Stockholm University

Master Thesis

Degree Project in
Marine Geology 60 hp

Diatoms from the late Holocene of the western Chukchi Sea, Arctic Ocean: environmental signals and palaeoceanography

Erik Browaldh

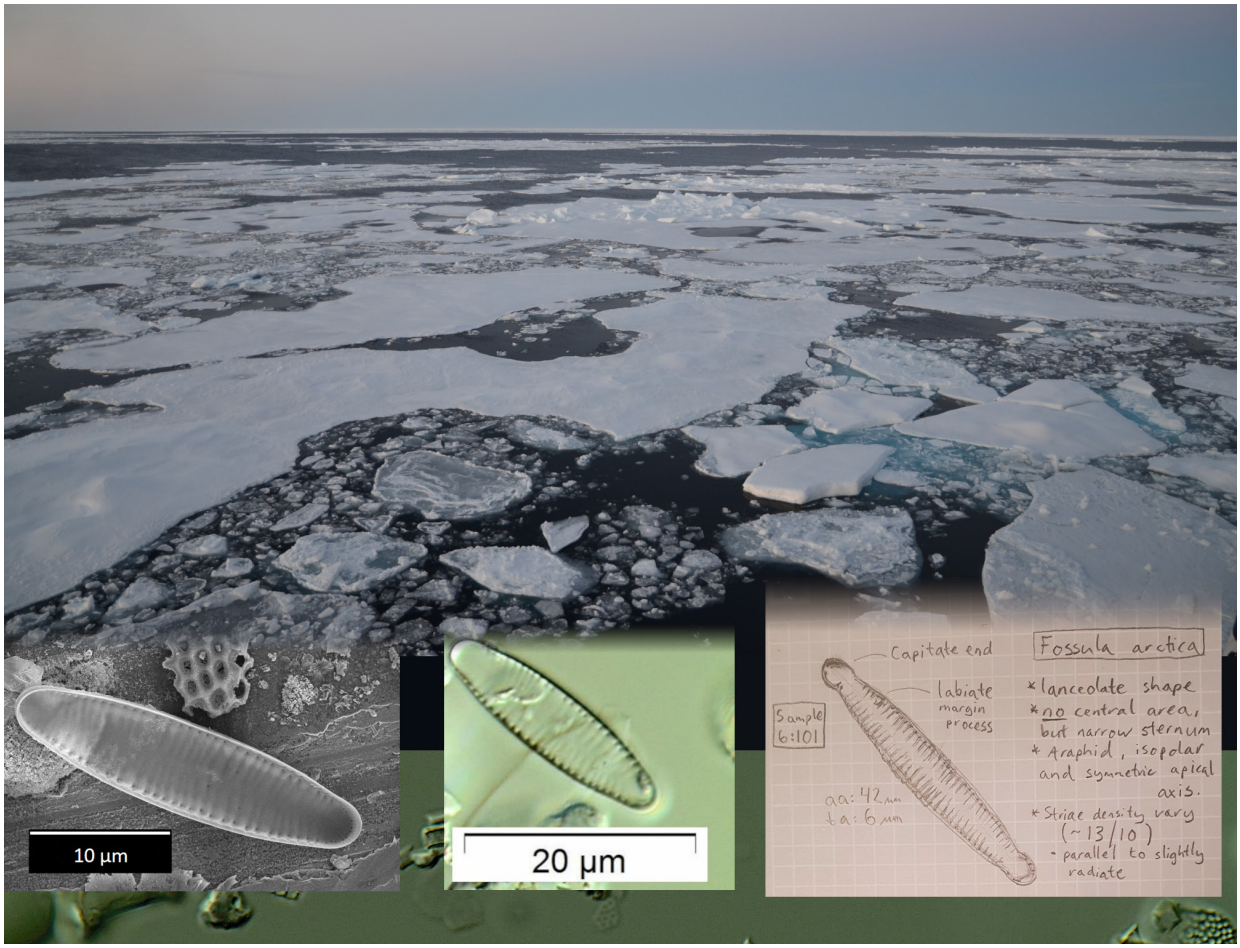

Stockholm 2022

Department of Geological Sciences
Stockholm University
SE-106 91 Stockholm

Diatoms from the late Holocene of the western Chukchi Sea, Arctic Ocean: environmental signals and palaeoceanography

Erik Browaldh

Master Thesis

60 credits

Department of Geological Sciences, Stockholm University

Abstract

The sediment Core SWERUS-L2-2-PC1 (2PC) retrieved from the Chukchi Sea, Arctic Ocean sits in an oceanographically dynamic location at the Arctic-Pacific Ocean gateway. The 8.3 m-long core was retrieved in Herald Canyon at the marginal ice zone at 57 m depth. Core 2PC is well-positioned to record variability in inflow of Bering Sea Water (BSW) and Pacific Water (PW) in Herald Canyon. With the 2PC high sedimentation rate (200 cm/kyr), two independent age models (radiocarbon and palaeomagnetism) based on tephra age markers, and a richness in well-preserved siliceous sediment, validate 2PC as an outstanding sequence for applying diatom assemblage analysis as a proxy for ocean-climate change back to 4250 years BP, including the past few hundred years where global warming and sea ice decline is recorded by instrumental records. These characteristics make Core-2PC a useful record for investigating the role of PW on sea ice variability in the Chukchi Sea, both in the past and predicting the future.

To investigate the impact of PW on ocean and sea ice conditions in the Chukchi Sea, diatom assemblage analysis was performed on 49 samples through the Late Holocene. The over-arching goal was to test the hypothesis, suggested by existing research on 2PC using benthic foraminifera Mg/Ca palaeothermometry, that the strength of PW inflow into the Chukchi Sea via Herald Canyon has varied on a time scales of ~500-1000 years in the past 4000 years. PW is slightly warmer than resident Arctic surface waters and is known to be an important control on Arctic sea-ice. The diatom assemblage approach assumes that there are recognizable differences between end-member diatom assemblages that are characteristic of PW versus Arctic Ocean type environments associated with extensive sea-ice conditions. The mapping of species in the Herald Canyon was used to test the idea of variability of sea-ice extent and the role of the Pacific Ocean forcings into the western Chukchi Sea.

The results reveal diverse diatom assemblages throughout the past 4000 years in Herald Canyon, showing this core to be very useful for diatom palaeoclimate reconstructions. A total of 126 species with abundance >1% are recognized. Several generalist species typically dominate assemblages especially *Chaetoceros*, ice-algae, marine-neritic and near ice or cold-water planktic centric diatoms. Distinct changes in stratigraphy are illustrated by changes in identified diatom assemblage zones. The 2PC diatom assemblages were contrasted with records from Chukchi-, Laptev-, East Siberian- and Bering Sea and North Pacific Ocean. At 2PC, sympagic (sea-ice related), planktic and neritic species abundance varies on time scales of ~500-1000 years. Importantly, there is a clear similarity between the timing of diatom assemblage changes and the 2PC benthic foraminifera Mg/Ca bottom water temperature (BWT) reconstruction. In particular, abundance changes in the warm water species *Thalassionema nitzschioides*, *Shionodiscus oestrupii* and *Thalassionema simonsenii*, tychoplanktic *Paralia sulcata,* Ice algae- and sympagic assemblages and cold-water indicators correspond best to BWT fluctuations shown by the Mg/Ca reconstruction. These oscillations are suggestive of changes in warmer PW inflow. Other aspects of the diatom data appear to correlate with colder and warmer climate events and suggest that changes in PW inflow amplified the effects of these events in the Chukchi Sea region through the Late Holocene in the Northern Hemisphere. It can thus, be concluded that diatoms from 2PC, support the palaeoceanographic reconstruction suggested by the benthic foraminifera Mg/Ca palaeothermometry and that variations in PW inflow through Herald Canyon is an important driver of sea ice variability on thousand-year time scales.

Front page: Two micrographs (mag. x2700, x1000) and a sketch of *Fossula arctica* (Hasle) Syvertsen & Quillfeldt 1996. Photo from SWERUS-expedition 2014, Arctic Ocean by Carina Johansson.

Contents

1. Introduction

The ocean cryosphere dynamics and forcings acting in the Arctic Ocean are not well understood. A piece of this puzzle can be investigated using diatoms – single-celled aquatic algae that are very sensitive to climate and environmental conditions and whose biomineral skeleton can contribute significantly to marine sediments in certain settings.

Sea ice in the Arctic Ocean (AO) can either melt or expand and is a key factor in the ocean-climate dynamics, defining the region. The heat transport from water masses from the Pacific Ocean can melt ice (Coachman et al., 1975). In the last two decades, research has narrowed the warm water-ice relationship to a few components. The reduced sea-ice formation in the western Arctic Basin, is one of the components, associated with the inflow of Pacific Water (PW) via the Bering Strait (Linders et al., 2017; Luchin and Panteleev, 2014; Stein et al., 2017; Woodgate et al., 2010). It's a common agreement, that the thermal conditions in the Chukchi Sea are established by warm PW. A typical August surface water temperature measured through Bering Strait 5-11°C (Woodgate et al., 2005a). Late Holocene trends show similar patterns in the sea-ice formation with other Arctic marginal seas (Stein et al., 2017). In addition to the physical changes, the marine eco-systems have also changed in the Arctic-Pacific region. The composition of marine species is believed to experience a shift in taxa due to increased seawater temperatures, sea-ice advance, and retreat (Grebmeier, 2012). However, the controlling mechanisms behind the PW inflow transiting the Chukchi Sea prior targeting the deeper, central basin of the Arctic Ocean (Stein et al., 2017) remain unclear. This includes present- and PW variability on millennial time scales. Proxy data like diatoms can help to resolve this.

Diatoms are unicellular algae with diverse ecologies and environmental tolerances (Karpuz and Schrader, 1990; Kilham et al., 1996). They are extremely sensitive to environmental change and are used extensively as proxies to reconstruct environmental conditions in the past (Karpuz and Schrader, 1990). In the Arctic Ocean diatoms have been studied from mid-20th century, and in the Chukchi Sea by Cleve (1883). Here they are used together with other proxies indicators, like dinoflagellates, biomarkers, $\delta^{18}O$ of foraminifera and ice-rafted debris to gain paleoclimate knowledge (Calvert and Pedersen, 2007). The Chukchi Sea is one of the most productive oceans in the Arctic Ocean region. The richness of the species is reflected in diatom abundance through late Holocene. Among the seas, the highest numerous variety among diatom taxa is in the Chukchi Sea region, where a variety of different marine sub-systems exist (von Quillfeldt et al., 2003).

In order to explore the relationship between Pacific Water inflow and the temperature fluctuations on the seafloor from the AO, a Bottom Water Temperature (BWT)-record was produced previously using benthic foraminifera Mg/Ca palaeothermometry, and a customized Arctic BWT calibration (Barrientos, 2018; Barrientos et al., 2018b). The Mg/Ca BWT reconstruction revealed temperature variability of -2.4 to 1°C at the seafloor in Herald Canyon over the past 4000 years (Figure 1a). Together with a correlated oxygen stable isotope ($\delta^{18}O$) from benthic foraminifera the results were interpreted to signal variability in Pacific inflow. However, It has remained unclear whether the benthic BWT signal was genuinely sourced from the Pacific or if there is a mixture of processes that resulted in the BWT-signal (Barrientos, 2018; Barrientos et al., 2018b).

1.1 Diatoms as environmental tracers in the Arctic Ocean: pack ice to open water conditions

A range of diatom habitats and ecologies can be recognized in the Chukchi Sea to Bering Strait region (Figure 1b). Starting with the multi-year pack-ice, a vast majority of the thickness is subsurface. If the sea-ice survive over two seasons, it accumulated to multiple ice-layer, else counted as first year ice. Thin ice has a lower strength than thicker layers, allowing rapid deformation and modifying the Arctic ice landscape (Herman, 1989). Communities like the ice-algae community live under such extreme conditions in the Arctic region. Here, the most crucial factor for these communities is access to light (Herman, 1989). Ice-algae (synonym: sympagic- or cryophilic species), are either attached to-, in- under- or above ice (Horner, 1989).

The Marginal ice zone (MIZ) is defined as a region with by 80% sea ice coverage. This sea surface ice is associated with seasonal built-up ice and stretches from the ice edge into the pack-ice. The MIZ contains sea ice causing highly active deformation in this zone. When ice starts to melt, a mixture of ice and cold shelf water coexist. Fragmenting sea-ice is floating in the water. The next zone is defined as around ice and early Spring bloomers. The first diatom spring bloom occurs when enough light can penetrate ice to initiate photosynthesis (Alexander and Chapman, 1981; Selz et al., 2018). Other communities grow in the water column around ice, melting ice, or in ice-free water

associated with the sea surface. As a rule of thumb, centric diatoms (circular shaped) are more frequent than pennales (elongate shaped) when shifting from sea-ice to cold water and ice-free pelagic conditions (Poulin et al., 2011).

With further melting of ice, the amount of ice free water increase until the ice free, cold water zone is reached (Hibler, 1989). Relatively closest to the Bering Strait of this succession described, are Pacific Water species from Bering Sea Water from a pelagic open water setting (Tsoy et al., 2017). In the Chukchi Sea, different diatom eco-habitats can be related to this ice-to-pelagic succession (Figure 1b).

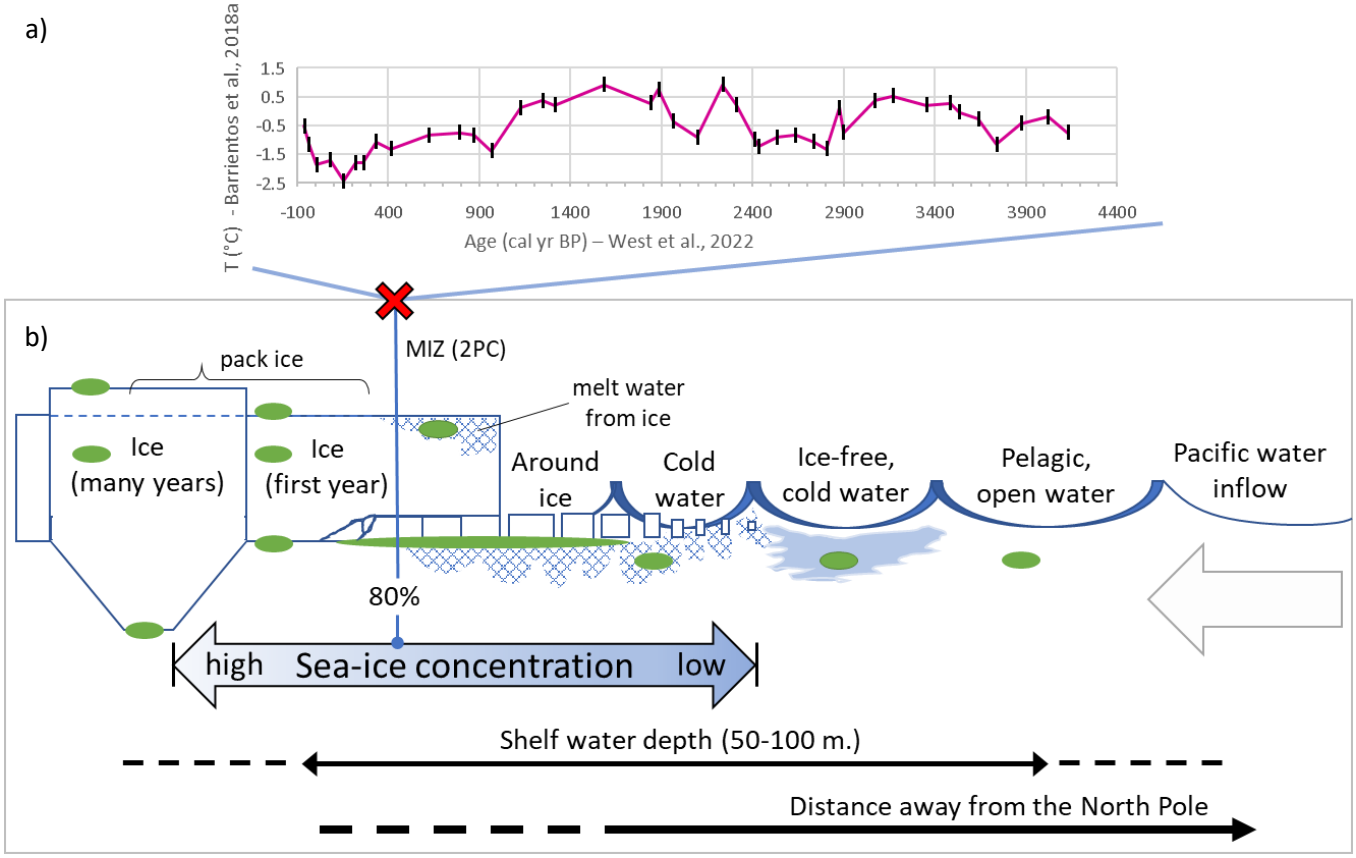

Figure 1. Bottom water temperature (BWT) integrated in same figure as a sea-ice to open water marine diatom habitats. **(a)** Bottom Water Temperature (BWT) history (Mg/Ca BWT proxy) at the Marginal ice zone (MIZ) in Herald Canyon as recorded from Core 2PC. **(b)** A seasonally- integrated schematic representation of sea ice to open water diatom habitats. Diatom habitats are represented by green ellipses. MIZ is where 2PC-Core (red cross) was retrieved. Dashed extension lines indicate variable start and end points of the conditional zones. Shelf water depth after Sancetta, (1981). The figure is not to scale.

1.2 Sea-ice: physical properties and recent changes

Sea ice extent fluctuates in space and time. Different types of sea ice in the Arctic Ocean are observed within a 100 km^2 patch. The sea ice density ranges from very thick to open water and the forces causing the ice to move, are mainly wind and currents (Hibler, 1989). Understanding sea ice variability over long time scales is challenging. Observations via satellite imagery have only been possible since the 1970s. A few polar expeditions were documenting the Arctic ice-sheet region since the end of 19th century, although technical improvements made the region easier to access in the middle of 20th century. In situ observations from submarine sonar profiles, concluded that during 1958–1978 the ice was more than 1 m thicker compared to 1993–1997 measurements in the Chukchi Sea, East Siberian Sea, Laptev Sea, Beaufort Sea and Central Arctic basin (Rothrock et al., 1999).

Ice surfaces can be calculated in two ways, either by area or by extent. Area is used when ice is packed together, while extent is ice concentration >25%. It includes cold water, melting ice, pack-ice, polynyas (open water areas by surrounding ice). It also includes the packed sea-ice area itself. Consequently, the extent is always bigger than the area. Ice can be seasonal with melting forces acting on the first-year ice-growth. This will eventually melt away every season. Ice surviving the season, enduring the summer melt season will accumulate with earlier ice layers building up the ice thickness that is less sensitive to the dynamics acting on sea ice reduction (Perovich and Richter-Menge,

2009). The data from NASA's Scanning Multichannel Microwave Radiometer (SMMR), shows a cyclic ice extent curve 1980–2008 (Comiso et al., 2008). Maximal peaks occurred during winter and early spring (13–16 x10^6 km^2), with minimum dips in late summer to autumn (4–7 x10^6 km^2). Since the 1970s, the sea ice extent has gradually decreased in the Northern Hemisphere with a trend of 30% yearly (NSIDC, http://nsidc.org). The largest sea ice reduction measured annually in August was contrasted in the year 1996 and the year 2012. Here, the relative extent decreased from 8.1 to 4.71 million km^2 from inset figure (2).

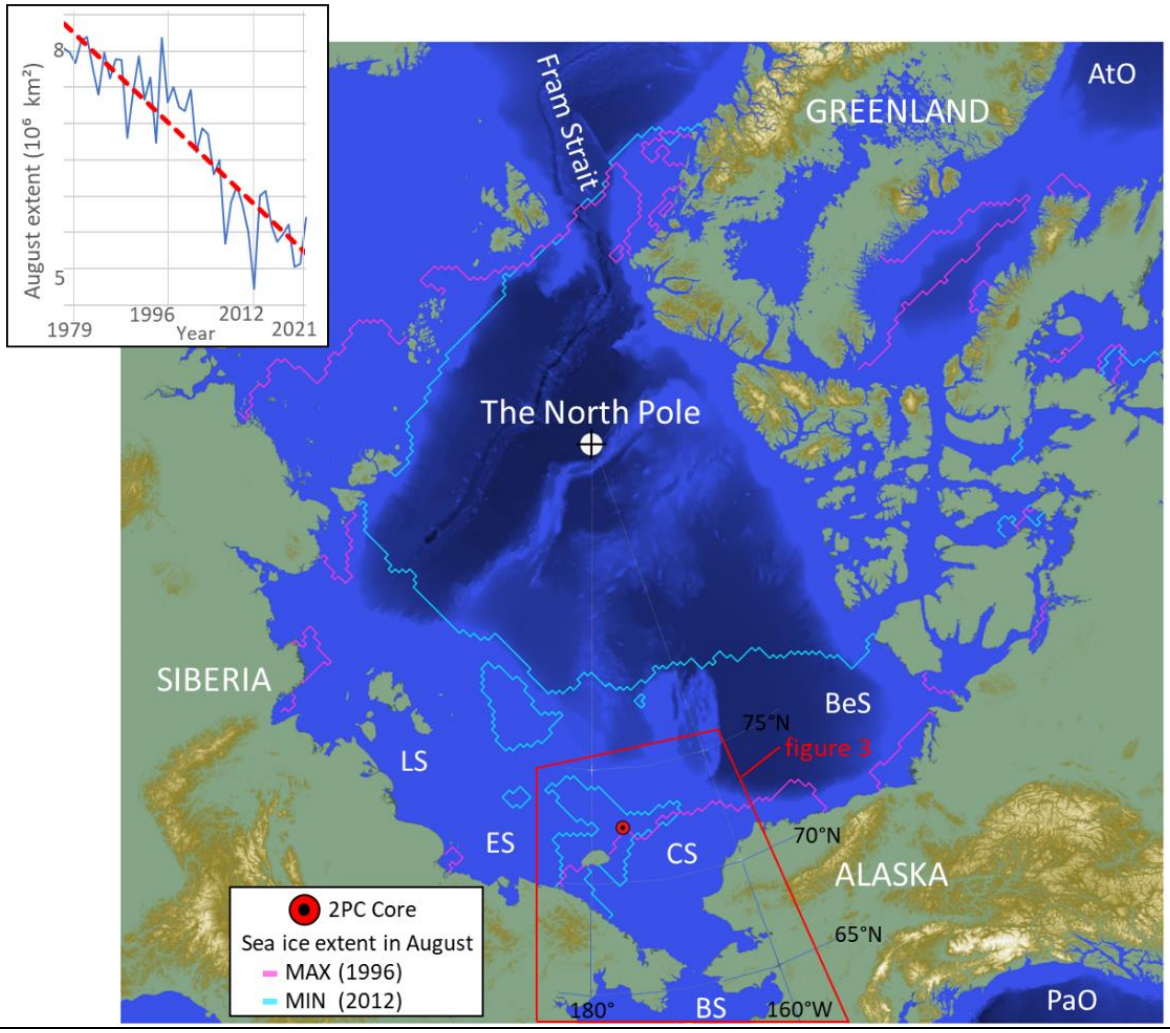

Figure 2. Map of the Arctic Ocean with 2PC Core marked and polylines (MIN, MAX) explained in the legend. The oceans and neighbouring seas AtO: Atlantic Ocean and PaO: Pacific Ocean, BS: Bearing Sea, CS: Chukchi Sea, ES: East Siberian Sea, LS: Laptev Sea and BeS: Beaufort Sea marked. Darker blue gradient from bathymetry >1000 meters depth after IBCAO v.4 (Jakobsson et al., 2020). Inset graph on the left side showing the Artic Ocean August ice extent 1979-2021 highlighting 1996 and 2012 with a linear trendline (dashed). Detailed setting of Chukchi Sea in figure 3. Vector polylines and sea ice extent data by NSIDC (http://nsidc.org [access: 2022-05-25]).

Core SWERUS-L2-2-PC1 (2PC) is from the Herald Canyon, western Chukchi Sea. This coring station has on decadal through millennial time scales experienced both sea-ice and cold open water (Figure 2). Recently, the freeze-extent line has varied some hundreds of kilometres around Herald Canyon (Woodgate et al., 2005a). 2PC was strategically located on the mean summer sea-ice extent between 1981 and 2010. Its position was favourable for monitoring the climate and marine conditions in the region, including PW inflow into the Chukchi basin (Stein et al., 2017). It contains abundant biogenic silica (BSi) throughout the core roughly 4000 year long core which is derived large from diatom fossils.

As diatoms are highly diverse and can be associated with different sea-ice habitats, they provide a valuable proxy and are helpful in reconstructing the palaeoceanographic setting including marginal ice zone (MIZ), water masses exchange and Sea Surface Temperatures (SST) estimates (Koç et al., 1993). Their diversity makes them suitable for palaeoceanographic analysis (Sancetta, 1981).

The 2PC-Core retrieved from MIZ (Figure 2), is unique because *i)* it is an expanded Late Holocene section, with extremely high sedimentation rates yielding high resolution of BSi-proxy data, *ii)* there is excellent down-core age control, provided by multiple methods (radiocarbon, palaeomagnetism, tephra), (Pearce et al., 2017; West et al., 2022), and *iii)* a diatom abundance that can be used to reconstruct Holocene palaeoceanographic changes. The third aspect consequently brings up the utilisation of diatom samples in this work.

1.3 Aim and research question to test.

The main goal is to test the hypothesis, suggested by existing research on 2PC using the benthic foraminifera Mg/Ca palaeothermometry, that the strength of Pacific water inflow into the Chukchi Sea has varied in a systematic way over the past 4000 years, and that this is an important control on sea ice variability in the region. It has been unclear whether the BWT-signal exclusively originated from the Pacific, or if there are a mix of processes that contributed to the BWT-signal.

The mapping of diatom species in 2PC was the tool to examine the role of Pacific Ocean forcings and its impact on the Western Chukchi Sea. Two aims (A and B) have been outlined, to drill down diatoms to individual signals related to the main goal.

A) The primary aim of this thesis is to use diatom assemblage analysis for reconstructing environmental conditions in the Herald Canyon in the late Holocene and use the down-core patterns of assemblage change as a proxy to investigate how Pacific water inflow to the Chukchi Sea has varied over this time period.

The following research questions will be addressed:

a.1) How does diatom species abundance vary over time in terms of life-form, salinity changes, and ice conditions between 4265 years BP to present date of the Western Chukchi Sea?

a.2) How do individual diatom taxa and abundance patterns of common species vary in the western Chukchi Sea compared Laptev-, East Siberian- and Bering Sea, and the North Pacific Ocean?

When the diatom assemblage approach is completed from Aim A, its assumed that there exist recognizable differences between end-member diatom assemblage that are characteristic of Pacific Water inflow contrasted with the sea-ice conditions of the Arctic Ocean.

B) The second aim of this thesis is to test whether there is a link between the diatom assemblage and the BWT proxy derived from Mg/Ca ratio from the same core (Barrientos et al., 2018a).

Here the following research questions will be addressed:

b.1) To what extent is the Mg/Ca BWT proxy comparable to diatom signals?

b.2) How do diatoms which indicate warm-water, cold-water and ice cover, respectively, from Core 2PC respond to paleoclimate events from the Northern Hemisphere through the Late Holocene?

2. Background

2.1 Oceanographic setting

The Arctic Ocean consists of marginal seas, and the Chukchi Sea is one of them (Figure 2). Bordered by Siberia and Alaska, the Chukchi Sea is connected to the Pacific Ocean via the Bering Strait. With a total area of 620 000 km^2, it is one of the largest shelf seas in the World (Jakobsson, 2002). An increased influx of Bering Sea water (BSW) starting in the transition of middle-late Holocene was the main contributor to the increased productivity in surface water of the shelf (Gusev et al., 2014). The bloom productivity is on average 12-98 g C m^{-2}, but highest in the shelf zones (Polyakova, 1989). The water depth across the shelf sea is typically 50-100 meters in the northern Bering Sea shelf and southern Chukchi Sea (Sancetta, 1981). The remainder Chukchi sea floor topography is generally flat, with depths of less than 50 meters and the shelf-break at ~73°N. The Chukchi Sea is seasonally ice free, the period of open water being 80-85% of the year in recent warm years, compared to a perennial ice cover throughout the year in the Central Arctic Ocean (Luchin and Panteleev, 2014). During winter time, polynyas (a crater of open water surrounded by ice) are formed around the coast (Woodgate et al., 2005a).The Herald Canyon has an enrichment of biogenic material (Grebmeier et al., 2006) and current transports is going through Herald canons shelf zone into deeper basin (Weingartner et al., 2005a).

In the past, Manley (2002) demonstrated that no inflow of fresh and nutrient-rich PW was possible before Last Glacial Maximum and an reopening of Bering occurred 10 ka calibrated years BP due flooding of the land bridge between the continents. Today, ocean water exchange in the Arctic Ocean is regulated by two gateways, one on the Atlantic side through the Fram Strait, and the other one with Pacific water flow through the narrow Bering Strait (85 km, 50 m deep). These two straits control the heat and ocean fluxes of the Arctic Ocean. The balance of freshwater and heat fluxes can change the Arctic sea-ice distribution (Woodgate et al., 2010). Thermal- and saline ranges in the Arctic Ocean are large, and differences between ice- and marine water is around S = 30 (Hibler, 1989). While atmospheric freshwater has a residence time of a week, ocean water stays on the decennial time scale. The freshwater-import through the Bering Strait answer to a third (30%) of all fluxes. Other sources into the Arctic Ocean include river runoff (38%) and net precipitation (Serreze et al., 2006), where snow contributing layer is ~30 cm thick (Hibler, 1989). Half of the outgoing freshwater transport is via Fram Strait as water or sea ice (26% respectively 25%) or along the Canadian coast (35%) through the Archipelago (Serreze et al., 2006). The freshwater outflow was 160 mSv (1 Sverdrup = 1 x 10^6 m^3s^{-1}) through Fram Strait and half of that outflow through the Canadian Archipelago (Dickson et al., 2008). Models have shown that a closure of the Bering Strait would have more impact on surface circulation in the Arctic and the North Atlantic Oceans with higher stratification and decrease of salinity in the upper 50 meters compared to little impact by closing the Fram Strait-Atlantic side (Karami et al., 2021). These observations and model results emphasize the importance of the Chukchi Sea in Arctic-exchange and climate, and thus provide motivation for careful study of its past ocean dynamics.

2.1.1 Ocean currents effecting the Chukchi Sea

Currents transiting Bering Sea into Chukchi Sea are primary driven by a difference in pressure-head between Pacific and AO (Coachman et al., 1975; Woodgate et al., 2005a). The currents have impact of salinity, water temperature, and may boost the Chukchi Sea with higher amounts of nutrient rich water (Coachman et al., 1975; Grebmeier et al., 2006; Stein et al., 2017; Weingartner et al., 2005a). Salinity and temperature vary over months studied with mooring data monitoring the flow from Bering Strait into Chukchi Sea. On average between 1990 to 2004, the near-bottom salinity was between ~31.9 in December with start of cooling followed by increased salinity until melting began in March associated with a peak in salinity of 33. Near-bottom temperature was between -1.8 to successively increased temperature until October maximum, 2.3 °C (Woodgate et al., 2005b). One part of the Bering Sea Water (BSW) flows through Herald Canyon, commonly termed branch one (Figure 3). In 1993, a well-mixed water column was measured in the canyon, moderately salty (~32.5) and warm (>2.0°C) originating Bering Sea Water (Weingartner et al., 2005b). There are three main water currents from the North Pacific heading northwards into the Chukchi Sea: Anadyr current (AC), Alaskan Coastal Water (ACW) and BSW (Springer and McRoy, 1993; Stein et al., 2017). In the North Bering Sea, they merge to two currents (figure 3). Besides impacting freshwater balance in the Arctic Ocean, these currents deliver variable amounts of ocean heat and nutrients into the Chukchi Sea (Woodgate et al., 2005a).

The three currents take distinctive pathways through the Bering Sea, flowing on western and eastern side through the passage due the seabed topography. On the western side AC is rich in nutrients from the Anadyr River and provides relatively cold and relatively high saline water into the Chukchi Sea. BSW also passes through the western side of Bering Strait, heading northeast of the AC, with an outflow to the Beaufort Sea (figure 3). The BSW provides the Chukchi Sea with relatively colder and higher salinity water surface water temperature compared with Alaska Coastal Water (Woodgate et al., 2005a). When salinity is increased by the sourced Pacific Sea Water, the ice-free water measure surface temperature of 2-3°C in Chukchi Sea, and even higher, up to 7-8 °C on Eastern side of Chukchi where Alaska Coastal Water (ACW), the third current, is flowing (Tsoy et al., 2017). The ACW is heated in the North Pacific, as shelf water surrounding the Aleutian Islands. It flows close to the eastern coast through the gateway into Chukchi Sea with relatively warm and relatively less saline water masses due river input from Yukon and Kuskokwim rivers. ACW flows from near the outer archipelago of Alaska in Eastern Chukchi basin before exiting on the marginal shelf of Beaufort Sea where the Canada Abyssal Basin is in contact with the shelf (Coachman et al., 1975; Springer and McRoy, 1993).

Around 0.8 Sverdrup (Sv) is yearly passed through the narrow strait into Chukchi basin from the Bering Strait-sourced flows (Woodgate et al., 2005a). The AC flows over the shelves at a depth of 100-200 meters and has similar densities to BSW, allowing them to mix along the current path. This in contrast to ACW that's more easily separated from the shelf water (Springer and McRoy, 1993). Freshwater contribution on the Eastern side through the Bering Sea contributes a much larger proportion of freshwater compared to the western side where the AC flows. This is explained by that the Yukon river delivers a six times higher contribution of freshwater compared with the freshwater discharge into the Gulf of Anadyr, Bering Sea (Coachman et al., 1975).

In the Chukchi basin the enriched nutrient western BSW-branch forks into three currents and the relatively less nutrient rich branch 2 and 3 of BSW current splits (Figure 3). The central and eastern currents are heading on the eastern side of Herald Shoal and the other branch is flowing parallel to the ACC. On annual average, the velocity in Bering Strait and Herald Canyon is 10-20 cm/s, and the Pacific water from central Chukchi is around 5 cm/s. The Herald Canyon has seasonally varying velocities, being strongest during Summer and Autumn (Woodgate et al., 2005a). The Siberian Coastal Current (SCC) is not derived from the Pacific but circulates from within the Central Arctic Ocean. It transits the Laptev Sea, East Siberian Sea and then follows along coast of Chukchi Sea. SCC is driven by wind, rivers and melting ice and provides the central Chukchi basin with fresh and cold waters (Weingartner et al., 1999). The volume is seasonally dependent on average ~0.1 Sv (figure 3).

2.1.2 Temperature (SST, BTW), and stratification

The thermal input from Pacific water into Chukchi Sea water is the reason for warmer influx in the basin (Coachman et al., 1975; Woodgate et al., 2005). Sea water temperature from Bering Strait has minimally increased with 0.012°C annually since 1941. The flow through Bering Strait is relatively stronger by warmer occasions, with a consequence of an increased current flow on the westward flow in the central Chukchi Sea (Luchin and Panteleev, 2014). Convection processes act in the Arctic Ocean, as heat travels northwards in the ocean and reach the ice layer through the warmer surface layers (Hibler, 1989). It has been shown that in recent years between 2001 and 2004 that the increased heat could melt 640 000 km^2 of 1 m thick ice in Chukchi Sea (Woodgate et al., 2006). The amount of freshwater into the Arctic Ocean is relevant since the basin is salinity stratified and less impacted of temperature (Suzuki et al., 2021). Temperature and salinity have been measured through the water column in Western Arctic Ocean. Since currents are seasonal, winter water from Pacific is coldest (-2°C to -1°C) with salinity up to 36 compared with warmer Pacific summer water, mostly ranging between -1°C to +3°C. Warmest is the ACW with ranges above from +3°C (Jin et al., 2017).

Similar to other oceans, the phytoplanktic zone of the Arctic Ocean retrieves nutrients from many sources, including atmosphere, precipitation, river input and upwelling. The upwelling, causes an admixture with the thermo- and halocline layers below (Andersen, 1989). The cold-water due floes serving as an ice-cap on surface providing a cold stratified layer on surface water in the Arctic Ocean. The Pacific Water inputs contribute to a stratified layer under this ice-or cold related surface water to maintain the upper halocline (Anderson et al., 2013). The halocline transit zone between the Pacific and Arctic Ocean water masses is traditionally in the Arctic at 33.1 (Woodgate and Peralta-Ferriz, 2021). During Summer, the Pacific water in Arctic Ocean cause a halocline stratification due water masses at

halocline of 50 meters, while the colder winter water sinks deeper and mix the AO halocline at ~120 meters (Woodgate et al., 2005b).

An oceanographic water column profile was sampled during the 2PC-retrievment in August 2014. The SST remained similar (<6°C) between 0-20 meters below sea level (mbsl) before it stratifies again prior the rapid decrease ~20-27 m b.s.s. (1°C), and then gradually decreasing to <0°C (57 mbsl) after which the curve nearly flattens out at seabed (<-1°C, 70 mbsl). The salinity was ~31.7 between 0-18 mbsl, with an increase to 32.3 at ~20 mbsl and then gradually increased to ~32.5 at 57 mbsl and below (credit: bolin.su.se/data/oden-swerus-2014-ctd-1).

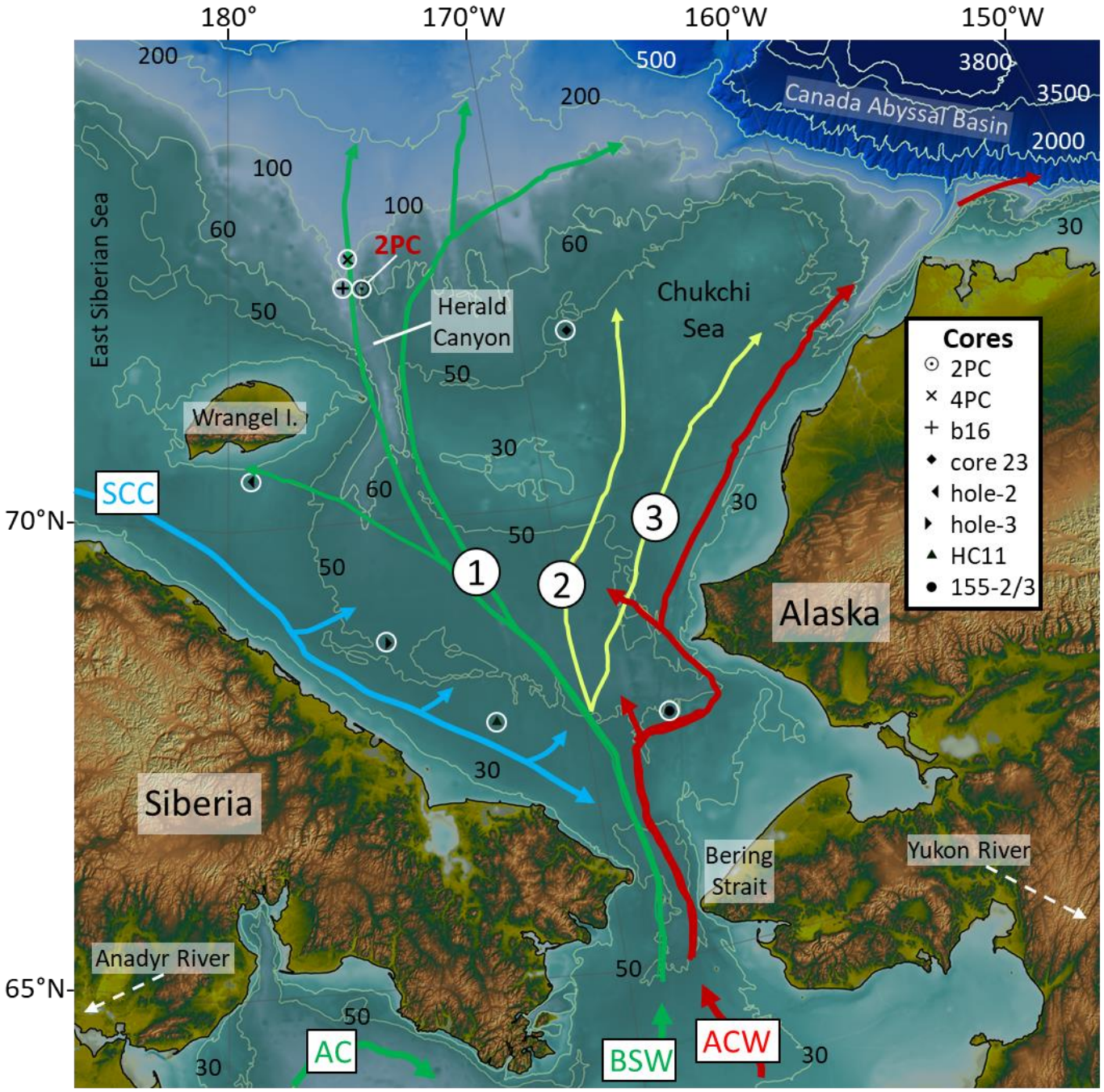

Figure 3. The Chukchi Sea oceanographic setting showing the relevant ocean surface currents and their origins. Core 2PC and other sample sites mentioned in this study are shown. Surface currents: ACW: Alaska Coastal Water, SCC: Siberian Coastal Current, AC: Anadyr Current and BSW: Bearing Sea Water. Three principal branches of BSW are identified: 1: highest amount of nutrients, via Herald Canyon before a northward exit in the deeper Chukchi Basin, and a flow to Wrangel Island, 2: the Central Channel, 3: BSW parallel to ACW. Relative water temperature of the currents is indicated by colours - red arrow: relatively warm water, blue arrow: relatively cold water. BSW (green lines) has a temperature that is relatively lower than the ACW but warmer than the SCC (after Coachman et al., 1975). Nutrient rich AC mixed with BSW (green northward arrow) (after Stein et al., 2017). Isobaths in meters. Basemap and modified bathymetry data: IBCAO v.4 (Jakobsson et al., 2020). Main flow directions and current properties modified after Grebmeier et al. (2006) and Stein et al. (2017).

2.1.3 Existing constraints on Holocene water temperature variability in Herald Canyon

Benthic foraminifera Mg/Ca palaeothermometry is a powerful tool for reconstructing BWT in the past. The method is derived by the Mg/Ca proxy using calcareous microfossils. Benthic foraminifera using Mg/Ca is almost temperate dependent and therefore a suitable tool for BWT (Lear et al., 2000). In existing research on the 2PC-core, BWT was found to vary between -2.4 to 1°C, over cycles of ~500-1000 years, which, together with δ^{18}Osw as a salinity proxy, was interpreted as signals of increased Pacific water inflow to Herald Canyon (Barrientos, 2018b). But wind and insolation are other components that must be considered besides PW inflow (Polyak et al., 2016; Stein et al., 2017; Woodgate et al., 2010). BWT was applied to reconstruct past seawater temperatures on geological timescale with 41 samples (Barrientos, 2018), with supplementary data (Barrientos et al., 2018a) in Appendix (A).

The climate events Roman Warm Period (RWP), the Dark Ages (DA), the Medieval Climate Anomaly (MCA) and Little Ice Age (LIA) occurred during the late Holocene BWT-samples (Mann et al., 2009; Mann and Jones, 2003; Matul et al., 2007; Neukom et al., 2019; Seidenkrantz et al., 2008).

2.2 Age model

Existing age constraints for Core 2PC have been used in this study. The age model is remarkably good for Arctic sediment sequences. Initially it was derived from radiocarbon analyses of mollusc shells and some foraminifera samples in addition to the recognition of a known tephra layer (Pearce et al., 2017). It was later improved through the measurement and correlation of paleomagnetic secular variation and additional 210Pbm, 137Cs and Hg measurements to constrain depositional rates in the last 100 years (West et al., 2022). The difference between the original and more refined age model were on average 15 years, and ~40 years at most. The greatest distinguishable adjustment were in the upper part of the core due to the inclusion of the Hg and additional 210Pb and 137Cs measurements (West et al., 2022).

2.3 Geological setting, geophysical- and geochemical properties

During the Cenozoic epoch, Chuckchi Sea was dominated by rifting and crustal stretching, causing a graben system. The Graben extends into Herald Canyon into the shelf edge of the north Chukchi basin. This caused an elongated neotectonic narrow structured belt on seafloor from Bering Sea, into the East Siberian coast (~67°N) up to 2PC (72°N), with a closing close to the Canada basin at 75°N (Shipilov et al., 1989). Low biogenic silica (BSi) is found in nearshore sediments (Gehlen and van Raaphorst, 1993), while diatomites contains high BSi (Mortlock and Froelich, 1989).
On the shelf, ~200 kilometres north of the Chukchi Coastal area, a plateau with a water depth of 50 meters is characteristic of the almost flat sea floor for tens of kilometres northwards on the shelf. The bathymetry changes closer to Wrangle Island, with a well-defined deeper canyon ~60 meters prior the study site (Figure 3).

The lithology of Core 2 PC is described as an olive-green silty clay (Pearce et al., 2017). In both 2PC and 4PC, physical properties of this lithology (Unit A as it is described) show similarities regarding density, magnetic susceptibility and $\delta^{13}C_{org}$. Unit A shows little variations down core and appears to be a relatively stable unit. In addition, biogenic silica (BSi) measured from the 4PC has throughout the unit A shown a high value, but associated with the transition to unit B, it drops to near zero-values (Jakobsson et al., 2017).

2.3.1 Site location and neighbouring cores and sample stations

The sedimentary 2PC-Core was cored in the Herald Canyon, 150 km northeast of Wrangel Island and additional 250 km from the Siberian coast (72.52° N, 175.32° W). The core length measured 830 cm and split into six sections prior a working- and archive half rounds division, sealed with endcaps. The 2PC was kept in a +4°C storage room. Core section 1 is the youngest and section 6 the oldest.

Core 2PC was retrieved on the shallower canyon flanks and boasts double the sedimentation rate compared to 4PC north of 2PC, towards the centre of the Chukchi basin (Jakobsson et al., 2017). The average sedimentation rate in 2PC is 0.2 cm annually or 200 cm/kyr (West et al., 2022). Three other cores with diatom studies within a radius of 20 km from 2PC are the SWR-L2-4-PC1 (4PC), b16 box corer dredger shows remarkable lower sedimentation rate and core length and the b9 to the East of 2PC, in Herald Canyon at depth of 100 mbsf diatom-described by (Vologina et al., 2016) with a core length of 37 cm (Figure 3). It showed similar sedimentation rates to 4PC ~100 cm kyr^{-1} The b16

core from same drill hole as b9, showed a higher organic carbon than on average in Chukchi Sea (A.S. Astakhov et al., 2020).

To the south of 2PC, the HC11 core was retrieved at water depth 49 m, with a core length of 111 cm long and an estimated sedimentation rate of 78 cm kyr-1 (A.S. Astakhov et al., 2020). The HC11, b9 and b16 (Figure 3) have been used in diatom palaeoceanographic and paleoclimate research aged back to 2300 years BP (Tsoy and Obrezkova, 2017). North from HC11, two gravity cores, LV77-3-1 and LV77-3-2 were retrieved at depth 51 m depth near the Bering Strait in the path of Bering Sea Water and measured 333 cm respectively 31 cm core length (A.S. Astakhov et al., 2020). The longer core was dated with radiocarbon and considered the age of 2PC by Pearce et al. (2017) to 4.7 ky (A.S. Astakhov et al., 2020).

On the Eastern side of the Chukchi Sea, the oldest recovered piston cores from the shelf (radiocarbon dated), back to 8.0 to 14.2 ka (Gusev et al., 2014) with hole 2 and 3 (Figure 3). Drill site 01GGC in Hope Valley ~50 mbsl, Eastern side of the marginal shelf of Chukchi Sea, sedimentation rate during the Late Holocene has been significant lower compared to 2PC, approximately 50 cm kyr^{-1} (Keigwin et al., 2006). The drill site 01GGC is close to where the ice cores (155-2/155-3) of first years ice diatoms studies (Figure 3) have been drilled (von Quillfeldt et al., 2003).

2.4 Diatoms

Diatoms are autotrophic algae and are abundant in marine to lacustrine environments, including snow and ice. They are photosynthetic, primary producers, restricted to the euphotic zone and depend on solar radiation for their blooms (Crosta and Koç, 2007). Diatoms are divided into centric and pennate shapes with sizes between 2 and 2000 µm, but most common sizes are between 10 and 200 µm (Hasle and Syvertsen, 1997). Key nutrients for diatoms dwelling are nitrogen and phosphorous. The amount of nutrients together with dissolved silica ($SiO_2.H_2O$) therefore controls the bloom (abundance) rates (Kilham et al., 1996). Diatoms in the Arctic Ocean of present-day is essential to address environmental changes in fossil assemblages. Many taxa and genera have an unknown ecology. However, using common diatom taxa, palaeoconditions can be reconstructed based on species associated with warm and cold water (Oksman et al., 2019), while others thrive in the Arctic Ocean ice-related setting. In the AO when the sea-ice begins to break up in early Spring, epontic blooms (diatoms under- or within sea-ice related to brine channels in ice) are replaced by MIZ-bloom (Alexander and Niebauer, 1981). In Summer, snow and ice start to melt and ponds are formed (Lüthje et al., 2006).

When the diatom dies, the algae cells (frustule) will eventually sink to the sea floor if not uptake or consumed by chemical- or biological processes in the water column. The exoskeleton of amorphous silica is now exposed for dissolution and eventually lithified by diageneses (diatomite). Other biosilica-producers include chrysophytes, radiolarians, silicoflagellates, and sponges. Among these, diatoms are by far the most abundant and greatest contributor to seafloor sediment, under conditions suitable for silica preservation (Ragueneau et al., 1996; Smol et al., 2001).

When considering marine diatom environmental preferences, they are contrasted geographically, for instance Northern Hemisphere or Greenland, Iceland and Norwegian seas (Karpuz and Schrader, 1990; Oksman et al., 2019), adjacent ocean or shelf seas (Sancetta, 1982), bipolar species (Gersonde and Zielinski, 2000), or sea-ice related habitats at higher latitudes where solar radiation needed for photosynthesis is strongly seasonal (Kang and Fryxell, 1992). Comparing studies in geological time involves palaeo-reconstruction with multiple environmental aspects being important, including geochemical- and geophysical conditions (Astakhov et al., 2019, 2014), salinity, or preservation (Warnock and Scherer, 2015), which can be compared between regions e.g. the Baltic Sea (Andrén et al., 2000). Diatom studies from the Chukchi Sea involve Holocene sediments (Tsoy et al., 2017), living diatoms in the water column (von Quillfeldt et al., 2003), surface sediments (Polyakova, 1989) and ice cores (Bauch and Polyakova, 2000; von Quillfeldt et al., 2003). It has been shown that the different species are variably-sensitive to sea-surface temperatures (SSTs), sea-ice conditions and amount of nutrients available (e.g. Crosta and Koç, 2007, and references therein). Some species are motile, especially benthic moving in sediments, but most of the diatoms are not. Most of the pelagic taxa float in the upper- photic part of the ocean, where lateral transport is in the direction of currents or surface waves. Other ways to perform a lateral transport, is with ice sheets, windblown surface currents, or with terrestrial transportation (Cremer, 1999).

Five (six) broad ecologic categories (eco-groups) of diatom can be recognized associated with the Arctic Ocean and defined below:

- Sea ice (sympagic) species (live within or attached to sea ice, throughout their life cycle or for a part of it)
- Species that attach at the seabed (benthic)
- Pelagic or Planktic species in shelf waters -neritic
    - *Chaetoceros* spp.: a subgroup of species that also thrive in productive- nutrient rich waters (upwelling) on the Chukchi shelf.
- Warm Water group

However, a diatom taxon is not always exclusively found in a single environment, and some are ecologically flexible globetrotters.

Sea-ice flora or ice-algae/ sympagic diatoms: Sea-ice flora or ice-algae have been studied for almost 200 years. Around 180 species have been detected in the Laptev-, East Siberian- and Chukchi seas. In the beginning of 20th century, Gran distinguished species that occurred both in ice and the water column for example *Nitzschia cylindrus*, *N. grunowii*, and *Melosira arctica*, and *Pauliella taeniata*. *Nitzschia grunowii*, was later *reinterpreted as Fragilariopsis oceanica,* and *Fragilariopsis cylindrus* instead of *N. cylindrus* (Lundholm and Hasle, 2010). The two *Fragilariopsis* species could be attached to drift ice as their blooming in cold water (Okolodkov, 1992). Cryophilic diatoms are a synonym commonly used to refer to Arctic Sea-ice diatoms. The species and individual taxa may vary, but generally, *Fragilariopsis* spp. and *Fossula arctica* are commonly grouped as dwelling in the lower ice surface and indicators of early phytoplanktic spring bloom (Tsoy and Obrezkova, 2017). Due to radiation attenuation in the Arctic region, the solar energy is very limited, and less than 1% reach through the euphotic layer in pelagic environments. However, the sympagic diatoms thrive in ice, and intensity of light can be around 0.1% (Crosta and Koç, 2007). *Fragilariopsis* spp. do not survive long in low-salinity melt water direct under the ice (Horner, 1989). *Fragilariopsis cylindrus* in contrast, has been reported as a bipolar and is also common in the Baltic Sea (Hasle and Syvertsen, 1997), and is commonly seen in the pack ice and the water column near the ice edge (Kang and Fryxell, 1992).

Benthic diatoms: Among benthic (sea-floor living) diatoms, the vast majority are pennates. The live closer to the seafloor, in shallow settings, living in sediments, for instance epiphytic, epilithic or epipsammic (Horner and Schrader, 1982). To this group, many of the Naviculoides belong, sometimes associated with river system like Lena River (Cremer, 1999). This in contrast to the open (pelagic) species, that vertically regulate their position according to their growth factors and remain buoyant (Kemp and Villareal, 2018). The spread in the water of this life-form, depends on available substrate and light penetration (Smol et al., 2001). Sublittoral species are planktic and benthic species dwelling in the sublittoral zone (Polyakova, 1989). Tychoplanktic species are either benthic or planktic, for example *Paralia sulcata* thriving in marine benthic littoral environment, as well as in the planktic setting (Hasle and Syvertsen, 1997). *Pseudogomphonema arcticum* and *Plerusigma rhomboides* are epibenthic and motile. They use other diatoms like cells of *Melosira artica* to transport themselves due gliding (Bauch and Polyakova, 2000; Poulin et al., 2014).

Pelagic species or Planktic neritic are planktic species. In the Western Chukchi area, they are restricted to the shelf zone. In the Arctic Ocean, one group of the planktic neritic could be considered a cold oceanic group. This because of the condition in the AO of sea ice to cold open water. The group consist mostly of centric species, like *Thalassiosira nordenskioldii*, *T. gravida*, *T. antarctica*, *Bacterosira bathyomphala*, and *Attheya septentrionalis* are examples of this eco-group (Polyakova, 1989). Further subgroups can be made with *T. nordenskioldii* described in ice-neritic habitat (Obrezkova et al., 2014; Tsoy et al., 2017) and *T. antarctica* in cold shelf water around ice (Obrezkova et al., 2014). Diatoms in the shelf water, may be panthalassic dwelling in both neritic and oceanic waters, often with cold water preferences in the Arctic Ocean. The panthalassics coexist in the sublittoral zone with the benthics.

Upwelling species -the *Chaetoceros* genera in Chukchi Sea is associated with upwelling areas, but also count as a vast majority of the neritic assemblage (Tsoy and Obrezkova, 2017), typical species in Western part of Chukchi Sea (Astakhov et al., 2015). They are associated with highly productive water column with vertical displacement in the water column (Polyakova, 1989; Sancetta, 1982) or productive surface water (Obrezkova et al., 2014). *Chaetoceros* resting spores tend to be robust and heavily silicified (Sancetta, 1982, 1981). *Chaetoceros furcellatus* however, is one

species that has been found in the marginal ice zone. Small specimen of *C. furcellatus* are difficult to distinguish from *C. socialis* (Quillfeldt, 2001), but the latter has also been identified in the marginal ice zone, MIZ (Caissie, 2012). A higher concentration of primary production is around the shelf seas of Bering and Chukchi (Springer et al., 1996). Diatom stages involved with environmental affecting processes in the Chukchi Shelf area are summarized in figure 4.

Warm water group is the last eco-group with typical warm water-temperate species sourced from Pacific Water, PW. Species include *Thalassionema nitzschioides, Thalassiosira simonsenii, Shionodiscus oestrupii* can be added sourced, together with a few *Coscinodiscus* species (Caissie, 2012; Hasle and Syvertsen, 1997; Obrezkova et al., 2014; Oksman et al., 2019)

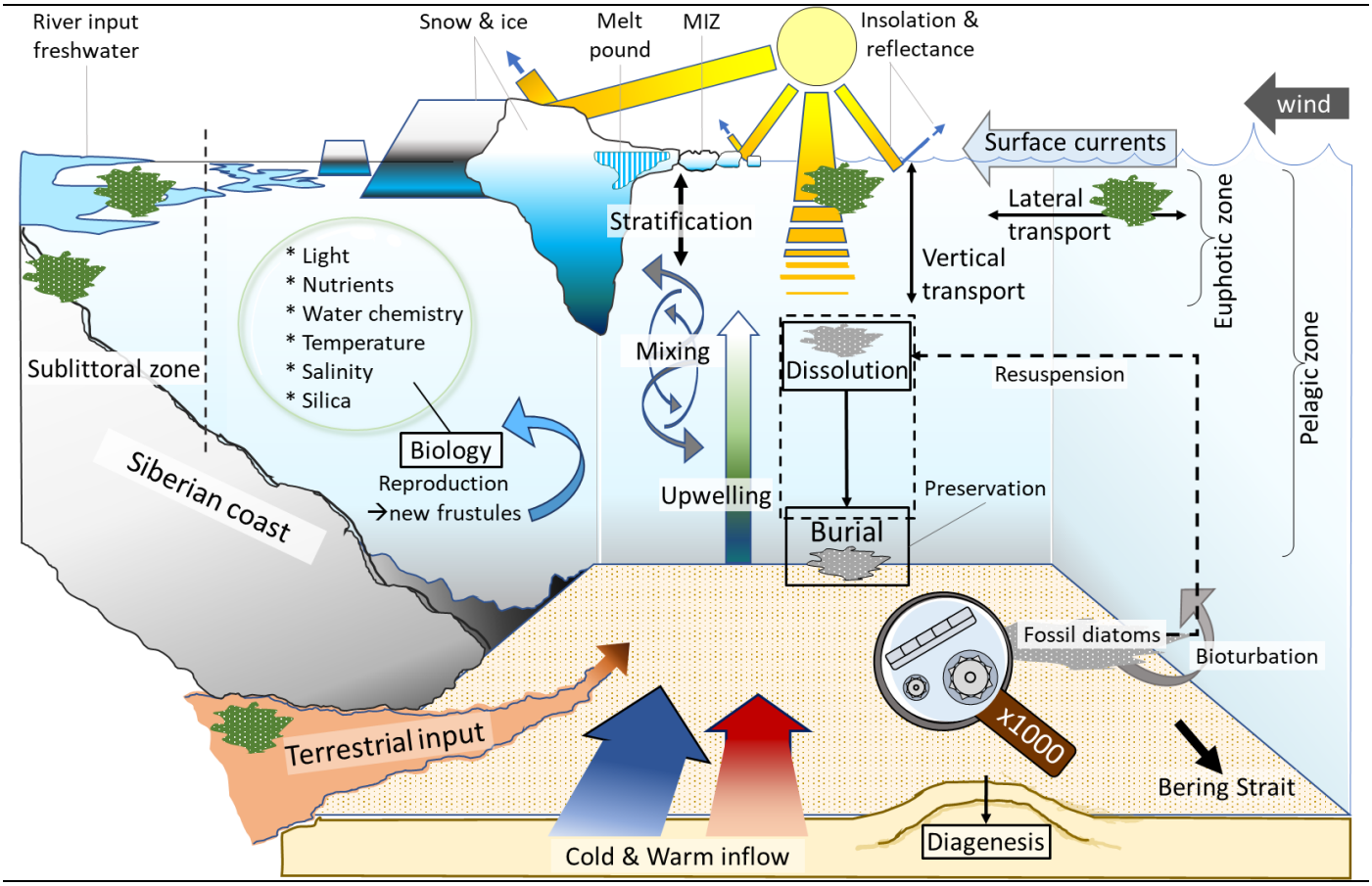

Figure 4. A schematic illustrating processes affecting diatom production and preservation at the sea floor in the shelf area of Chukchi Sea. See text for further explanations. Solid black frames identify four different diatom states: living - biology, dissolution, burial, and diagenesis. Green dotted splashes represent living diatoms with essential and limiting factors for their bloom. Grey dotted clouds are fossil diatom deposits, eventually viewed through microscope (magnification: x1000). Black arrows indicate approximate path directions. Dotted black lines are potential pathways. Arrow in lower right corner points out a southward direction towards Bering Strait. Cold and warm currents after (Coachman et al., 1975), various solar reflectance, with surface albedo larger on ice than ice free where radiation is absorbed by the water surface (Gersonde and Zielinski, 2000; Stroeve et al., 2007). Figure Inspired by Cremer, 1998 (Fig. 20).

2.4.1 Transect of species from The Arctic Ocean to the North Pacific.

The East Siberian Coast is shared by many Arctic sub basins. The East Siberian Sea and the Laptev Sea are located west of the Chukchi Sea, sharing the East Siberian coast. From these neighbouring basins, Tsoy and Obrezkova (2017) counted to 425 taxa grouped in 125 genera by coring. Most of the freshwater taxa was found from studies around the Laptev Sea and it's Lena delta river system (87.1%). Outside the Siberian Arctic coasts, terrestrial material influences the regions, allowing benthic species to thrive there. Leaving the coastland northwards to deeper shelf settings, a drastic decrease of freshwater species in favour for marine species (Bauch and Polyakova, 2000).

The marine *Chaetoceros* enrichment in samples reached ≤54% abundance in surface sediments associated with marginal shelf slope around Herald Canyon (Obrezkova et al., 2014). Core HC 11 from late Holocene ranging over last 2300 years was retrieved at 47 m water depth in the south Chukchi Plain with core positioned by the Bering Sea Water flow, 100 km from Siberian coast. By analysing 38 diatom samples, the study identified 97 species grouped into 41 genera with marine species up to 90%, oceanic up to 10%, benthic varying between scarce to frequent and fresh water <1% (Tsoy et al., 2017). In the adjacent shelf sea to Bering Sea, Sea of Okhotsk cold-water diatoms also predominate ~90%, while warm-water species were 0.5-3.4%. The neritic species *Bacterosira bathyomphala* were predominant in the surface sediment with a vast majority while *Paralia sulcata*, *Thalassionema nitzschioides*, *Fragilariopsis oceanica*, *F. cylindrus* and *Thalassiosira antarctica* are frequently occurring in the assemblages and *Probascia subarctica*, *Rhizosolenia hebetata*, *Thalssiosthrix longissima*, *Shionodiscus oestrupii*) were occasionally recorded in the samples (Tsoy et al., 2009). A latitudinal transect of diatom research is summarized (Table 1).

Table 1. A geographical transect from Herald Canyon, Chukchi Sea to North Pacific Ocean with diatoms after latitude (lat.) with Core-ids from some of the Chukchi Sea studies (Figure 3). A semi-quantitative separation of major and minor abundance of diatoms and sample type abbreviations W: water column, S: sediment: SS: surface sediment or I: ice core from the respectively reference-study.

Region (+ Core)	Lat.	Major species, life-form, and or eco-group	Minor species, life-form, and or eco-group	Typ	Reference
Laptev Sea shelf	76-79	Sympagic sp., *Thalassiosira antarctica, Chaetoceros* spp.	*Pinnularia* spp., *Navicula* spp.	SS	Cremer 1999; 1998
Laptev Sea coast	71-73	Freshwater sp., *Navicula* spp.	*Pinnularia* spp.	SS	Cremer, 1999, 1998
Herald Canyon	~72	sympagic, neritic, *T. antarctic*a	Oceanic-, Bering Sea Species, warm water species	SS	Obrezkova et al., 2014
Herald Canyon (b16)	~72	*Chaetoceros* spp.	*Thalassiosira* spp.	SS	Vologina et al., 2016
Chukchi Sea shelf (hole 2/3)	69-71	*Thalassiosira* spp. *Chaetoceros* spp., sympagic	Bering Sea water- and thermophilic species	S, SS	Gusev et al., 2014
East Siberian shelf	69-70	*Chaetoceros* spp., sympagic, *T. antarctica*, *T. nordenskioldii*	brackish- and freshwater, *Navicula* spp.	S	Polyakova, 1989
Chukchi Sea	66-70	Neritic-, cold water sp.	*Coscinodiscus* spp.	S	Polyakova, 1989
Central Chukchi Sea (core 23)	~69	*Chaetoceros* spp., Sympagic sp., *T. antarctica*, *T. nordenskioldii*	*Coscinodiscus* spp. Bering Sea Species, warm water sp.	S	Polyakova, 1989
Southwest Chukchi Sea	67-68	*Chaetoceros* spp., sympagic sp.	Oceanic species, Planktic warm water sp.	SS	Obrezkova et al., 2014
Southwest Chukchi Sea (HC11)	~67	Marine-, sympagic sp., *T. antarctica, T. nordenskioldii, Bacterosira bathyomphala*	Oceanic- and freshwater sp.	S	Tsoy et al., 2017
South Chukchi Sea (155-2/3)	~67	Marine species, sympagic, Nitzschia frigida, N. transitans	brackish- and freshwater sp.	I, W	von Quillfeldt et al., 2003
South Herald Canyon	~67	*Chaetoceros* spp., sympagic, *T. antarctica, T. nordenskioldii*	*Thalassionema nitzschioides*	S	Polyakova, 1989
Bearing Strait	65-66	*Chaetoceros* spp. (West side of the strait), *Paralia sulcata* (East Side of the strait, else scarce)	*Porosira glacialis, Thalassiosira hyalina, Thalassiothrix longissimia*,	SS	Sancetta, 1982
Bering Sea	55-65	*Chaetoceros* spp.	*Bacterosira bathyomphala*	SS	Sancetta, 1982
North Pacific Ocean	60	*Chaetoceros* spp,. small centric sp. (*Minidiscus*)	*Thalassiosira* spp., *Pseudo-nitzschia* spp.	W	Endo et al., 2018
North Pacific Ocean	40-60	Open ocean sp., *Actinocyclus* spp., *Pseudo-nitzschia* spp.	*Thassiosira* spp., *Fragilariopsis* spp.	W	Endo et al., 2018

2.4.2 Ice algae assemblages and cold-water indicators

Ice-algae diatoms comprises a diverse set of taxa, and the pennate species are more abundant than centric species (Horner, 1989). Sympagic diatoms have been separated from other marine life-forms in studies from the Chukchi Sea (Astakhov et al., 2015; Cremer, 1999; Obrezkova et al., 2014; Tsoy et al., 2017; von Quillfeldt et al., 2003), or in the

Laptev Sea (Bauch and Polyakova, 2000; Cremer, 1999). As the ice algae vary over time, their abundance generally shows the sea-ice dynamics (Bauch and Polyakova, 2000).

In the Arctic ice realm, *Fragilariopsis* spp. *(F. cylindrus, F. oceanica*) and *Fossula arctica* are associated where ice is present and are among the most abundant species. These species bloom in early spring (Hasle and Syvertsen, 1997; Okolodkov, 1992; Quillfeldt, 2000) and are the bulk members of the sympagic community. There are other species associated within- or around ice. Before the sympagic assemblage was commonly classified, taxonomic literature observed *Pauliella taeniata*, *Bacterosira bathyomphala*, *Attheya septentrionalis* with similar distribution pattern in the Arctic Ocean (Hasle and Syvertsen, 1997). *Pauliella taeniata* is considered as an early Spring bloomer after the sea-ice melt (Oksman et al., 2022) and found incorporated in first year ice and the water column (von Quillfeldt et al., 2003). Melosira arctica is recorded from the long-term pack ice where its predominating among various diatom species in the Arctic Ocean, but also considered pelagic and on the ice (Obrezkova et al., 2014; Snoeijs, 1993a). Finally, *Porosira glacialis* is a robust indicator of cold water species and *Actinocyclus curvatulus* are a cold water indicators (Hasle and Syvertsen, 1997; Oksman et al., 2019; von Quillfeldt et al., 2003).

2.4.3 Preservation of species

Well preserved diatom frustules are essential to have identifiable species in the samples. Generally, thin- smaller- and delicate species dissolve faster during settling (Cremer, 1998). The preservation is better in times of high rates of diatom production and sediment accumulation (Khalil et al., 2007; Konfirst et al., 2011; Ryves et al., 2001).

Species in the Laptev Sea like *Thalassiosira antarctica, Paralia sulcata* and the resting spores of *Chaetoceros* are relatively more robust than *Fragilariopsis oceanica*, *F. cylindrus* and *Fossula arctica* (Cremer, 1998). *I*n the Sea of Okhotsk *Bacterosira bathyomphala* (resting spore), *Thalassionema nitzschiodes*, and cold neritic diatoms *Thalassiosira antarctica* and *T. nordenskioldii* are among the heavy silicified and robust species (Nakamura et al., 2020). Generally, centric diatoms (excluding vegetative cells of *Chaetoceros* spp.) were the last to undergo a complete dissolved stadium (Warnock and Scherer, 2015). The most vulnerable parts of diatom frustules are girdle bands, and the least silicified delicate structure of the valves, and lightly silicified taxa (Smol et al., 2001). Warm water species tend to generally have these thinner silicious walls (Warnock and Krueger, 2020). Except dissolution of the silica, bad preservation can be caused when frustules are mechanically broken into incomplete, fragmented frustules (Nakamura et al., 2020)..

Apart from diatoms, Chrysophyte cysts are also photosynthetic siliceous species. They are typically found in open water, but also benthic and epiphytic taxa exist. Cysts sink to the sea floor after being formed in surface water, where they may reproduce themself under favourable conditions. Cysts are relatively well preserved and influenced by salinity when studied in lake settings (Smol et al., 2001 and references therein).

3. Materials and methods

3.1 Core and samples

The sediment samples used in this study are from 2PC gravity core, collected during leg 2 from the expedition in the Arctic Ocean 2014. Total core length of 2PC measured 8.3 metres with 92% recovery. The six sections from 2PC have been kept in a cold room at +8°C at the Department of Geological Sciences, Stockholm University. The samples used in this thesis were subsampled between 1 and 820 cm. Interval 1-36 cm in section one used the archived half of the core, due to the limited amount of available sediment in its work-replicate. The inner diameter of the liner halves measured nine cm each. Core section 1 is the youngest and section 6 the oldest.

By the naked eye observations, the lithology of the 2PC is homogeneous without no observed layers, distinct or gradual colour shifts, or distinct change in grain size. Throughout it is appear as well mixed nuance between olive green to dark grey silty clay, apart from two orange-coloured nodules (3-4 cm^2 each) at ~587 and ~675 cm core depth, avoided by sample picking.

All samples were carefully scraped off the core perpendicular to the core length, using a small spatula on the flat surface of the half rounds. They were taken from the same positions as the sample set of Barrientos, et al. (2018). The samples were retrieved as close to the centre as possible and at least 2 cm from the inner liner boarder. A total number of 49 samples were subsampled (~0.1 gram each).

Most of them were subsampled at the same stratigraphic depth ± 1 cm as the samples used for palaeothermometry (Barrientos et al., 2018a) presented in Appendix (A). A further eight samples from the original 41 samples, were taken to improve the stratigraphic resolution of the study.

3.2 Sample preparation

The sediment subsamples were stored in zip-sealed plastic bags in a freezer for 36 hours (-18°C) prior freeze-drying in a Labogene Scanvac coolsafe freeze-drier for 78 hours at about -50°C at the School of Natural Sciences, Technology and Environmental Studies, Södertörn University. The now dried powdered samples with a mass of ~0.1 g each, were weighted with 5 decimals accuracy (Figure 5, step 1).

Each sample was put in cleaned 100 mL glass beakers and soaked with a few drops of 10% hydrogen chloride (HCl) to remove carbonates. Samples were then submerged into 30% hydrogen peroxide (H_2O_2), to a total volume of 20-25 ml and left overnight in room temperature in a fume cupboard. Organic material was removed by heating up each sample to 150°C and let them fizzle out with a beaker cover. After two hours the heated hydrogen peroxide had oxidized all organic substance leaving a cleaned silica sample (Figure 5, step 2).

A decanting process to remove clay particles followed repeating these steps: fill each beaker with distilled water. allow sedimentation (settlement of particles in the silt fraction and larger) with four hours between each separation of solid and liquid phase. Then wash away clay particles in suspension. Before adding up new distilled water, the sample beaker was carefully stirred. Three decants were performed to clean chemical substances added earlier. Then a weak ammonium solution 0.5 mL ammonium (NH_3, concentration 25%) per litre water was added, allowing clay particles to repel, and separated from clustered fractions. Then another five to six decants were performed until the water was totally clear, prior the siliceous slurry was transferred in tagged plastic bottles (Figure 5, step 3,4).

Preparation of diatom slides used dried cleaned cover slips submerged into ethanol (>99%) were put on a stable plate to avoid vibrations. To achieve the concentration of diatoms in valves/gram dry weight of sediment (absolute abundance) microspheres were added to the cleaned slurry. These act as a known number of microscopic markers in solution (6.19 x 10^6 / mL) measured with pipette set on 1000 µL. A sub sample of the cleaned sediment slurry was transferred to a test tube. To avoid contamination between each sample depth, disposable Pasteur pipettes were used to fill the cover slip completely with the cleaned sediment slurry. A Vortex mixer (Vortex-Genie 2) was used before the subsample, and by applying the desired amount on a cover slip.

To avoid too concentrated slides, two cover slips per sample were used with an extra dilution of distilled water for the second cover slip. Cover slips were then left to gently dry overnight allowing the (siliceous) content to settle randomly (Figure 5, step 5).

Slides were before use permanently fixed with the Naphrax™ (refraction index 1.65). The cover slips were put on the glass slides together with a drop of the mounting media and heated on a hot plate in the fume cupboard for the toluene to vaporize. A temperature < 130°C was used, else the microspheres made by divinylbenzene may deform (Figure 5, step 6).

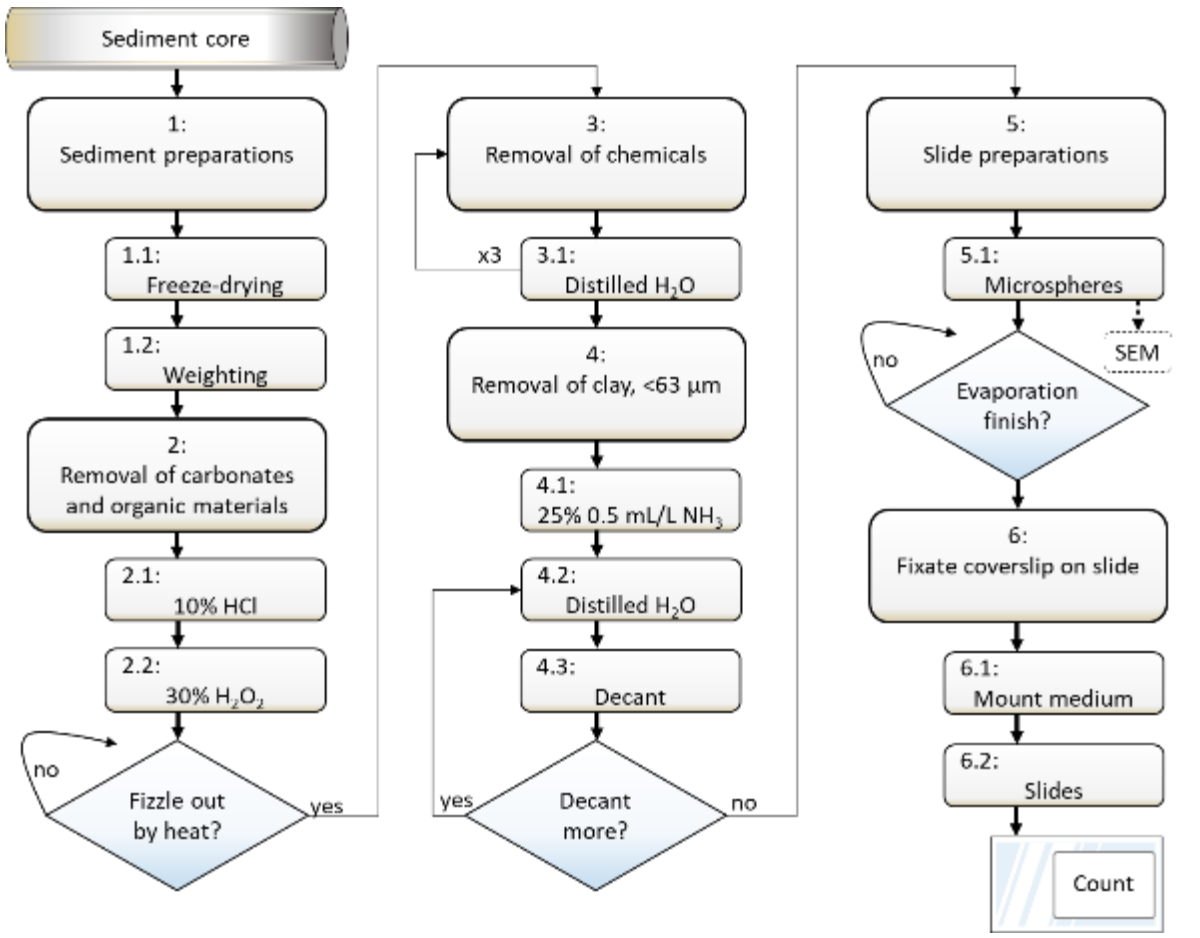

Figure 5. Core to count with process steps referred in text. Adopted from Battarbee (1986) flowchart.

3.2.1 Scanning electron- and tabletop microscope and image processing

A scanning electron microscope (SEM) was used to help with morphological and taxonomic identifications. Aluminium stubs were cleaned overnight in ethanol (>99%). The preparation from step 5.1 (figure 3) follows the same procedure as the slide preparations for disposable Pasteur pipette and vortex treatment between samples. Finally, aliquots of the cleaned diatom samples were carefully distributed on individual stubs to gently allow random settlement during air-drying overnight.

The stubs were gold-sputter-coated and observed at the Department of Materials and Environmental Chemistry (MMK), Stockholm University, Sweden. The coating configuration was set to 10mA, 30s, distance of 70mm (JFC-1200). The SEM-observations and image captures were made with Field Emission Microscope (JEOL JSM-7000F) and a software package (EOS 7000F). A tabletop microscope (TM3000) with PC software (Hitachi High-Technologies corporation, version 02-03-02) was additionally used for a rapid taxa identification prior the SEM usage. TM3000 used same prepared stubs at MMK.

Light micrographs of diatoms were captured with a camera module attached to the microscope (Olympus SC30) with software analysis getIT by Olympus Soft Imaging Solutions GmbH (ver. 5.2, Build 3554), configure with pixel sharpened values (1-20, default 10) emphasizing small features like thin striae appear more distinct when saved to jpeg. SEM and TM3000 micrographs were captured images to the lossless tiff-raster format.

3.3 Taxonomy and identification of siliceous microfossils

At least 400 diatom valves per slide were counted, and primarily identified to species level when possible. Since *Chaetoceros* spp. have mass occurrence in most samples, the valve count considered two thresholds to reach sufficient counts per sample: i) ≥200 diatoms and ii) ≥400 valves (*Chaetoceros* included). Afterward, the relative abundance (%) was defined in scarce, regular, common, and frequent (Table 2).

The diatom slides were analysed with an Olympus BX53 light microscope (LM) at the School of Natural Sciences, Technology and Environmental Studies, Södertörn University. To obtain as high resolution as possible the LM used Nomarski Differential interference contrast (DIC). Counting was performed with highest magnification (x1000) available on the microscope using oil immersion (refractive index 1.65). The counting convention suggested by Schrader and Gersonde (1978) was used (Figure 6a). Descriptive terminology to describe species was used according to Anonymous (1975).

The diatoms were identified following the taxonomic frameworks presented in monographs and floras (Cleve-Euler, 1951; Cremer, 1998; Krammer and Lange-Bertalot, 1986; Lange-Bertalot et al., 2000; Pankow, 1971; Pascher, 1930; Snoeijs, 1993b; Tsoy and Obrezkova, 2017) and key articles with taxa description, distribution, ecology and diatom plates to identify diatoms (Fryxell and Hasle, 2022, 1980, 1972a; Hasle, 1978; Hasle et al., 1996; Kang and Fryxell, 1992; Quillfeldt, 2001, 2000).

In each sample chrysophyte cysts were counted due different morphology of the cell wall, as well as dinoflagellates and sponge spicules. Silicoflagellates were observed but not counted and appeared occasional or at most on scarce abundance level throughout the core. *Attheya septentrionalis* is missing data in four samples. The same preparation used for Chrysophyte cysts as diatoms, the same slides were used counting them in all samples. The cysts are commonly merged into one group (Smol et al., 2001), and Chrysophyte cysts have been identified on genus level.

Table 2. Relative diatom abundance classes in 2PC.

Class	Rel. abundance
scarce	<2%
regular	≥2%
common	≥5%
frequent	≥15%

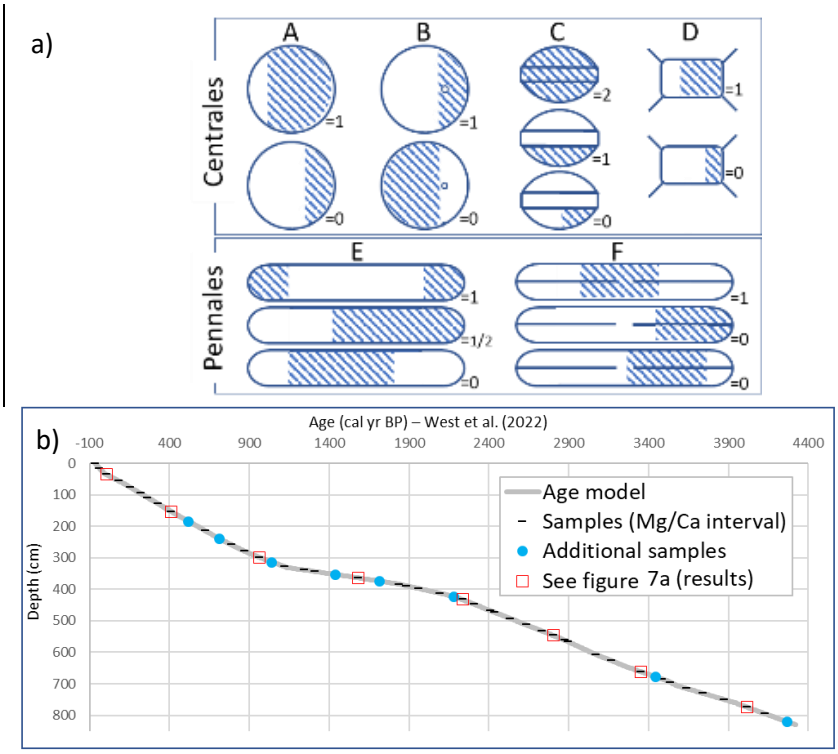

Figure 6. (a) Counting convention of diatom valves in microscope. A: Centrales without central process or nodule, B: The visible part that contains a pseudonodule is counted, C: A cell in pervalvar view with girdle band, D: Vegetative spore with filaments. E: Araphid valves, F: Raphe-bearing valves. Numbers to the right are how they were counted. Modified after Schrader and Gersonde (1978). **(b)** The age model of sediment Core 2PC with the 49 analysed samples distributed over core depth/age. The Mg/Ca interval after Barrientos et al. (2018a).

3.3.1 Diatom ecological preferences, salinity tolerance and geographic distribution of diatom species

Interpretation of diatom life-forms, salinity requirements, cold- and warm water preferences, as well as geospatial distribution of diatoms assigned to different water masses in Chukchi and neighbouring seas and oceans, are based on knowledge of diatom ecology from previous studies on Arctic and Pacific Ocean diatom floras (Cremer, 1998, 1999; Hasle and Syvertsen, 1997; Lange-Bertalot et al., 2000; Okolodkov, 1992; Pankow, 1971; Poulin, 1990; Poulin and Cardinal, 1982; Snoeijs, 1998, 1996, 1993a; Tsoy and Obrezkova, 2017).

Freshwater species together with unidentified *Navicula* (i.e., *Navicula* spp.), *Chaetoceros* sp. *7*, *Haslea* cf. *spicula*, *Sinerima marigela*, *Thalassiosira* cf. *pacifica* and small *Thalassiosira* spp. (<10 µm in diameter) are classified as ungrouped life form.

Absolute diatom abundance (concentration) was calculated in each sample as a proxy for diatom productivity. Changes over time in abundance can be interpreted as paleo primary productivity (Wolfe, 1997). Absolute Diatom Abundance (ADA) is a measurement of diatom valves per mass unit, and calculated using the formula by Battarbee and Kneen (1982):

$$\mathrm{ADA} = \frac{(ms\ introduced\ x\ diatoms)}{(counted\ ms\ x\ dw)} \tag{1}$$

Where the introduced microsphere concentration (ms) per litre is multiplied with diatoms counted, divided by counted microspheres multiplied with the dry weight (dw) of each specific sample.

3.4 Statistical methods and data analysis

Diatom assemblage diversity was assessed using standard diversity indices including Shannon, Simpson and an absolute measurement of unique specimen per samples. Diversity index was utilized to achieve information about a community. Shannon's H'-index (Shannon, 1948):

$$\mathrm{H}' = -\sum_{i=1}^{R} pi \ln pi \tag{2}$$

Where H' typically is a number between 1.5 to 3.5.

The Shannon index was used to examine diversity of communities and provide a hint if some taxa is more dominant. Low H'-numbers are less diverse, and high numbers mean that the sample is towards evenly distribution, and more diverse. Minor species may play a huge role in finding small abundance signals in ecosystem, and Shannon index may overlook very rare species, so as a complementary index, Simpson diversity index (SDI) was used (Simpson, 1949):

$$SDI = 1 - \sum_{i=1}^{R} \frac{ni(ni-1)}{N(N-1)} \tag{3}$$

Where SDI is the probability ranging between 0 and 1. An SDI towards 1 reflect higher diversity.

SDI is the probability that two individuals from a community will be different. Unlike H'-index, SDI is not as sensitive to rare species.

Species richness is showing the total number of species in a sample, describing the community structure (Maurer, 2011), and is the third way to numerically describe the data, here used as absolute number of species present in a sample. A sample with a higher number of individuals is considered richer. Little benefit has been shown for species counted over 300 diatoms as a minimum (Battarbee et al., 2001), however, when a genus with same eco-group signal is dominating in abundance (e.g. *Chaetoceros*) other less abundant species will show weaker signals. By adding number of individuals detected over time spent (workload), a complimentary method was presented to measure if new species are continuously detected at same rate when calculating more than 300 species.

Initially, a rapid rate of new species are detected in a rapid rate, but less new species are detected the more transects that are examined and the curve flattens out (Battarbee et al., 2001). Eight samples (Figure 6b) were used to measure the new individuals detected over transects. The samples were evenly age-distributed over the core to monitor this change. First, the diatom abundance was counted prior 2/3 (~67%) of each base sum was reached. Then the rest of desired base sum (i.e., 100%) was reached. Species on genus level (e.g., *Thalassiosira* spp.) counted as one and varia (seven specimen in total) was left out. In addition, species richness was performed on the complete data set when counting was complete.

A species diagram was compiled in Tilia (version 3.0.1) suitable for microfossil graph-plots with stratigraphic records. All taxa with ≥2% abundance at least on one occasion were included in the diagram. In the species diagram, taxa were grouped after life form, where the sympagic group was separated from the neritic species assemblage and is further seen as a synonym for the merged abundance of *Fossula arctica*, *Fragilariopsis cylindrus*, *F. oceanica* and *F. reginae-jahniae*. These four species are the bulk members of the sympagic group. *Melosira arctica* and *Pauliella taeniata* have been grouped as other ice-algae species.

The software uses a built-in plugin of CONISS, a cluster analysis that divides the stratigraphy into clusters and used to define stratigraphic diatom zones with the least square method. The zonation is stratigraphically constrained, allowing neighbour samples to be grouped together. An advantage with CONISS, is that diatom relative abundance data (%) can be processed together with other data (e.g., ADA). At most N-1 samples give N zones (Grimm, 1987). In this dataset, four diatom assemblage zones (DAZ) were used. The species diagram displays taxa with relative abundance ≥2% and CONISS-clustering was made with the exclusion of *Chaetoceros* assemblage.

The IBM SPSS software (version 28) was used to perform the statistical analyses. The distribution of the different species of diatoms was evaluated using Q-Q plots and histogram. In two of the cases (*Thalassionema nitzschioides* and *Bacterosira bathyomphala*) an outlier was detected and removed from the data. The correlation between different species of diatoms was evaluated by Pearson's correlation coefficient for normally distributed and Spearman's correlation coefficient for not normally distributed data. The results were considered statistically significant at P value < 0.05. To run statistical analysis with 49 diatom samples against the 41 samples from the Mg/Ca data set, eight imputed values were performed with linear interpolation.

The xy-plots were produced with the independent BWT-variable on x-axis and the depending diatom species on the y-axis. Warm water species were subdivided into two group, warm water group 1 (*Thalassionema nitzschioides*, *Thalassiosira simonsenii* and *Shionodiscus oestrupii*) *and warm water group 2 (Coscinodiscus marginatus* and *Rhizosolenia hebetata* f. *semispina added to* warm water group 1). *Paralia sulcata*, chrysophyte cysts and sympagic group were plotted against Mg/Ca BWT during cold and warm events on the Northern Hemisphere (e.g. Neukom et al., 2019 and references therein). Subboreal- and subatlantic intervals were added as stages from Northern Europe (Ponel, 2013). The recent warming (industrial warming) with extending the interval from Matul et al. (2007) of industrial warming to -63 BP (2014 EC). The uppermost (i.e., youngest) data point during industrial warming was removed when considered the regression line and associated R^2-value for *Thalassionema nitzschioides*.

Maps were produced using QGIS (version 3.8 Zanzibar), and Python (version 2.7) and R-programming (RStudio version 1.2.5019) applied to geographically sort the abundance of diatoms between northern Pacific Ocean and Laptev Sea, East Siberian Sea and Chukchi Sea from PANGEA db (https://doi.pangaea.de/10.1594/PANGAEA.904147 [access: March 2022]) and the Artic Ocean Atlas Tsoy and Obrezkova (2017).

4. Results

4.1 Overview and preservation of diatoms

A total of 49 samples between 1 and 820 cm were analysed for siliceous microfossil relative and absolute abundance. The occurrence of each taxa follows the classification are found in Table 1. A diatom species list of all taxa found in 2PC with life-form and salinity preferences can be found in Appendix B. The subsampling over core depth was shown in figure (6b). Species richness after 67% of effort completed had a diversity of 21 to 39 per sample. When a sample was 100% completed, new species were summarised, and they showed a richness between 1 and 6 species (Figure 7a).

Absolut diatom abundance was between 402 and 644 x10^6 valves gdw-^{1} when *Chaetoceros* spp. was counted, and between 203 and 285 x10^6 valves gdw^{-1} when not included. A centrales-pennales (C,P) distribution for all species except all *Chaetoceros* spp. and *Attheya septentrionalis*. The pennate fraction was 55% on average (Figure 7b).

126 species were identified in total (including varieties of *Chaetoceros* spp. and *Attheya septentrionalis*) belonging to 56 genera (appendix B,C,D). Around a third of these have been recorded in at least half of the counted samples. The most diverse genus of the benthic taxa was *Navicula* (15 taxa), followed by *Nitzschia* (7 taxa) and *Pinnularia* (8 taxa). Of the pelagic, *Thalassiosira* was the most diverse with 10 species (Appendix B). Throughout the core, *Navicula* species varied between 0 and 4%, *Nitzschia* species between 0 and 7%, *Pinnularia* species 0 and <2% with dominance within the benthic *P. quadratarea* group, and *Thalassiosira* between 13 and 31%, where *T. antarctica* and *T. nordenskioeldii* dominated the record. The recorded *Nitzschia* spp. were exclusively marine taxa, except *N. linearis* with a high contribution to the freshwater assemblage. *Pinnularia* spp. contributed with a smaller proportion to freshwater and the varieties of *P. quadratarera* to the marine assemblage.

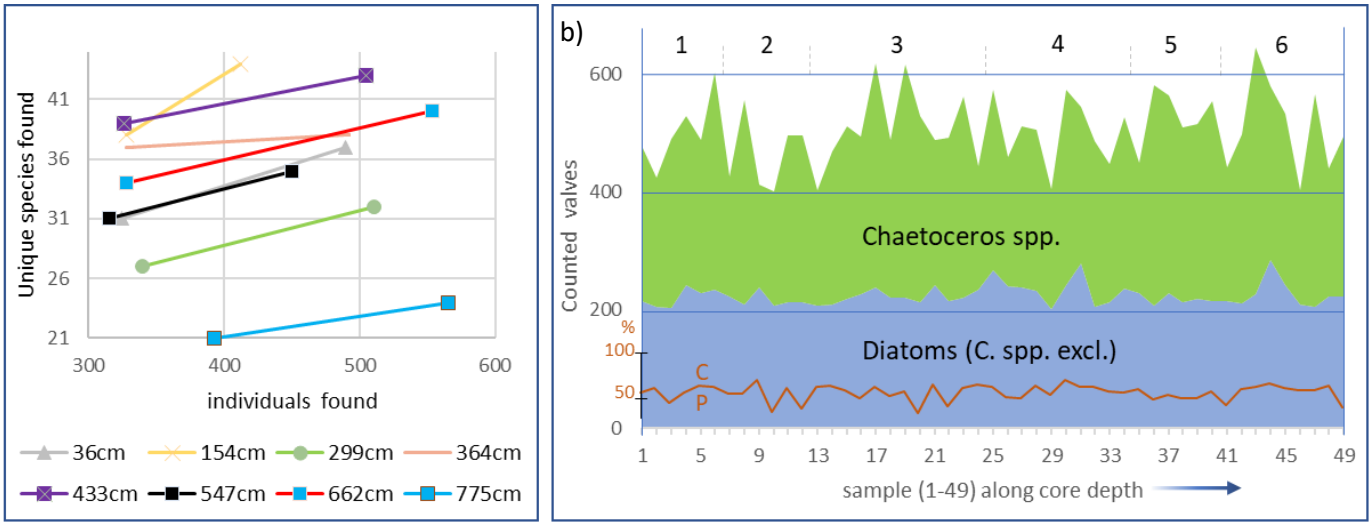

Figure 7. (a) Experimental species richness profiles. **(b)** Absolute Diatom Abundance with 2PC Core sections (1-6) on top and centric-pennate (C-P) proportion from diatoms (excl. *Chaetoceros*). Arrow increased depth.

The *Chaetoceros* spp. group is the most frequent group with approximately 40%-65% abundance. Some neritic *Chaetoceros* species were identified including *Chaetoceros cinctus*, *C. debilis*, *C. diadema*, *C. didymus*, *C. furcellatus*, *C. lorenzianus*, *C. ingolfianus*, *C. holsaticus*, *C. mitra*, *C. vanheurckii*, *C.* sp. *2* sensu Cremer 1998 (Cremer, 1998: pl. 5, Fig. 5.), *C.* sp. *3* (Appendix C, plate 5) and assumed neritic *C.* sp. *7* (Appendix E: supplementary Figure 1). The vast majority of the *Chaetoceros* spp. were recorded as resting spores.

Beside the *Chaetoceros* group, the sympagic group is the most frequent assemblage being present in all samples, with between 46% and 16%. Species being present in >90% of the samples were *Bacterosira bathyomphala* (common), *Paralia sulcata* (regular to common), *Pauliella taeniata* (mostly regular to common), *Porosira glacialis* (scarce to regular), *Thalassionema nitzschioides* (mostly regular), *Thalassiosira antarctica* including *T. gravida* (mostly common), *T. hyalina* (mostly scarce to regular) and *T. nordenskioldii* (mostly common to frequent). *Rhizosolenia* was observed in most of the samples, dominated by *R. hebetata* except for five occasional warm water indicator possible recorded *R. hebetata* f. *semispina* (Appendix C).

4.2 Diatom stratigraphy

The diatom stratigraphy using the CONISS analysis identifies four diatom assemblage zones (DAZ). The occurrence of each taxa following the classifications (Table 1) with life-form and salinity preferences (Appendix B).

The main scope of the most abundant species contributed with ~80% per diatom assemblage zone, where *Fossula arctica* and *Fragilariopsis oceanica* alone answered for 26-32%, and *Thalassiosira nordenskioldii* 10%-12%, *Thalassiora antarctica* ~7%-8%, *Bacterosira bathyomphala* ~10%, and *Paralia sulcata* 4.0-7.1%. The rest of the assemblage had regular to scarce abundance with *Pauliella taeniata* ~4%, *Thalassionema nitzschioides* 2.7-4.2% and *Porosira glacialis* ~2%.

The sympagic group has its highest average abundance in DAZ 1 and is then successively decreased through zone 2 to 4. Neritic (excluding *Chaetoceros* spp.) taxa are recorded frequently dominating all the zones (average. 36%). Other life-forms share a proportion of <8% on average, distributed on benthic (3.4%), tychoplanktic (2.6%) and oceanic species (1.8%) proportions through the core. The planktic neritic *Thalassiosira hyalina* shows a saw-tooth pattern throughout all zones, with its abundance corresponding well with *P. sulcata.* Species richness varies through the first zone between 27 and 41, following the relative abundance fluctuations of pennate assemblages (*Nitzschia* spp., *Navicula* spp., and *Pinnularia* spp. in the zone and the other three DAZs. *Neodenticula seminae* at most abundant classified as scarce, shows a maximum abundance in zone 2, else relatively lower abundance and in DAZ 1 its only present in two samples close to DAZ 2. *Melosira arctica* shows scattered scarce distribution with lowest abundance in first zone, while highest peaks in the two youngest zones. Each diatom assemblage zone is described from the oldest to the youngest (Figure 8).

DAZ 1 (4265 to 3460 years BP)

The first zone starts with 4265 years Before Present (2316 EC). At the deepest sample, the sympagic group experiences the lowest abundance (~30%). *Fossula arctica* and *Fragilariopsis oceanica* contribute most to this zone, with 16% each. *Pauliella taeniata* is common, reflecting the sympagic group abundance pattern through all zones, whereas *P. sulcata* shows a negative relationship to the ice algae. *Thalassiosira bulbosa* was counted scarce and with highest abundance in DAZ 1. Although the tychoplanktic species *Odontella aurita* was scarce with pulsing abundance in the first zone, it correlated with the peaks of *P. sulcata* in all zones, and consequently amplified the tychoplanktic abundance pattern. *Neodenticula seminae* appeared first around 3650 years BP. Absolute diatom abundance was lowest among the zones in DAZ 1 on average, starting with a low minimum at the core bottom (2.5 $x10^7$ number of valves gdw^{-1}) gradually increasing to a spike similar to a maximal *Chaetoceros* spp. abundance ~3500 years BP.

DAZ 2 (3460 to 1775 years BP)

The second DAZ involves the largest subset of data, with 19 of 49 data points spanning from 3500 to 1700 years BP. The sympagic group lower until 2900 years BP, decreased in the lowest 150 cm of the zone, while *Bacterosira bathyomphala*, *Thalassiosira nordenskioeldii* and *T. antarctica* showed a slight increase in abundance. These species then decrease to ~5%-7% while the sympagic groups increase at ~2600 years BP. The sympagic assemblage then ends in decreased abundance at the transition to the next zone. *Melosira arctica* corresponds moderately with peaks of *P. sulcata* and *O. aurita*. A few peaks of *D. confervacea* (scarce to regular) correspond to a higher abundance of *D. suriella* (scarce) in this zone and the following (Figure 8). The neritic *Chaetoceros* spp. increased relatively compared with other marine species in the lower half of this zone, mirroring the sympagic group at the same time. A slightly higher concentration in benthic and tychoplanktic species is seen in the lower part of the zone, and then in increasing amount exiting the zone. The species richness is between 31 and 43 in the zone following the fluctuations of the genera *Navicula, Nitzschia* and *Pinnularia*. The absolute diatom abundance (inclusive *Chaetoceros* spp.) showed a spike pattern, and on average the zone had the highest number of valves per gram freeze dried sediment counted (6.9 $x10^7$ gdw^{-1}) including the highest two diatom abundant peaks through the record at ~2600 years BP and ~2200 years BP where number of valves were 1.3 $x10^8$ gdw^{-1} (Figure 8).

DAZ 3 (1775 to 750 years BP)

Saw-pattern in this and zone 4 for sympagic groups with two of the lowest abundances of the sympagic group reaching ~18% each at ~1700 years BP and ~1400 years BP. Tychoplanktic (2.9%) and benthic (3.7%) are above the core average of abundance, while the neritic taxa drop to 34% in Zone 3. When starting at the end of zone 2, benthic and tychoplanktic species showed concentrated higher abundance together with an increase in *T. nitzschioides*. These stripes of higher abundance continue to the middle of zone 3. ADA (inclusive *Chaetoceros*) began with low numbers ~2.5 $x10^7$ valves gdw^{-1} increasing gradually through the zone and apart from a spike at 1200 years BP core

depth similar to peaks in DAZ 2, the ADA ends at ~5.0 x 10^7 gdw^{-1} at the end of DAZ 3. On average through the zone, ADA was 6.9 x10^7 number of diatom valves per gram of freeze-dried sediments (Figure 8).

DAZ 4 (750 to -63 years BP)

Although *Pseudogomphonema arcticum* and *Navicula transitans* have a high occurrence in the complete data set, their highest peak (regular) is in zone 4. This zone shows an above average of ~1% each of benthic and tychoplanktic species, starting at the border between zones 3 and 4, and two more relatively high benthic and tychoplanktic boosts (~400 and ~150 years BP).

Zones 3 and 4 have the same amount of species richness found (average 36), although, zone 4 fluctuates less. Although ADA (inclusive *Chaetoceros*) has a jagged pattern in DAZ 4, including an ending with three gradually decreasing spikes (~100–0 cm), the zone presents the total highest number of diatoms values of all four zones. At 900 years BP, it began with low absolute abundance of ~2.5 x10^7 gdw^{-1} valves, increasing gradually through the zone and apart from a spike (~1130 years BP) similar to peaks in DAZ 2, the ADA ends at ~5.0 x 10^7 valves gdw^{-1} at the end of DAZ 4 (Figure 8). The last zone ends in -63 years Before Present (2013 EC).

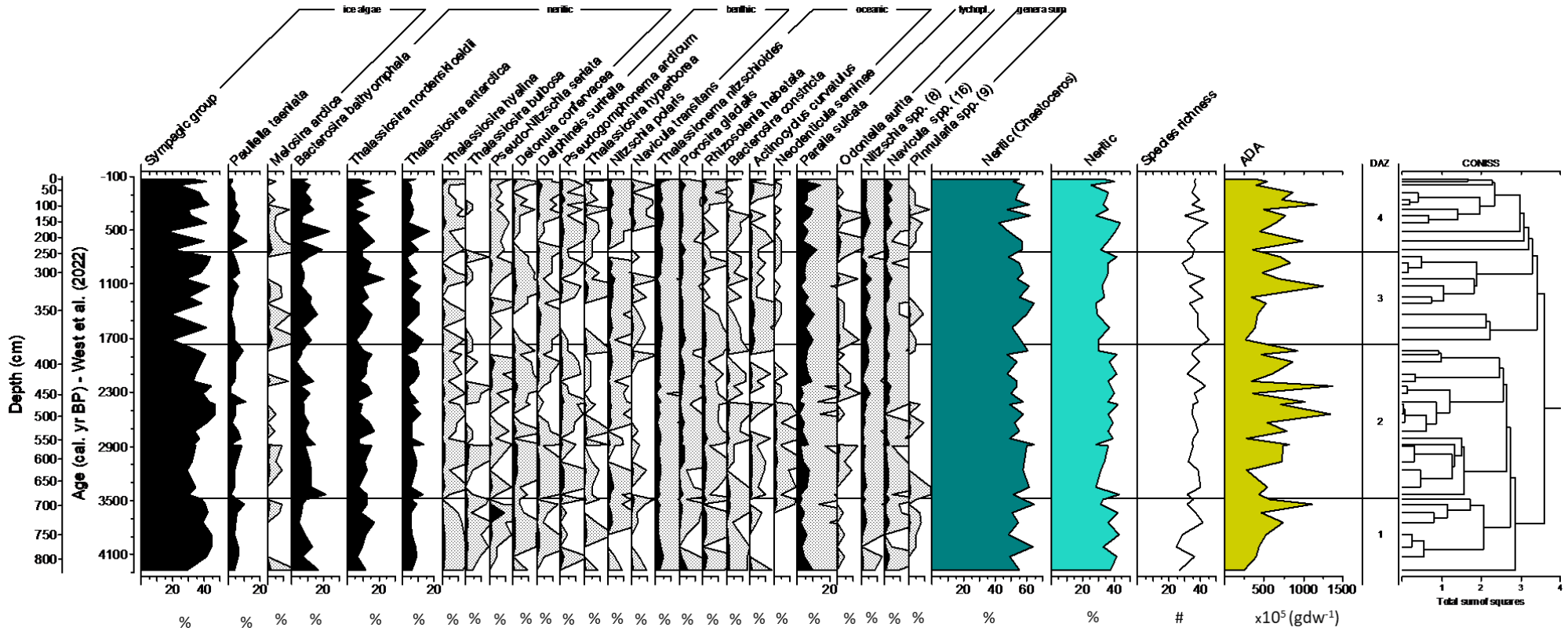

Figure 8. Species diagram from samples between 0-820 cm core depth, with ≥2% abundance (excluding *Chaetoceros*), Diatom assemblage zones (DAZ 1-4), Absolute diatom abundance (ADA) and two area charts with proportion of neritic *Chaetoceros* and other neritic diatoms. Solid area grey graphs are by a factor of x10 exaggerated. A scale bar tick is 5 for the %-axis. Age model within -63 to 4265 years BP after West et al. (2022).

4.2.1 Species composition and surface water salinity

Most of the species belong to the marine eco-group, oscillating between 30 and 50%. The rest belongs to *Chaetoceros*-marine except a smaller proportion of brackish species 2%-6%. Freshwater species 0-2% and unknown were 0.16% on average.

The marine species were diverse between the diatom assemblage zones on average. It was highest in DAZ 4 and lowest in zone 3. The assemblage classified as brackish was highest in DAZ 1 and similarity in the other three zones, while freshwater species showed an increasing trend from DAZ 1 to 4 (Figure 9a). The sum of both *Chaetoceros* and other neritic species including the sympagic group range between 84% to 98% with a gradual decrease in abundance from oldest part of the core to the youngest (Figure 9b).

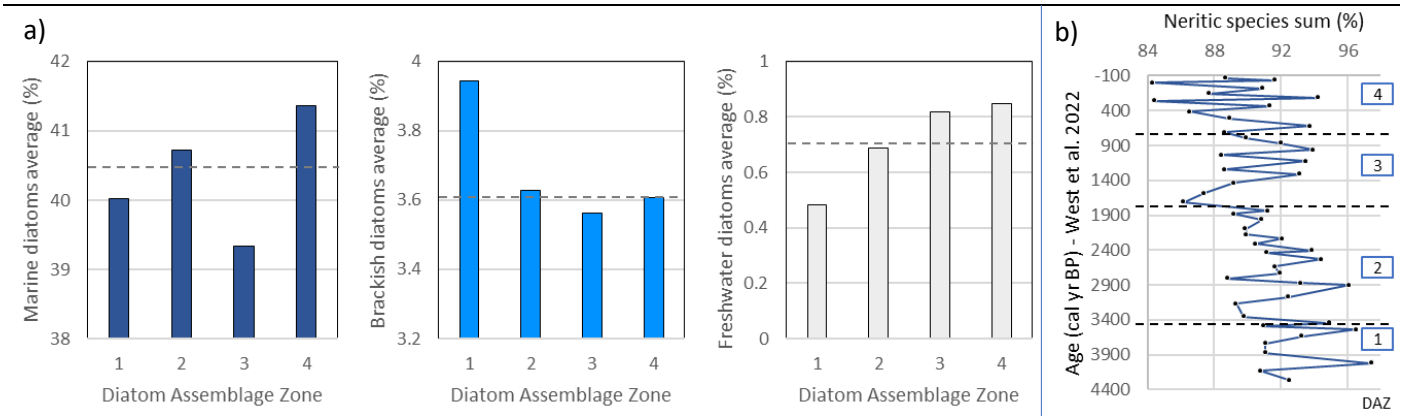

Figure 9. (a) Diatom relative abundance divided into salinity requirements (marine, brackish, freshwater) in diatom assemblage zone, DAZ 1-4. DAZ 1: 4265 to 3460 cal yr BP, DAZ 2: 3460 to 1775 cal yr BP, DAZ 3: 1775 to 750 cal yr BP, and DAZ 4: 750 to -63 cal yr BP. Dashed lines are the average of all zones. **(b)** The sum (%) of all marine-neritic species separated by DAZ 1-4 (dashed lines).

4.3 Common Arctic ice- and cold-water diatom taxa

Species being regular to frequent reported, thriving in the cold region of Arctic are *Fossula arctica*, *Fragilariopsis cylindrus*, *F. oceanica*, *F. reginae-jahniae*, *Pauliella taeniata*, *Thalassiosira antarctica*, *T. nordenskioeldii*, *and Chaetoceros furcellatus* and *Attheya septentrionalis*. These species have been presented in the previous section, except for *C. furcellatus* and *A. septentrionalis*. The proportion of *C. furcellatus* was near regular (avg. ~2%) in 84% of the samples, and *A. septentrionalis* was commonly classified (average 5.2%) in 92% of the samples. Apart from species, an absolute abundance (ADA) with all species, and diversity index (H' and SDI) are graphically represented (Figure 10).

Maximal peaks in the dataset were truncated. The ADA three spikes occurred between 2535 to 1124 with 77-/74 and 77 valves x10^6 gdw^{-1}. Neritic ADA both spikes were ~50 valves x10^6 gdw^{-1}, benthic truncated peaks were 5.5 and 4.7 valves x10^6 gdw^{-1}. *Thalassiosira nordenskioeldii spike was 10.7% at 1*040 years BP. *Chaetoceros* and neritic species show mirrored relationship, while oceanic with low abundance (<3%), mostly fluctuating between 1-2% following the abundance of neritic species (Figure 10).

Fragilariopsis reginae-jahniae and *F. cylindrus* show an anti-correlation almost throughout the sample set, except 1700 to 1300 yr BP, where all sympagic species and *Pauliella taeniata* have high spikes. Same negative relationship is seen between *F. cylindrus* show low (or 0-values) when *F. arctica* is high and vice versa, except for the modern sample (from 330 yr BP) up to core top, where they instead are positively aligned. The results of sympagic group were further dissected in their individual abundancies together with *P. taeniata* (Figure 10). A direct relationship is seen between *Fossula arctica* and *Fragilariopsis oceanica*, apart from some dips the latter experience. Adding *P. taeniata*, it also follows these species except in age interval ~3900 to 3050, and 2300 to 2100 yr BP. The four maximal peaks of *F. arctica* are well followed by *F. reginae-jahniae, F. oceanica* and *T. nordenskioldii*. The ice algae sum and *T. antarctica* are positively related except at 2876 cal yr BP and an interval between ~2000 to 1400 yr BP, ~900 to 330 yr BP, and age in modern time ~260 to core top (-65) years BP (Figure 10).

Attheya septentrionalis and *Thalassiosira antarctica* have a strong positive correlation, except in the top sediment and the last three data points at the core bottom (Figure 10). *Chaetoceros furcellatus* and *T. antarctica* show a strong relationship, except for the three oldest data points and ~1000-year anomaly (1300 to 2200 cal yr. BP) where *C. furcellatus* instead directly is related to the abundance *F. oceanica*. The Shannon index (H') and Simpson Diversity Index (SDI) are oscillated with small changes seen. The relative ratio of SDI and the logarithmic richness of H' follow the species richness positively throughout except for slightly opposite trends at ~3700, 2400, 600 and 330 cal years BP. The minima coincide well with peaks of either *F. oceanica* or *F. reginae-jahniae* (Figure 10).

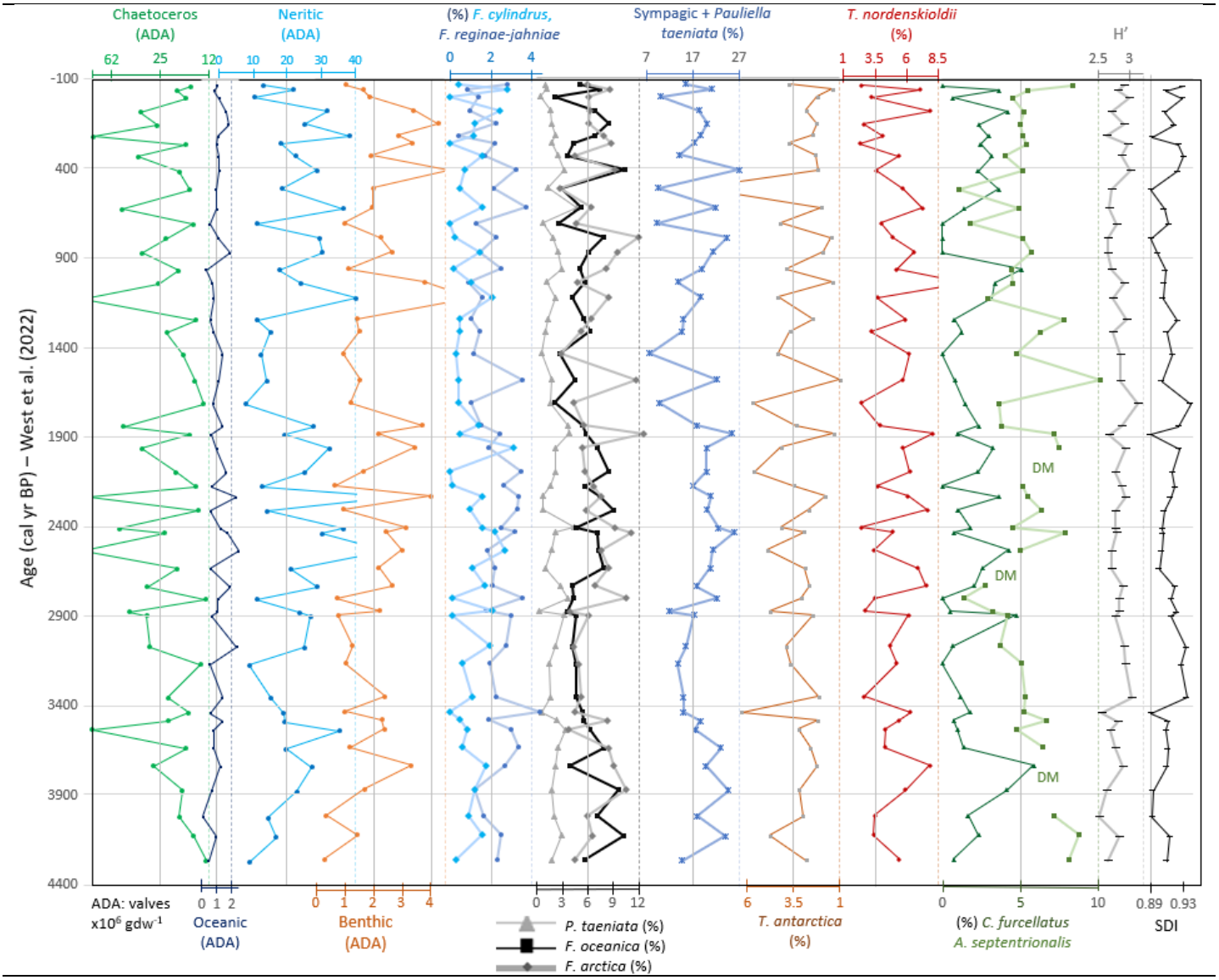

Figure 10. Sympagic and cold pelagic eco groups juxtaposed with ADA of Neritic-, Benthic-, Oceanic- and Chaetoceros species. All Absolute diatom abundance (ADA) expressed in valves x10^6 gdw^{-1} and species, and species groups expressed in relative abundance (%). Ice-algae sum: sympagic group and *Pauliella taeniata*. DM: data missing. Shannon index (H') and Simpson diversity index (SDI) are unit less. Observe the flipped x-axis of *Chaetoceros* and *T. antarctica*.

The sympagic species *Fossula arctica* and *Fragilariopsis oceanica* showed a very low significant number when compared with each other indicating how likely a pattern in the data set was by chance were small when contrasting eco-groups set up in two table columns (Table 3). Same low results were given when planktic species were contrasted to each other. Between the cold planktic species only *Thalassiosira antarctica* and *Thalassiosira nordenskioldii* show a negative correlation (i.e. opposite directions). Last, *Thalassiosira antarctica* and *Bacterosira bathyomphala* have a positive significant correlation (Table 3).

Table 3. Statistic correlation between eco-group a and eco-group b. Eco-groups are Sympagic group: *Fragilariopsis oceanica*, *Fragilariopsis cylindrus*, *Fragilariopsis reginae-jahniae*, and *Fossula arctica*. Warm water group 1: *Thalassionema nitzschioides*, *Thalassiosira simonsenii* and *Shionodiscus oestrupii*. The N-value shows number of sample counts (N≤49).

Eco-group a	Eco-group b	Species or assemblage compare	Significance (2-tailed)	Correlation coefficient [1]	N
Sympagic	Sympagic	*F. arctica, F. oceanica*	0.015	0.346	49
Sympagic	Sympagic	*F. arctica, A. septentrionlis*	0.04	0.308	45[2]
Planktic	Planktic	*T. antarctica, B. bathyomphala*	0.012	0.359	48[3]
Planktic	Planktic	*T. antarctica, T. nordenskioldii*	0.034	-0.304	49
Planktic	Sympagic	*T. nordenskioldii, C. furcellatus*	0.04	0.295	49
Warm water	Sympagic	*T. nitzschioides, F. oceanica*	0.341	0.140	48[3]
Warm water	Sympagic	*T. nitzschioides, F. arctica*	0.069	0.265	48[3]
Warm water	Sympagic	*Warm water-, sympagic group*	0.182	0.196	48[3]
Tychoplanktic	Sympagic	*P. sulcata, F. oceanica*	0.234	-0.173	49
Tychoplanktic	Sympagic	*P. sulcata, F. arctica*	0.192	-0.189	49
Tychoplanktic	Sympagic	*P. sulcata, sympagic group*	0.051	-0.281	49
Tychoplanktic	Warm water	*P. sulcata,* Warm water group	0.112	0.232	48[3]
Planktic	Warm water	*B. constricta, W*arm water group	0.103	-0.238[4]	48[3]

[1] Pearson's Correlation Coefficient unless otherwise stated.

[2] Only 45 samples were evaluated due to the technical limitations.

[3] An outlier was removed from the data.

[4] Spearman's Correlation Coefficient.

4.4 Warm water diatom taxa versus other species and bottom water temperatures

To further explore the potential correlations between warmer water key indicators from the data set, and Mg/Ca BWT, the warm water groups, *Thalassionema nitzschiodes*, *Paralia sulcata,* sympagic group and chrysophyte cysts were plotted against Mg/Ca BWT.

The tychoplanktic species *Paralia sulcata* had the best significance and highest negative correlation coefficient when indivicual taxon of the sympagic group were summarized (Table 3). *Paralia sulcata* has a sawtooth pattern, where each low to high abundance vary roughly between 2-5%. The oldest part is gradually decreasing until ~2300 years BP, where the abundance thereafter experiences an increased bump. From there, a new bumpy increase in abundance, followed by high abundance spikes (maximal peak ~6%). In the uppermost sediment, *P. sulcata* experience the highest peak ~6%. Apart from the core bottom, *P. sulcata* and *T. nitzschioides* show a moderately positive relationship through the core. A negative relationship in abundance between *Paralia sulcata* and Chrysophyte cysts is recorded through the core (Figure 11).

Shionodiscus oestrupii, *Thalassionema nitzschioides* and *Thalassiosira simonsenii*, are the warm water species from group 1, associated with Pacific Water and has a moderately positive correlation coefficient with *Paralia sulcata* (Table 3). The relative abundance of *T. nitzschioides* has slightly increased intervals between ~3874 to 2735, 2235 to 1245 and 966 to 263 years BP and the youngest two spikes at 154 years BP, respectively the two samples at core top. The two highest peaks were at core bottom 4129 years BP and at 1 cm depth (4.3%, truncated). Abundance of *Shionodiscus oestrupii* and *Thalassiosira simonsenii* appeared in pulses, partly overlapping in the oldest half of sample set. None of the species showed high relative abundance. Maximum was ~0.6%, and the pulses between 0.2 and 0.4% (Figure 11).

Thalassiosira eccentrica has a positive correlated pattern with warm water species around 700 to 0 years BP, where *T. eccentrica* also experience its highest peak values. The warm water species and *T. eccentrica* are further well- to moderately positive aligned in correlation from 1300 to the near oldest section of 2PC. There exists a mirrored relationship between *B. constricta* and *T. eccentrica*, while *T. eccentrica* and warm water group 1 are positively matched curves (Figure 11).

Between *Bacterosira constricta* has its largest minimums during the positively BWT-cycles. *Thalassiosira simonsenii* and *Shionodiscus oestrupii* occasional scarce abundance coincide well with the cyclic ranges where BWT is oscillating over -0.5°C. In the same BWT intervals, *Thalassiosira eccentrica* also has abundance peaks throughout the core except older than 3400 years BP (Figure 11).

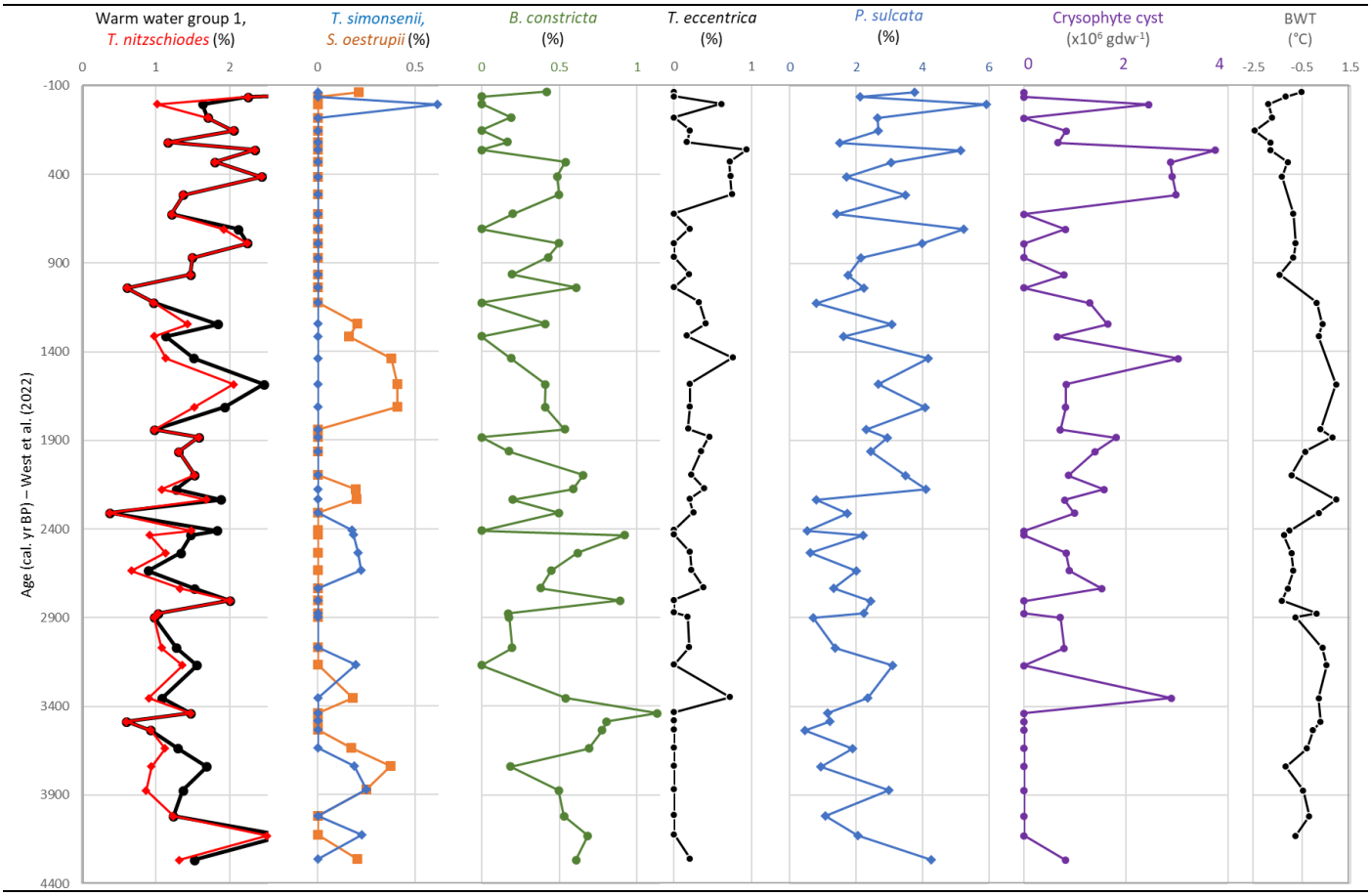

Figure 11. Warm water indicators together with *Bacterosira bathyomphala, Paralia sulcata* and chrysophyte cyst. The rightmost graph is the Mg/Ca BWT as reference point (Barrientos et al., 2018a).

4.5 Diatoms, chrysophyte and BWT

Prior summarizing the results in a concluding graph, various trendlines and R-square values are presented to further explore the potential correlations between key species-groups and Mg/Ca BWT. The data plots were clustered into five different intervals, partly overlapping with climate events from bottom: Subboreal warming (~3700 to 3100 years BP), Subatlantic cooling (~2900 to 2300 years BP), Roman Warm Period to Dark Ages (~1900 to 1300 years BP), Medieval Climate Anomaly (~1100 to 500 years BP) and Industrial Warming (300 to -63 years BP) at top (Figure 12).

Thalassionema nitzschioides and warm water group 1 had similar trendlines, including negative trendlines during Subatlantic cold and during Medieval Climate anomaly (MCA), while positive slopes during Roman Warm Period (RWP) to Dark Ages (DA). The R^2 values are slightly higher in Warm water group 1 compared with group 2. The tychoplanktic species *Paralia sulcata* and the sympagic group both have low R-square values, but they are of all intervals opposite trendlines to each other, except the green line (DA-RWP) that has a positive correlation for both (Figure 12). The correlation coefficient between sympagic data set and the BWT was not significant (-0.16, p-value = 0.294). Crysophyte cyst had high R-square values, except interval of modern time (Industrial warming). The correlation line was negative except during MCA where R^2 was highest (Figure 12).

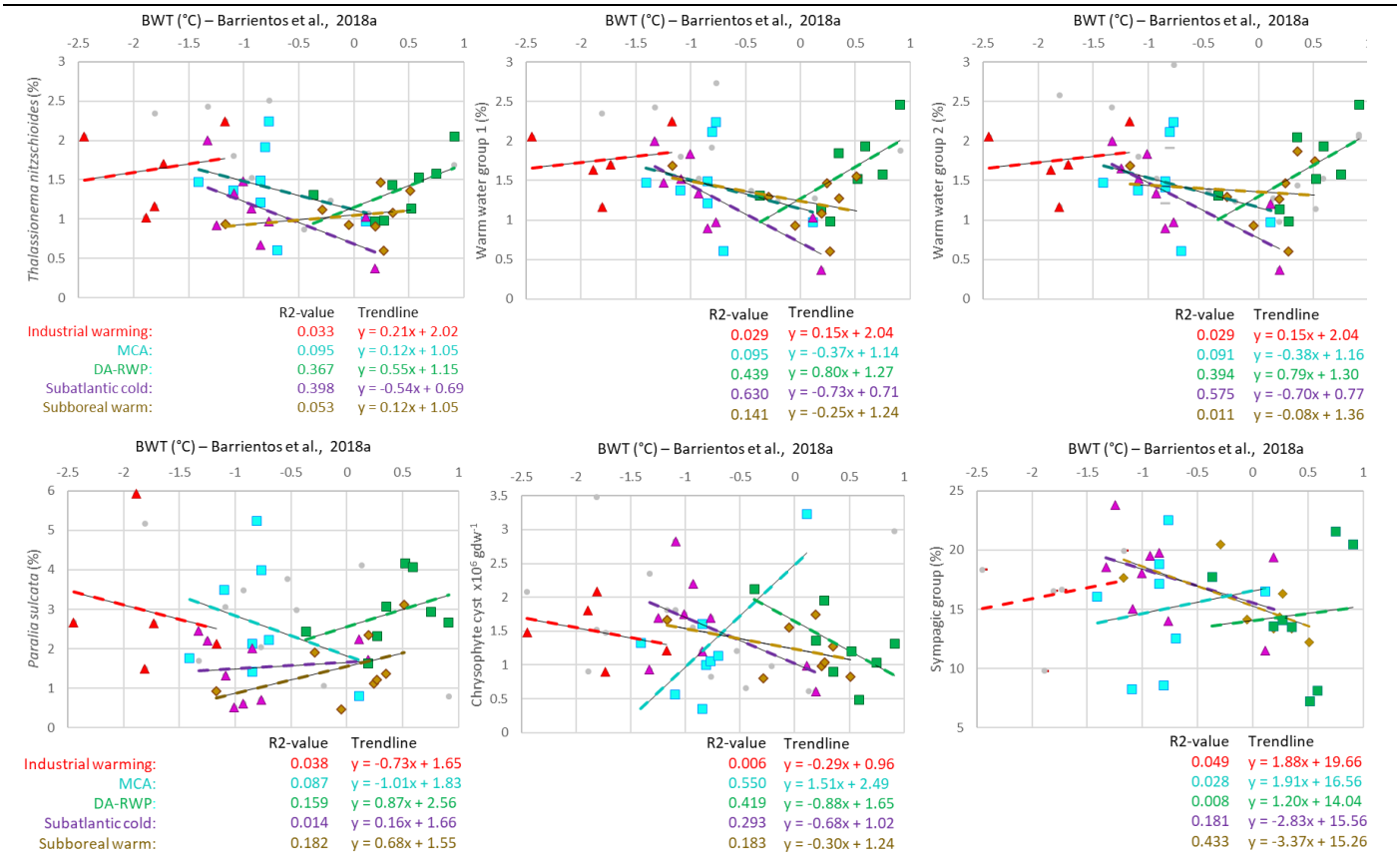

Figure 12. Six xy-plots between BWT temperature (°C) and T*halassionema nitzschioides*, and Warm water group 1 and 2, *Paralia sulcata*, Crysophyte cyst and Sympagic group. All plots with dashed regression lines. R2-value and linear trendline equation under each graph. The plots with trendlines are in the interval within late Holocene with colour in parentheses, starting with oldest (bottom to up): Subboreal warming (dark yellow), Subatlantic cooling (purple), Roman warming period through Dark Ages (green), Medieval climate anomaly (cyan), and Industrial warming (red). These events shown as double ended arrows over age intervals (see Fig. 13). The grey dotted points are the other samples outside the targeted intervals.

The final data exploration composition of various species from ecological warm-water, sympagic-, cold-water-, planktic, neritic- diatom groups together with chrysophyte cysts, and Simpsons SDI-index juxtaposed. The graph further include bottom water temperature (BWT) and $\delta^{18}O_{SMOW}$ (Barrientos, 2018) and the xy-plots time intervals (Figure 12) following the same colour scheme. Last, climate events are mentioned in a separate column (Figure 13).

Except previously explained relationships (i.e. Fig. 10-12; Table 3) A strong correlation between abundance of *Bacterosira bathyomphala* and *Thalassiosira antarctica* is graphically seen with BWT and $\delta^{18}O$ (Barrientos, 2018) and overlayed by coloured climate events. An increase in the SDI, correspond positive with higher abundance of warm water and reverse pattern of the neritic graph without *Chaetoceros* almost throughout the 2PC (Figure 13).

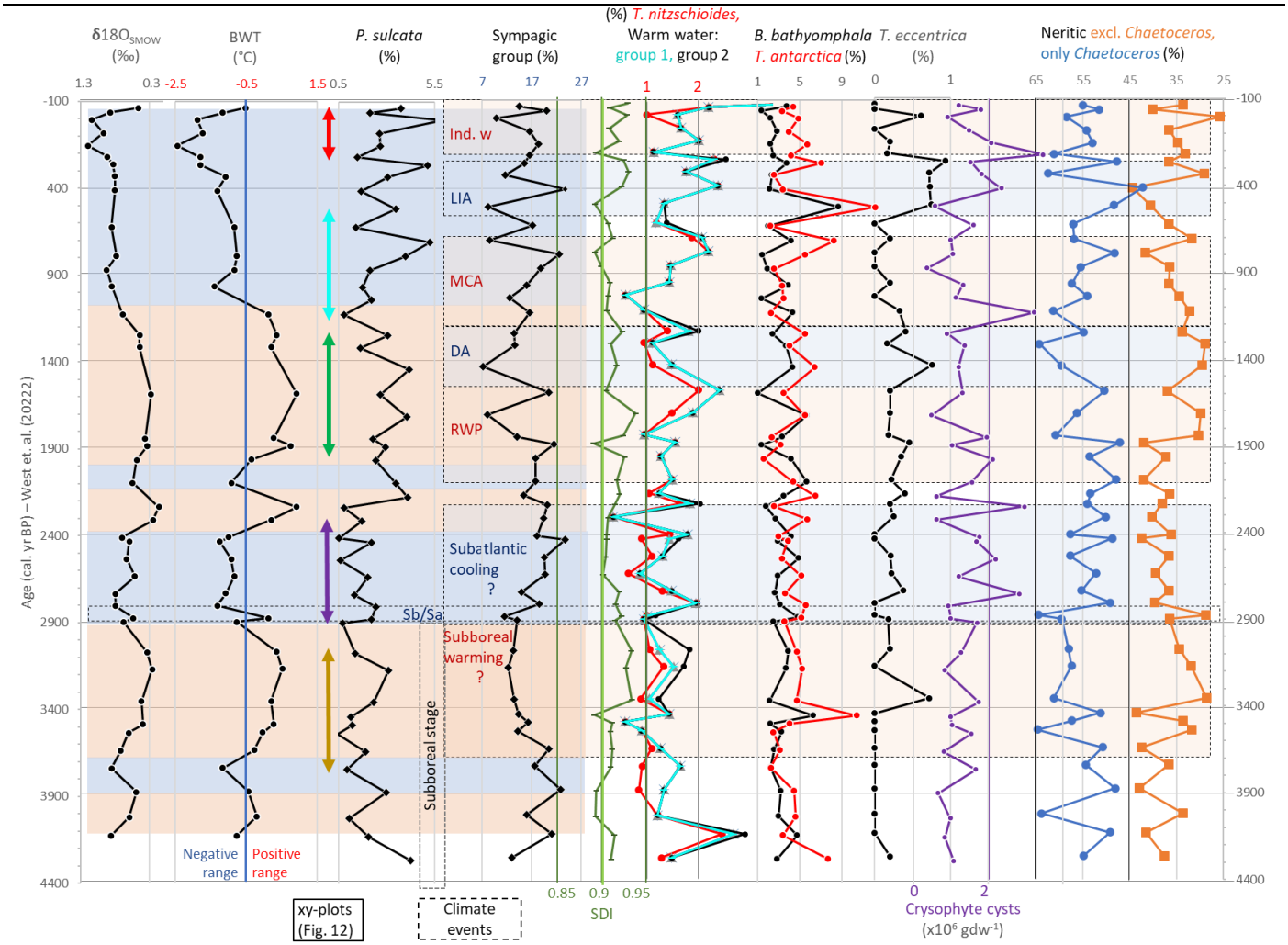

Figure 13. A multivariate proxy data set from all defined eco-groups, chrysophyte cysts and SDI. Red and blue overlay of climate events, representing warm- and cold events or stages. Sb/Sa: Subboreal-Subatlantic transition, RWP: roman warm period, DA: dark ages, MCA: medieval climate anomaly, LIA: little ice age, Ind. w: Industrial warming (Campbell et al., 1998; Mann et al., 2009; Mann and Jones, 2003; Neukom et al., 2019; Seidenkrantz et al., 2008). Subboreal- and Subatlantic stages after Ponel (2013) overlap with warming- and cooling events (question marked) Cooling middle Ages party overlap Dark Ages and Industrial warming adopted by Matul et al. (2007). Double ended arrows with cross-reference to figure (12). SDI-index with green baseline at 0.9. BWT and $\delta^{18}O$ SMOW graphs with relatively warmer and cooler climatic intervals interpreted relative to the -0.5°C blue base line, after Barrientos et al. (2018a).

5. Discussion

Many components are involved in the Arctic Ocean sea-ice advance and retreat. The sea-ice variability over the late Holocene has been tested if Pacific Water inflow is an important control or if the dynamics are related to other factors in the Arctic Ocean. The bottom water temperature had a signal, but it was unclear if the fluctuations were source from PW or a mix of other components. The main goal was to use diatoms as a tool to resolve this issue.

Diatom species have been recorded in every sample from the 2PC core from the Herald Canyon, Western Chukchi Sea, Arctic Ocean. The core had a high diversity of 25 to 40 diatom taxa per sample and over 120 different species in total. A small subset of these species was further used to analyse their sensible signals of their dwelling environment on centennial to millennial time frames during the late Holocene. Diatoms blooming near the surface, reflecting the surface temperature, were contrasted with another proxy, a geochemical Mg/Ca derived palaeothermometry (BWT) reflecting the temperature at the bottom of the ocean (Barrientos, 2018). To explore the species, they were divided into different eco-groups, that thrive in various habitats from the end nodes sympagic eco-group (ice-algae) to the warm water, Pacific Water inflow end node eco-group, and the eco-groups in between (Figure 1b). It was shown that the sympagic group follows the generally BWT oscillation pattern throughout best, while the warm water species sourced from Bering Strait Water had an occasional match at some intervals in the dataset.

To achieve a high-resolution oceanographic setting, other species would complement the sympagic group, and the warm water end node species presented. The species compared within the sympagic group, adding sea-ice related species *Attheya septentrionalis* and *Chaetoceros furcellatus* with Marginal Ice Zone (MIZ) *Thalassiosira nordenskioldii*, and cold planktic diatom species *Bacterosira bathyomphala* and *Thalassiosira antarctica* all show significance (<0.05) when eco-groups were compared with each other (Table 3). This suggests that a combination with sympagic, cold-oceanic and MIZ-related species could complement the picture to achieve a detailed high resolution oceanographic setting (Figure 10–13). Additionally, the tychoplanktic diatom *Paralia sulcata* align with higher abundance during positive ranges of BWT and vice versa from the oldest core part with uncertainty from 800 years BP to -63 years BP (Figure 13).

Aim A: Diatoms as proxy for reconstructing environmental conditions in the Herald Canyon in the Late Holocene.
The 2PC diatom dataset was stratigraphically constrained into four different diatom assemblage zones (DAZ 1–4). Absolute diatom abundance (ADA) in valves per gram dry sediment was significantly higher than in studies in the Laptev Sea, and showed similar high valve concentration compared with studies in the Chukchi Sea (Cremer, 1999; Polyakova, 1989).

The various zones showed that the neritic marine assemblages were pending from ~85-95% through the core, with a neritic decrease through the zones from oldest to youngest. The most distinct one was the gradual decrease in DAZ 2 (Figure 9b). Apart from this sum of neritic species, 3.5% benthic species, <2% oceanic- and <1% freshwater species were recorded. To the south on the Chukchi Plain in Core HC11, less marine species, while more oceanic- benthic-, and freshwater were recorded (Tsoy et al., 2017). Similarities of diatom species are seen, with higher abundance of planktic *Thalassiosira nordenskioldii* and *T. antarctica* compared with core 2PC, but the same negative correlation between them. Another core through a similar age span as 2PC on the Chukchi plain are LV77-3-1 and LV77-3-2 north of HC11 (Astakhov et al., 2020).

Both HC11 and LV77-3-1/2 are on the path of Bering Sea water with an increase in *T. antarctica* indicating ice free periods. The peaks do not coincide with 2PC, but the general pattern that sympagic with *T. nordenskioldii* (ice advance) and cold-water indicators *T. antarctica* and *Bacterosira bathyomphala* exist. The sea ice cover decreased at the beginning of the late Holocene in both LV77-3-2 and 2PC Cores with a gradual decrease until a smaller gradual increase advance and shorter ice-free intervals (jagged pattern) from 1900 year BP in 2PC (1500 year BP in LV77-3-1). These differences may indicate that LV77-cores are more exposed to both SCC and situated closer to the Bering Strait, influenced by the higher amount of mixing of these currents. Further north, almost at the end of the shelf break, b16 is situated with less *Thalassiosira nordenskioldii* and *T. antarctica than* the 2PC Core (Vologina et al., 2016).

The neritic diatoms, excluding *Chaetoceros* have abundance around 30-40% and is goes up when the sympagic group increases, and down when the sympagic group decreases in abundance. During the intervals of lower abundance of this neritic group, the absolute abundance of marine neritic *Chaetoceros* taxa increase. This is interpreted that they do not compete in the same ecological niche, and when ice growth is higher, the abundance of neritic, particularly

the sympagic species, increase. This is interpreted as a boost of nutrient-rich water from the BSW is in favour of the *Chaetoceros* species with increased abundance, which probably is reflected better closer to the Bering Strait (e.g. core LV77-3-1, HC11, and hole 3).

The small number of fresh-water species with a gradual increase from the oldest part of Core 2PC to the youngest (Figure 9a) is believed to not originate from the coastal parts of the Siberian, influenced by river systems and then migrated up to the Herald Canyon. Instead, these diatoms are suggested to be associated with closed melt ponds from the Summer melt of the sea-ice with an increase in more recent time (Kilias et al., 2014).

A geospatially distribution of diatoms, comparing results among findings of 126 taxa showed that 24 species are exclusively within the Chukchi Sea. Among these, 10 species that have not been reported in Chukchi Sea earlier, including one *Chaetoceros* (*Chaetoceros* sp. *7*) suggestes a new recorded diatom. These species not recorded in Late Holocoene sediments from the East Arctic Seas are *Cymbella gracilis*, *Denticula subtilis*, *Haslea cf. spicula*, *Navigeia paludosa*, *Pinnularia subcapitata*, *Thalassiosira bulbosa*, *Thalassiosira cf. pacifica, Sinerima marigela* and *Stauronella arctica.* The species *Encyonema silesiacum*, *Odontidium mesodon*, *Navicula frigida*, *Opephora mutabilis* and *Pinnularia quadratarea var. maxima* are assumed to be observed in the samples, but only seen in the Laptev Sea and/or East Siberian Sea according to the East Arctic Seas Atlas (Tsoy and Obrezkova, 2017). It should be noticed, that although a meridional transect could show abundance fluctuations among species, it is important to keep in mind that a shorter distance between geographic settings, not necessarily reflect similarity in species assemblages, statistically proven in the sub basins of the Arctic Sea (Gogorev and Samsonov, 2016).

Aim B: Exploring the link between the diatom assemblages and the BWT-palaeothermometry. The regional setting in the Western Chukchi Sea is seen as an interplay between various currents, affecting the palaeoceanographic landscape. It is found that during colder years the relatively warmer Pacific water is minimised and most of the PW then flows via the Alaskan coast into Barrow Canyon. This in contrast to the warmer years, where PW is flowing more through the Herald Canyon (Luchin and Panteleev, 2014). How the surface water temperatures from diatoms and bottom water temperatures (palaeothermometry) are coupled have first been addressed with the sympagic- and then the warm water species.

The sympagic group and BWT with the statistical methods chosen did not show either a good p-value, distinct trend lines, or high R^2-score. However, the overall graph clearly follows the BWT trends on cyclic pattern. When BWT is going up (positive range), the ice-algae are going down and vice versa (Figure 13). It is possible that the smaller ups- and downs within each BWT 500 to 1000 years BP are contributing to the low statistical values. This implies that another kind of statistical method might be suitable to better capture the oscillations within each BWT cycle for the sympagic group. The neritic species excluding *Chaetoceros* (where sympagic group is included as part of the neritic life-form) show a similar negative pattern, while the *Chaetoceros* followed the oscillation of BWT (Figure 13). *Pauliella taeniata* added to the sympagic group also showed a good negative correlation with BWT except in the uppermost negative range (Figure 10, Figure 13). *Pauliella taeniata* is considered an ice algae with dual signals (von Quillfeldt et al., 2003, p. 20043) that would explain the incomplete overlap with the abundance of *Fragilariopsis* spp. bulk-members of the sympagic group. It's a diatom in the sea-ice succession placed somewhere between MIZ and around ice (Figure 1b).

The warm water groups were divided into the warm water groups 1 and 2 and *Thalassionema nitzschioides* separately. Thalassionema nitzschioides shows a negative trendline during the medieval climate anomaly (MCA) event while BWC is in a negative range, while positive trend during the Dark Ages to Roman Warm Period (DA-RWP) aligning with the positive range of BWT, while the cold cyclic range of 500 years coincide with a negative trend of *T. nitzschioides* and flips to a positive range and positive regression line on the 1000-year event between 2900 to 3800 years BP (Figure 12). This suggests that *Thalassionema nitzschioides* is a good signal following BWT except the recent warming (industrial warming). Here, *Thalassionema nitzschioides* has a positive trendline in industrial warming event, that may align with that this is a warming event for the modern warming period and not a negative range as displayed in the BWT graph (Figure 13). Warm water species show similar trends with *T. nitzschioides*, except for a negative regression line in the sub boreal warming event.

In the oceanographic setting of the Western Chukchi Sea, influenced by nutrient enriched BSW water, abundance of various species are suggested to relate to relatively warmer current, that may impact the sea-ice dynamics and seen in the BWT-record. *Thalassionema nitzschioides* is thriving close to ice-free conditions and is suggested to come with the ACW-current (Astakhov et al., 2015; A.S. Astakhov et al., 2020, p. 20120; Oksman et al., 2019). The diatom *T. nitzschioides* together with *Paralia sulcata* thrives in vertically mixed waters, less saline also freshened water from ACW (Artemova et al., 2018; Astakhov et al., 2015; Obrezkova et al., 2014; Sancetta, 1982). *Shionodiscus oestrupii* is another warm indicator (Hasle and Syvertsen, 1997) but is rare in the Chukchi Sea (Table 1) including the few records in the 2PC Core. In the Bering Sea, Shionodiscus *oestrupii* and *Thalassiosira eccentrica* were less than 5% (Caissie, 2012).

Paralia sulcata shows a mirrored well match associated with the BWT except for the most recent 1000-years negative ranged BWT-cycle (Figure 11,13). It has been suggested, that *Paralia sulcata* is an indicator of freshened water from the Alaskan Coastal Water (A.S. Astakhov et al., 2020; Obrezkova et al., 2014; Polyakova, 1989). This would then be supported by the mirrored relation to sympagic species becoming relatively less abundant the same time (Figure 13).

Between the succession of the endmember sympagic- and warm water species, other species thriving in MIZ and cold pelagic water according to other ice-conditions have been recorded (Figure 1b). Therefore, a mix of various species may better explain various intervals, and at the best, fit well to different climate events (Figure 10,11,13).

The climate events used (Figure 13) are from various sources given, including European time frames (Ponel, 2013; Seidenkrantz et al., 2008). However, many of these events did not occur at the same time globally, rather regional (Neukom et al., 2019). Additionally, events can be viewed on various time scales with relative warmth compared to the Late Holocene with other intervals of Holocene. Here, a warm interval is outlined between 3500 and 1000 years BP (Andreev and Klimanov, 1999). Roman Warm Period (RWP) and Dark Ages (DA) are compromising the time frame from Seidenkrantz et al. (2008) and start of Cooling of Middle Ages (Matul et al., 2007). Industrial Warming is assumed to coincide with the start of the European event Industrial revolution (1850 EC).

During the Subboreal-Subatlantic transition, the BWT and all the graphs have either a sudden increase or decrease in abundance (Figure 13), emphasising a transition zone between the two stages presented. *Paralia sulcata*, *Thalassiosira eccentrica*, the Warm water groups and *Thalassionema nitzschioides* show an abundance jump in abundance during the Maunder Minimum (~200 to 250 years BP), closely related to the global minimum of BWT (Figure 13).

Thalassiosira nordenskioldii is a stable signal of the cold water species (Oksman et al., 2019) and blooms after the sympagic group and is considered an ice-neritic species at the ice margin (Tsoy et al., 2017). It contributes to the MIZ with its abundance linked to it (Sancetta, 1981). With this it follows that a higher abundance of *T. nordenskioldii*, the MIZ is situated for better conditions for *T. nordenskioldii* with longer duration of ice cover more than six months. *Chaetoceros furcellatus* is another species in the MIZ (von Quillfeldt, 2001) confirming the longer ice cover pattern in the Western Chukchi Sea.

Thalassiosira antarctica forms resting spore and is well preserved due its heavy silicification (Cremer, 1999). It had from the results a reflective relationship to *T. nordenskioldii* (Figure 10). This has also been recorded in other studies through the late Holocene in the Chukchi Sea (e.g. Tsoy et al., 2017). The *Fragilariopsis* spp. are the first to bloom during ice-melt and has its highest abundance when *T. antarctica* is less abundant. This consequently mean that the positive relationship between sympagic group and *T. nordenskioldii* is due to same blooming in Spring, also recorded in studies (e.g. Ran et al., 2014).

Bacterosira bathyomphala is another robust signal indicating cold water, with vast majority of the species around ice (Oksman et al., 2019; von Quillfeldt et al., 2003). An increase of *B. bathyomphala* is an indication of BSW and therefore an increase of salinity (A.S. Astakhov et al., 2020).

The Chrysophyte cysts mirrored relationship with *Paralia sulcata* might indicate different levels of salinity the species thrive in. While *Paralia sulcata* dwells good in vertically mixed waters, with freshened water from Alaska Coastal

Current. A lower abundance of *P. sulcata* may indicate low phosphorus concentrations, stratified water columns (due less ACC freshened input). The thriving of Chrysophyte cysts is indicating with an opposite oceanographic setting, i.e., less mixing, the salinity of surface water is reduced – the environmental factors keeping a lower abundance of *P. sulcata* (McQuoid and Nordberg, 2003). It is speculated that the diversity of Chrysophyte cysts in Herald Canyon prefer low salinity and a decrease of phosphorous favour smaller species the Herald Canyon (Firsova et al., 2015; Jin et al., 2017). This correlates well with less inflow of saline water from the Pacific Ocean. When *T. nitzschioides* is showing less abundance, and an advance of cold planktic species *Thalassiosira antarctica* and *Bacterosira bathyomphala*, chrysophyte increase, suggesting less intense inflow of BSW when colder in the AO.

Thalassiosira eccentrica is an open and oceanic, panthalassic diatom, thriving in water without sea ice (Fryxell and Hasle, 1972a; Polyakova, 1989). *Thalassiosira eccentrica* is showing stronger signals and to some extent reflect BWT signals through the events RWP to industrial warming, suggesting that the species is less reliable in the lower parts of the core as a palaeoceanographic proxy. At least from 4200 to 3400 years BP, *T. eccentrica* is not a trustable indicator. This in contrast to *Bacterosira constricta*, that show an abundance signal through complete 2PC, negatively correlated with *T. eccentrica* (Figure 11). This indicates thriving in various pelagic settings between them. *Bacterosira constricta* is recorded in the Arctic, subarctic cold to temperate regions (Cremer, 1998; Gusev et al., 2014; Pearce et al., 2014) while *T. eccentrica* has been identified as both cold water species (Fryxell and Hasle, 1972b) and a cosmopolitan warm water species recorded in the Bering Sea (Caissie, 2012). A possible warm water signal of *T. eccentrica* should not be overlooked, due its positively match with warm water group 1 (Figure 11). However, *Thalassiosira eccentrica*, *T. pacifica* and *T. trifulta* have historically been mismatched with each other in the Bering- and Okhotsk seas (Sancetta, 1982).

The higher influxes of neritic species are associated with the sympagic species, suggesting a stronger SCC-current with colder surface water temperature since the cold-water species are increased, and hence advance ice formation. This in contrast during warmer periods, where the Chukchi Sea is halocline driven rather than thermocline. At warmer times, the ice-free periods get more months and oceanic species take over with more stratified water and less nutrients mixing in the water column. In a study including the southern Chukchi Sea, the impact of *Chaetoceros*, *Fragilariopsis* and *Thalassiosira* species abundances are related to stratification (Suzuki et al., 2021).

Semi-opened melt ponds with access to marine water in the Arctic Ocean influence locally the salinity. The marine-neritic species (*Chaetoceros* and other neritic diatoms) have through the Diatom assemblage zones 1–4 gradually decreased (Figure 9b). This could be explained by larger amounts of opened melt pounds or speculating that these are open and accessible for marine Arctic Sea water in the Herald Canyon over more months in the most recent time, now (DAZ 4) compared with the past, oldest (DAZ 1), implying a slightly warmer climate over the Late Holocene affecting the Western Chukchi.

Simpson Diversity Index, SDI with a value between 0 and 1 is marked with a baseline at 0.9 (Figure 13). When warm water groups are increased in abundance, the SDI index increased above 0.9, and the neritic group without *Chaetoceros* is decreased. This is interpreted as a link between a more diverse diatom flora during warming events, including industrial warming. When the diversity is going up, the neritic shelf group (excl. *Chaetoceros*) experiences a decrease in abundance. The BWT follows the same described pattern except for the negative range during the recent warming (Figure 13). The notches in SDI can be explained by less diversity due an advance of ice formation in the Herald Canyon coupled with an abundance increase in *Fragilariopsis reginae-jahniae*, *F. oceanica* and *F. arctica* (Figure 10). At the end of the Little Ice Age (400–250 years BP), the SDI increased while warm species, cold water species and neritic groups are oscillated, implying that during LIA species richness is driven by something else than associated with higher abundance of Pacific Water flow species.

The Anthropocene impact of recent warming is derived from sample data in the upper section of core 1 (i.e. top 3–5 samples), here also termed Industrial warming. In the northern part of the Chukchi Sea, close to Core 2PC, the last decades show an increase in the abundance of *Paralia sulcata* and Planktonic ocean species (Astakhov et al., 2019).

In the most recent years, the last two decades between 1990 to 2019, an increase of BSW occurred annually 0.010 ± 0.006 Sv with a temperature over 0°C five months a year in the 1990s to above seven months year 2017 (Woodgate and Cecilia Peralta-Ferriz, 2021). In the last decades, typical species from warm Pacific waters is

predominating, including the tychoplanktic species *Paralia sulcata* (Astakhov et al., 2019). While the BWT is still in the negative range, the warm water group 1 and 2 are increased indicating a warmer inflow of Pacific Water into the Arctic Ocean. In the top three (youngest) data points, *P. sulcata*, Warm water group (Figure 13) and *Attheya septentrionalis* (Figure 10) correlated with BWT in recent time indicating them as following the geochemical Mg/Ca proxy well here.

Minor findings related to diatoms. The observations of the diatoms *Actinocyclus curvatulus*, *Thalassiosira bulbosa*, *Delphineis suriella*, *Neodenticula seminae* and *Sinerima marigela* are added to expand the observations of their abundance pattern and the oceanographic setting.

Actinocyclus curvatulus was mostly considered scarce from the dataset and dwells in around-ice with less ice concentration then found in the edge zone of marginal ice zone, MIZ (Figure 1b). The species has considered a near sea ice, but not marginal ice sea, a "summer pack ice" species or a thermophilic taxon brought from the Bering Sea (Gusev et al., 2014; von Quillfeldt et al., 2003). Abundance of *A. curvatulus* seem to be related with greater relative abundance while sympagic group show lowest minima ~1600-1700 years BP (Figure 8). This further support the various dwelling patterns that the sea-ice concentration breaks up, speculating longer Spring and Summer months leaving a longer range for species around ice to expand their abundancy.

Thalassiosira bulbosa was very scarce, occasionally only found at two stations in Laptev Sea (Cremer 1998) and absent from other studies in the western Chukchi Sea. *Thalassiosira bulbosa* also thrive in other surface waters such as temperate (Hasle and Syvertsen, 1997; Syvertsen and Hasle, 1984), with a possible migrated connection into the Chukchi Sea via North Pacific or shelf areas from the Bering Sea.

Delphineis suriella indicate transportation associated attached with sand within cold to temperate waters. Similar to *P. sulcata, D. suriella* can be stirred up in turbulent waters (Ran et al., 2014). Its therefore speculated as a benthic long lateral transportation signal through the Herald Channel, or from the coast outside Wrangel Island.

In the 2PC Core, very few records were found of *Neodenticula seminae*. The long transport is suggested for the *N. seminae, being a* signal of deeper oceanic settings, most abundant outside the shelf water around the Aleutian Islands. *Neodenticula seminae* further dwells in high saline water in the North Pacific above 42°N with less productive water (Sancetta, 1982). It has been used as an indicator of the Alaskan stream water (Caissie, 2012).

Finally, *Sinerima marigela*, has been detected in the Bering Sea and along the Canadian coastal waters and described as an indicator of high ice concentration >70% (Nesterovich, 2019). Due its recent detection, an increase in this specimen in other marginal seas of the Arctic region is expected, or a possible transfer from similar recorded species (e.g. *Porosira glacialis*).

In a wider geographical perspective, its elaborated, that not many large palaeoceanographic oscillations have occurred with increased sea level changes in the Arctic Ocean (Keigwin et al., 2006). Regarding the amount of Bering Sea Water inflow, this was monitored over last 5 kyr from the station LV77-3 (Astakhov et al., 2020). Due the high resolution, diatom fossil data of the 2PC Core may be suitable with the advantage of an increased sample resolution to achieve than performed in this study to achieve a better palaeoceanographic reconstruction in the Western Chukchi Sea.

The results so far have been related to the Northern Pacific and Arctic Ocean, especially emphasised marginal seas of Western- and central Chukchi Sea, Bering Strait, and Bering Sea, touching the North Pacific Area outside these marginal seas. However, the paleoclimate over the Holocene, might be a concern on global scale addressing a northern Hemisphere process (De Boer and Nof, 2004). In recent years, decrease of ice. In case of more imbalance of retreating ice sheet associated with warmer water temperatures or decreased salinity in the Chukchi region, may change the vertical distribution of nutrients, the stratification may be more pronounced (Suzuki et al., 2021).The upwelling condition would then affect the diatoms and jeopardise the food web balance from the Arctic Ocean.

6. Conclusions

The Core SWERUS-L2-2-PC1 (2PC) retrieved in Western Chukchi Sea with a supported age model has been analysed of siliceous material with a focus on diatoms.

On the cyclic BWT variations of 500–1000 years in the past 4000 years, it has been tested that diatom, narrowed to eco-groups sympagic and neritic assemblages, the best fit with the palaeothermometry is the sympagic species and both neritic groups, either following BWT or an anti-relationship to it. The Neritic exclusively *Chaetoceros* have increased abundance where the BWT shows a positive range, while the *Chaetoceros* alone mirrors this statement.

A palaeoceanographic setting in the west Chukchi Sea, is shown by signals of oscillated abundance of cold-around ice species *Thalassiosira antarctica* and *T. nordenskioldii* thriving in the marginal ice zone. These species reflect reduced and advanced sea-ice formation. Their abundance is further supported by cold water around the ice species *Bacterosira bathyomphala*, sympagic species including *Chaetoceros furcellatus*, and ice algae diatom *Attheya septentrionalis*.

Paleoclimate events in the west Chukchi Sea partly coincide with the Tychoplanktic species *Paralia sulcata* with the warm species group, *Thalassiosira eccentrica*, and climatic events throughout the late Holocene, but none of these species alone correlate completely with all climate events or a strong BWT correlation. Chrysophyte cysts have an oscillating signal through the core, that seem to have a striking reflective pattern to *P. sulcata*. It is further suggested that Crysophyta cysts show a salinity range relationship to ocean-pelagic species *Bacterosira bathyomphala* and *Bacterosira constricta*. The *Bacterosira* genera are concluded to dwell in different pelagic settings (cold versus Bering Sea water influenced).

Aim A.1 concludes that species with abundance throughout the late Holocene (-63 to 4265 year BP) have been described with a multivariate diagram including life form, salinity variations and species richness of water masses. Species have been related to four different diatom assemblage zones (DAZ), explaining the variability with the four zones (DAZ) in terms of fluctuations of taxa, genera and assemblages. Species richness linked with diversity indices, is shown to belong to *Navicula* spp. and freshwater species.

Aim A.2 concludes that the Arctic Ocean is related to different eco-groups, especially neritic assemblages, sympagic species, a few oceanic species with subgroup division of cold-oceanic species, and MIZ thriving species and species around ice. Some species are exclusively recorded in the Chukchi Sea when contrasting with Laptev- and East Siberian Seas. Other species have a stronger signal at lower latitudes, sourced from Pacific water.

Aim B.1 concludes that certain groups of diatoms can show party overlap correlations with BWT and proposes that the results from diatoms, separated from the foraminifera Mg/Ca proxy-extracted foraminifera record, align with a correlation supporting the bottom water temperature (BWT), best seen with the sympagic group, and can therefore independently show a relationship of inflow of Pacific water and the impact of bottom water temperature on cyclic patterns of 500–1000 years.

Aim B.2 concludes from the perspective of climate in the Northern Hemisphere, that sympagic- and ice-algae, Pacific warm water species, *Paralia sulcata,* chrysophyte, and some cold-water indicators, address interesting aligning similarities with warm and cold events on a larger scale for the northern hemisphere. The species abundance as a palaeoceanographic signals, and subsequently the paleoclimate, provide insight in the western Chukchi Sea regarding ice-dynamics - possible longer than the Late Holocene, and indirectly achieve predictions into future climate. In the upper part of the core, addressing the Anthropocene climate change, more records are needed with higher resolution of diatom samples.

A recommendation of at least 400 valves, including a dominant species of 40%-70% is recommended. The 2PC is outstanding in terms of high preservation and the two independent age-models with a tephra horizon age-marker. The 2PC further contributes to valuable insights into the richness of species in the Western Chukchi Sea, suggesting that the proportion of species from 2PC are balanced in the Arctic region around MIZ, and proposed to be added as a baseline of diatom species abundance for future research within the late Holocene.

Finally, it is believed that preserved diatom assemblages downcore through the Late Holocene correlate well with the palaeoceanographic setting in the Western Chukchi Sea, and with other strategically positioned and well-dated cores, reconstructed sea surface temperatures sensitive down to a decennial resolution could draw an improved map of the sea-ice dynamics in the Arctic Ocean.

Acknowledgements

A comprehensive piece of the dynamics-forcings puzzle in the Arctic Ocean is viewed through diatoms - silica bearing algae and their sedimentary imprint carved in glass. I would like to first express my gratitude to three persons with their experienced lenses accompanying my path to complete this project. First, my supervisor Elinor Andrén at Södertörn University - not only the library access to your books was open 24-7, but you have also been there from first- to last chapter of this project including lab- and microscopy. Your knowledge and positive vibes about diatoms have been essential to me. Then many thanks to co-supervisors at Stockholm University: Helen Coxall for your profession and open door when I know you were busy, fruitful discussions, suggestions, and inspirational steps and Matt O'Regan for advice, knowledge around the core and tips and tricks I tried to copy or at least follow.

Some more people I would like to mention during completion of this work within the diatom field: The coeditor of the Atlas of Russian East Arctic Seas, Ira Tsoy: for insightful comments, and help with some species – thank you. Diatomist Jan Risberg and Pollen expert Martina Hättestrand at Stockholm University Quaternary geology for both showing early guidance and inspiration. Renat Gogorev for guiding advice describing *Chaetoceros* sp. *7*. Andrzej Witkowski for comments and suggestions and the warmth greeting to be a diatomist colleague. Beth Caissie for an optimistic view and all the best good luck with PAGES-project. David U. Hernández-Becerril for valueble assistance within *Chaetoceros*, and Holger Cremer, your Diatom Flora of the Laptev Sea followed me throughout this project.

Thank you all, hope I can contribute back to you.

Also, I would like to thank at Stockholm University: Gabriel West - technical questions regarding the sedimentary core 2PC, Kjell Jansson at MMK for SEM assistance and nice chats, Carina Johansson with assistance providing cores to SLAM-lab and front picture of this thesis.

During my time at Södertörn University, chats lifted my daily life outside the bubble of Natural science, including Anders, Christian, Fred, Martin D., Mats G., Mona, Igne, Patrik D., Thérese, Thomas A. and of course Anushree Sanyal for nice conversations and experiences you shared with me.

Peter Sundgren - for valuable readings and comments. Grateful thanks to my parents and my sister. Finally, to my inner family unit - S.E.A. Shirin Ziaei for patience and increasing space for me, in contrast to our smallest family member for impatience and stealing time. Both ways expanded my ability to accomplish this thesis and beyond.
I love you.

References

Alexander, V., Chapman, T., 1981.
The role of epontic algal communities in Bering Sea ice, in The Eastern Bering Sea Shelf: Oceanography and Resources, edited by D.W. Hood and J.A. Calder. University of Washington Press, Seattle, Washington 773-780.

Alexander, V., Niebauer, H.J., 1981. Oceanography of the eastern Bering Sea ice-edge zone in spring1. Limnology and Oceanography 26, 1111–1125. https://doi.org/10.4319/lo.1981.26.6.1111

Andersen, O.G.N., 1989. Diatoms in Arctic Shallow Seas Sediments, in: Herman, Y. (Ed.), The Arctic Seas. Springer US, Boston, MA, pp. 147–192.

Anderson, L.G., Andersson, P.S., Björk, G., Peter Jones, E., Jutterström, S., Wåhlström, I., 2013. Source and formation of the upper halocline of the Arctic Ocean. Journal of Geophysical Research: Oceans 118, 410–421. https://doi.org/10.1029/2012JC008291

Andreev, A.A., Klimanov, V.A., 1999. Quantitative Holocene climatic reconstruction from Arctic Russia 12.

Andrén, E., Andrén, T., Kunzendorf, H., 2000. Holocene history of the Baltic Sea as a background for assessing records of human impact in the sediments of the Gotland Basin. The Holocene 10, 687–702. https://doi.org/10.1191/09596830094944

Anonymous, 1975. Proposals for a standardization of diatom terminology and diagnoses. Nova Hedwigia, pp. 323–354.

Artemova, A.V., Sattarova, V.V., Vasilenko, Y.P., 2018. Distribution of diatoms and geochemical features of holocene sediments from the Kuril Basin (Sea of Okhotsk). Deep Sea Research Part II: Topical Studies in Oceanography 154, 10–23. https://doi.org/10.1016/j.dsr2.2017.12.019

Astakhov, A., Bosin, A., Kolesnik, A., Obrezkova, M., 2015. Sediment Geochemistry and Diatom Distribution in the Chukchi Sea: Application for Bioproductivity and Paleoceanography. Oceanog 28, 190–201. https://doi.org/10.5670/oceanog.2015.65

Astakhov, A.S., Bosin, A.A., Liu, Y.G., Darin, A.V., Kalugin, I.A., Artemova, A.V., Babich, V.V., Melgunov, M.S., Vasilenko, Yu.P., Vologina, E.G., 2019. Reconstruction of ice conditions in the northern Chukchi Sea during recent centuries: Geochemical proxy compared with observed data. Quaternary International 522, 23–37. https://doi.org/10.1016/j.quaint.2019.05.009

Astakhov, A.S., Markevich, V.S., Kolesnik, A.N., Wang, R., Kononov, V.V., Obrezkova, M.S., Bosin, A.A., 2014. Possible conditions and the formation time of the Chukchi Plateau pockmarks. Oceanology 54, 624–636. https://doi.org/10.1134/S000143701404002X

Astakhov, A.S., Shi, X., Darin, A.V., Kalugin, I.A., Hu, L., Tsoy, I.B., Kolesnik, A.N., Obrezkova, M.S., Alatortsev, A.V., Babich, V.V., Plotnikov, V.V., 2020. Reconstructing ice conditions in the southern Chukchi Sea during the last millennium based on chemical composition of sediments and diatom assemblages. Marine Geology 427, 106220. https://doi.org/10.1016/j.margeo.2020.106220

Astakhov, A.S., Shi, X., Darin, A.V., Kalugin, I.A., Hu, L., Tsoy, I.B., Kolesnik, A.N., Obrezkova, M.S., Alatortsev, A.V., Babich, V.V., Plotnikov, V.V., 2020. Reconstructing ice conditions in the southern Chukchi Sea during the last millennium based on chemical composition of sediments and diatom assemblages. Marine Geology 427, 106220. https://doi.org/10.1016/j.margeo.2020.106220

Barrientos, N., 2018. Arctic Ocean benthic foraminifera preservation and Mg/Ca ratios : Implications for bottom water palaeothermometry. Diss. Stockholm University, Stockholm.

Barrientos, N., Coxall, H.K., Lear, C.H., Pearce, C., Muschitiello, F., O'Regan, M., Stranne, C., de Boer, A., Cronin, T.M., Koshurnikov, A., Jakobsson, M., 2018a. Late Holocene variability in Arctic Ocean Pacific Water inflow through the Bering Strait. [Unpublished manuscript].

Barrientos, N., Lear, C.H., Jakobsson, M., Stranne, C., O'Regan, M., Cronin, T.M., Gukov, A.Y., Coxall, H.K., 2018b. Arctic Ocean benthic foraminifera Mg/Ca ratios and global Mg/Ca-temperature calibrations: New constraints at low temperatures. Geochimica et Cosmochimica Acta 236, 240–259. https://doi.org/10.1016/j.gca.2018.02.036

Battarbee, R.W., 1986. Diatom analysis. In B. E. Berglund (Ed.), Handbook of Holocene palaeoecology and palaeohydrology, in: Diatom Analysis. Wiley, Chichester, pp. 527–570.

Battarbee, R.W., Jones, V.J., Flower, R.J., Cameron, N.G., Bennion, H., Carvalho, L., Juggins, S., 2001. Diatoms, in: Smol, J.P., Birks, H.J.B., Last, W.M., Bradley, R.S., Alverson, K. (Eds.), Tracking Environmental Change Using Lake Sediments: Terrestrial, Algal, and Siliceous Indicators, Developments in Paleoenvironmental Research. Springer Netherlands, Dordrecht, pp. 155–202. https://doi.org/10.1007/0-306-47668-1_8

Battarbee, R.W., Kneen, M.J., 1982. The use of electronically counted microspheres in absolute diatom analysis. Limnology and Oceanography 27, 184–188. https://doi.org/10.4319/lo.1982.27.1.0184
Bauch, H.A., Polyakova, Y.I., 2000. Late Holocene variations in Arctic shelf hydrology and sea-ice regime: evidence from north of the Lena Delta. International Journal of Earth Sciences 89, 569–577. https://doi.org/10.1007/s005310000122
Caissie, B.E., 2012. Diatoms as recorders of sea ice in the Bering and Chukchi Seas: Proxy development and application (PhD thesis). University of Massachusetts Amherst.
Calvert, S.E., Pedersen, T.F., 2007. Elemental Proxies for Palaeoclimatic and Palaeoceanographic Variability in Marine Sediments: Interpretation and Application 78.
Campbell, I.D., Campbell, C., Apps, M.J., Rutter, N.W., Bush, A.B.G., 1998. Late Holocene ~1500 yr climatic periodicities and their implications. Geology 26, 471–473. https://doi.org/10.1130/0091-7613(1998)026<0471:LHYCPA>2.3.CO;2
Cleve, P.T., 1883. Diatoms, collected during the expedition of the Vega, Vega-expeditionens vetenskapliga iakttagelser 3, 455-517.
Cleve-Euler, A., 1951. Die Diatomeen von Schweden und Finnland. Kungliga Vetenskapsakademiens Handlingar I-V. Stockholm: Almqvist & Wiksell. 4:e serien 2:1 (1951), 3:3 (1952), 4:1 (1953), 4:5 (1953), 5:4 (1955).
Coachman, L. K., Coachman, Lawrence K., Aagaard, K., Tripp, R.B., 1975. Bering Strait: The Regional Physical Oceanography. University of Washington Press.
Comiso, J.C., Parkinson, C.L., Gersten, R., Stock, L., 2008. Accelerated decline in the Arctic sea ice cover. Geophysical Research Letters 35. https://doi.org/10.1029/2007GL031972
Cremer, 1998. Die Diatomeen der Laptevsee (Arktischer Ozean): Taxonomie und biogeographische Verbreitung Diatoms in the Laptev Sea (Arctic Ocean): Taxonomy and biogeographic distribution. Ber. Polarforsch. 260.
Cremer, 1998. Bibliotheca Diatomologica, The Diatom Flora of the Laptev Sea (Arctic Ocean). 169 pp. 40 pl. Band 40. Gebrüder Borntraeger Verlag. Berlin Stuttgart.
Cremer, H., 1999. Distribution patterns of diatom surface sediment assemblages in the Laptev Sea (Arctic Ocean). Marine Micropaleontology 38, 39–67. https://doi.org/10.1016/S0377-8398(99)00037-7
Crosta, X., Koç, N., 2007. Chapter Eight Diatoms: From Micropaleontology to Isotope Geochemistry, in: Developments in Marine Geology. Elsevier, pp. 327–369. https://doi.org/10.1016/S1572-5480(07)01013-5
De Boer, A.M., Nof, D., 2004. The Bering Strait's grip on the northern hemisphere climate. Deep Sea Research Part I: Oceanographic Research Papers 51, 1347–1366. https://doi.org/10.1016/j.dsr.2004.05.003
Dickson, R.R., Meincke, J., Rhines, P., 2008. Arctic-subarctic ocean fluxes: defining the role of the Northern seas in climate. Springer, Dordrecht.
Endo, H., Ogata, H., Suzuki, K., 2018. Contrasting biogeography and diversity patterns between diatoms and haptophytes in the central Pacific Ocean. Sci Rep 8, 10916. https://doi.org/10.1038/s41598-018-29039-9
Firsova, D.A., Bessudova, A.Y., M. Sorokovikova, L., V. Tomberg, I., V. Likhoshway, Y., 2015. The Diversity of Chrysophycean Algae in an Arctic Zone of River and Sea Water Mixing, Russia. AJPS 06, 2439–2452. https://doi.org/10.4236/ajps.2015.615246
Fryxell, G.A., Hasle, G.R., 2022. The Marine Diatom Thalassiosira Oestrupii: Structure, Taxonomy and Distribution 12.
Fryxell, G.A., Hasle, G.R., 1980. The Marine Diatom Thalassiosira Oestrupii: Structure, Taxonomy and Distribution. American Journal of Botany 67, 804–814. https://doi.org/10.2307/2442672
Fryxell, G.A., Hasle, G.R., 1972a. Thalassiosira Eccentrica (ehrenb.) Cleve, T. Symmetrica Sp. Nov., and Some Related Centric Diatoms1. Journal of Phycology 8, 297–317. https://doi.org/10.1111/j.1529-8817.1972.tb04044.x
Fryxell, G.A., Hasle, G.R., 1972b. Thalassiosira Eccentrica (ehrenb.) Cleve, T. Symmetrica Sp. Nov., and Some Related Centric Diatoms1. Journal of Phycology 8, 297–317. https://doi.org/10.1111/j.1529-8817.1972.tb04044.x
Gehlen, M., van Raaphorst, W., 1993. Early diagenesis of silica in sandy North sea sediments: quantification of the solid phase. Marine Chemistry 42, 71–83. https://doi.org/10.1016/0304-4203(93)90238-J
Gersonde, R., Zielinski, U., 2000. The reconstruction of late Quaternary Antarctic sea-ice distribution—the use of diatoms as a proxy for sea-ice. Palaeogeography, Palaeoclimatology, Palaeoecology 162, 263–286. https://doi.org/10.1016/S0031-0182(00)00131-0
Gogorev, R.M., Samsonov, N.I., 2016. The genus Chaetoceros (Bacillariophyta) in Arctic and Atarctic. Novosti sistematiki nizshikh rastenii 50, 56–111. https://doi.org/10.31111/nsnr/2016.50.56
Grebmeier, J.M., 2012. Shifting Patterns of Life in the Pacific Arctic and Sub-Arctic Seas. Annu. Rev. Mar. Sci. 4, 63–78. https://doi.org/10.1146/annurev-marine-120710-100926
Grebmeier, J.M., Cooper, L.W., Feder, H.M., Sirenko, B.I., 2006. Ecosystem dynamics of the Pacific-influenced Northern Bering and Chukchi Seas in the Amerasian Arctic. Progress in Oceanography 71, 331–361. https://doi.org/10.1016/j.pocean.2006.10.001

Grimm, E.C., 1987. CONISS: a FORTRAN 77 program for stratigraphically constrained cluster analysis by the method of incremental sum of squares. Computers & Geosciences 13, 13–35. https://doi.org/10.1016/0098-3004(87)90022-7

Gusev, E.A., Anikina, N.Yu., Derevyanko, L.G., Klyuvitkina, T.S., Polyak, L.V., Polyakova, E.I., Rekant, P.V., Stepanova, A.Yu., 2014. Environmental evolution of the southern Chukchi Sea in the Holocene. Oceanology 54, 465–477. https://doi.org/10.1134/S0001437014030011

Hasle, G.R., 1978. Some Thalassiosira species with one central process (Bacillariophyceae). Norwegian Journal of Botany 25, 77-110.

Hasle, G.R., Syvertsen, E.E., 1997. Marine Diatoms. In C. R. Tomas (Ed.), Identifying Marine Phytoplankton, San Diego: Academic Press, 5–385. doi:10.1016/B978-012693018-4/50004-5.

Hasle, G.R., Syvertsen, E.E., von Quillfeldt, C.H., 1996. Fossula arctica gen. nov. spec. nov., a marine Arctic araphid diatom. Diatom Research, 11, 261-272.

Herman, Y. (Ed.), 1989. The Arctic Seas: Climatology, Oceanography, Geology, and Biology. Springer US, Boston, MA. https://doi.org/10.1007/978-1-4613-0677-1

Hibler, W.D., 1989. Diatoms in Arctic Shallow Seas Sediments, in: Herman, Y. (Ed.), The Arctic Seas. Springer US, Boston, MA, pp. 47–92.

Horner, R., Schrader, G.C., 1982. Relative Contributions of Ice Algae, Phytoplankton, and Benthic Microalgae to Primary Production in Nearshore Regions of the Beaufort Sea. ARCTIC 35, 485–503. https://doi.org/10.14430/arctic2356

Horner, R.A., 1989. Diatoms in Arctic Shallow Seas Sediments, in: Herman, Y. (Ed.), The Arctic Seas. Springer US, Boston, MA, pp. 123–146.

Jakobsson, M., 2002. Hypsometry and volume of the Arctic Ocean and its constituent seas. Geochemistry, Geophysics, Geosystems 3, 1–18. https://doi.org/10.1029/2001GC000302

Jakobsson, M., Mayer, L.A., Bringensparr, C., Castro, C.F., Mohammad, R., Johnson, P., et al., 2020. The international Bathymetric chart of the Arctic Ocean version 4.0. Scientific Data, 7(1), 176. https://doi.org/10.1038/s41597-020-0520-9.

Jakobsson, M., Pearce, C., Cronin, T.M., Backman, J., Anderson, L.G., Barrientos, N., Björk, G., Coxall, H., de Boer, A., Mayer, L.A., Mörth, C.-M., Nilsson, J., Rattray, J.E., Stranne, C., Semiletov, I., O'Regan, M., 2017. Post-glacial flooding of the Bering Land Bridge dated to 11 cal ka BP based on new geophysical and sediment records. Clim. Past 13, 991–1005. https://doi.org/10.5194/cp-13-991-2017

Jin, H., Zhuang, Y., Li, H., Chen, J., Gao, S., Ji, Z., Zhang, Y., 2017. Response of phytoplankton community to different water types in the western Arctic Ocean surface water based on pigment analysis in summer 2008. Acta Oceanol. Sin. 36, 109–121. https://doi.org/10.1007/s13131-017-1033-z

Kang, S.-H., Fryxell, GretaA., 1992. Fragilariopsis cylindrus (Grunow) Krieger: The most abundant diatom in water column assemblages of Antarctic marginal ice-edge zones. Polar Biol 12. https://doi.org/10.1007/BF00236984

Karami, M.P., Myers, P.G., de Vernal, A., Tremblay, L.B., Hu, X., 2021. The role of Arctic gateways on sea ice and circulation in the Arctic and North Atlantic Oceans: a sensitivity study with an ocean-sea-ice model. Clim Dyn 57, 2129–2151. https://doi.org/10.1007/s00382-021-05798-6

Karpuz, N.K., Schrader, H., 1990. Surface sediment diatom distribution and Holocene paleotemperature variations in the Greenland, Iceland and Norwegian Sea. Paleoceanography 5, 557–580. https://doi.org/10.1029/PA005i004p00557

Keigwin, L.D., Donnelly, J.P., Cook, M.S., Driscoll, N.W., Brigham-Grette, J., 2006. Rapid sea-level rise and Holocene climate in the Chukchi Sea. Geol 34, 861. https://doi.org/10.1130/G22712.1

Kemp, A.E.S., Villareal, T.A., 2018. The case of the diatoms and the muddled mandalas: Time to recognize diatom adaptations to stratified waters. Progress in Oceanography 167, 138–149. https://doi.org/10.1016/j.pocean.2018.08.002

Khalil, K., Rabouille, C., Gallinari, M., Soetaert, K., DeMaster, D.J., Ragueneau, O., 2007. Constraining biogenic silica dissolution in marine sediments: A comparison between diagenetic models and experimental dissolution rates. Marine Chemistry 106, 223–238. https://doi.org/10.1016/j.marchem.2006.12.004

Kilham, S.S., Theriot, E.C., Fritz, S.C., 1996. Linking planktonic diatoms and climate change in the large lakes of the Yellowstone ecosystem using resource theory. Limnology and Oceanography 41, 1052–1062. https://doi.org/10.4319/lo.1996.41.5.1052

Kilias, E.S., Peeken, I., Metfies, K., 2014. Insight into protist diversity in Arctic sea ice and melt-pond aggregate obtained by pyrosequencing. Polar Research 33, 23466. https://doi.org/10.3402/polar.v33.23466

Koç, N., Jansen, E., Haflidason, H., 1993. Paleoceanographic reconstructions of surface ocean conditions in the Greenland, Iceland and Norwegian seas through the last 14 ka based on diatoms. Quaternary Science Reviews 12, 115–140. https://doi.org/10.1016/0277-3791(93)90012-B

Konfirst, M.A., Kuhn, G., Monien, D., Scherer, R.P., 2011. Correlation of Early Pliocene diatomite to low amplitude Milankovitch cycles in the ANDRILL AND-1B drill core. Marine Micropaleontology 80, 114–124. https://doi.org/10.1016/j.marmicro.2011.06.005

Krammer, K., Lange-Bertalot, H., 1986. In Ettl, H., Gärtner, J. G., Gerloff, J., Heynig, H. & Mollenhauer, D. (Eds.), Süsswasserflora von Mitteleuropa Bd 2. Stuttgart: Fischer. T. 1, Naviculaceae (1986), T. 2, Bacillariaceae, Epithemiaceae, Surirellaceae (1988), T. 3, Centrales, Fragilariaceae, Eunotiaceae (1991) and T. 4, Achnanthaceae (1991).

Lange-Bertalot, H., Witkowski, A., Metzeltin, D., 2000. Iconographia Diatomologica. annotated diatom micrographs: Diversity - Taxonomy - Identification : Diatom Flora of Marine Coasts I 7 7. A.R.G. Gantver Verlag K.G., Ruggell.

Linders, J., Pickart, Robert.S., Björk, G., Moore, G.W.K., 2017. On the nature and origin of water masses in Herald Canyon, Chukchi Sea: Synoptic surveys in summer 2004, 2008, and 2009. Progress in Oceanography 159, 99–114. https://doi.org/10.1016/j.pocean.2017.09.005

Luchin, V., Panteleev, G., 2014. Thermal regimes in the Chukchi Sea from 1941 to 2008. Deep Sea Research Part II: Topical Studies in Oceanography, Understanding Ecosystem Processes in the Eastern Bering Sea III 109, 14–26. https://doi.org/10.1016/j.dsr2.2014.05.007

Lundholm, N., Hasle, G.R., 2010. *Fragilariopsis* (Bacillariophyceae) of the Northern Hemisphere – morphology, taxonomy, phylogeny and distribution, with a description of *F. pacifica* sp. nov. Phycologia 49, 438–460. https://doi.org/10.2216/09-97.1

Lüthje, M., Feltham, D.L., Taylor, P.D., Worster, M.G., 2006. Modeling the summertime evolution of sea-ice melt ponds. Journal of Geophysical Research: Oceans 111. https://doi.org/10.1029/2004JC002818

Manley, W.F., 2002. Postglacial Flooding of the Bering Land Bridge: A Geospatial Animation: INSTAAR, University of Colorado, v1, http://instaar.colorado.edu/QGISL/bering_land_bridge.

Mann, M.E., Jones, P.D., 2003. Global surface temperatures over the past two millennia. Geophysical Research Letters 30. https://doi.org/10.1029/2003GL017814

Mann, M.E., Zhang, Z., Rutherford, S., Bradley, R.S., Hughes, M.K., Shindell, D., Ammann, C., Faluvegi, G., Ni, F., 2009. Global Signatures and Dynamical Origins of the Little Ice Age and Medieval Climate Anomaly. Science 326, 1256–1260. https://doi.org/10.1126/science.1177303

Matul, A.G., Khusid, T.A., Mukhina, V.V., Chekhovskaya, M.P., Safarova, S.A., 2007. Recent and Late Holocene environments on the southeastern shelf of the Laptev Sea as inferred from microfossil data. Oceanology 47, 80–90. https://doi.org/10.1134/S0001437007010110

Maurer, B.A., 2011. Measurement of species diversity (ed: Magurran, A. E, McGill, B. J). Oxford University Press chaps. 5, pages 11.

McQuoid, M.R., Nordberg, K., 2003. The diatom Paralia sulcata as an environmental indicator species in coastal sediments. Estuarine, Coastal and Shelf Science 56, 339–354. https://doi.org/10.1016/S0272-7714(02)00187-7

Mortlock, R.A., Froelich, P.N., 1989. A simple method for the rapid determination of biogenic opal in pelagic marine sediments. Deep Sea Research Part A. Oceanographic Research Papers 36, 1415–1426. https://doi.org/10.1016/0198-0149(89)90092-7

Nakamura, H., Okazaki, Y., Konno, S., Nakatsuka, T., 2020. An assessment of diatom assemblages in the Sea of Okhotsk as a proxy for sea-ice cover. J. Micropalaeontol. 39, 77–92. https://doi.org/10.5194/jm-39-77-2020

Nesterovich, A., 2019. Quantitative Diatom-based Proxy for Sea Ice Extent in the Bering and Chukchi Seas (PhD thesis). Iowa State University, United States -- Iowa.

Neukom, R., Steiger, N., Gómez-Navarro, J.J., Wang, J., Werner, J.P., 2019. No evidence for globally coherent warm and cold periods over the preindustrial Common Era. Nature 571, 550–554. https://doi.org/10.1038/s41586-019-1401-2

Obrezkova, M.S., Kolesnik, A.N., Semiletov, I.P., 2014. The diatom distribution in the surface sediments of the Eastern Arctic seas of Russia. Russ J Mar Biol 40, 465–472. https://doi.org/10.1134/S1063074014060170

Okolodkov, Y.B., 1992. Cryopelagic flora of the Chukchi, East Siberian and Laptev Seas.Proc. NIPR Symp. Polar. Biol. 5, 28-43.

Oksman, M., Juggins, S., Miettinen, A., Witkowski, A., Weckström, K., 2019. The biogeography and ecology of common diatom species in the northern North Atlantic, and their implications for paleoceanographic reconstructions. Marine Micropaleontology 148, 1–28. https://doi.org/10.1016/j.marmicro.2019.02.002

Oksman, M., Kvorning, A.B., Larsen, S.H., Kjeldsen, K.K., Mankoff, K.D., Colgan, W., Andersen, T.J., Nørgaard-Pedersen, N., Seidenkrantz, M.-S., Mikkelsen, N., Ribeiro, S., 2022. Impact of freshwater runoff from the southwest Greenland Ice Sheet on fjord productivity since the late 19th century (preprint). Other/Ocean Interactions. https://doi.org/10.5194/tc-2021-373

Pankow, H., 1971. Algenflora der Ostsee. G. Fischer.

Pascher, A., 1930. Die Süsswasser-Flora, Deutschlands, Österreichs und der Schweiz, 2nd ed. Fischer, Jena. https://doi.org/10.5962/bhl.title.21607

Pearce, C., Varhelyi, A., Wastegård, S., Muschitiello, F., Barrientos, N., O'Regan, M., Cronin, T.M., Gemery, L., Semiletov, I., Backman, J., Jakobsson, M., 2017. The 3.6 ka Aniakchak tephra in the Arctic Ocean: a constraint on the Holocene radiocarbon reservoir age in the Chukchi Sea. Clim. Past 13, 303–316. https://doi.org/10.5194/cp-13-303-2017

Pearce, C., Weckström, K., Sha, L., Miettinen, A., Seidenkrantz, M.-S., 2014. The Holocene marine diatom flora of Eastern Newfoundland bays. Diatom Research 29, 441–454. https://doi.org/10.1080/0269249X.2014.925508

Perovich, D.K., Richter-Menge, J.A., 2009. Loss of Sea Ice in the Arctic. Annu. Rev. Mar. Sci. 1, 417–441. https://doi.org/10.1146/annurev.marine.010908.163805

Polyak, L., Belt, S.T., Cabedo-Sanz, P., Yamamoto, M., Park, Y.-H., 2016. Holocene sea-ice conditions and circulation at the Chukchi-Alaskan margin, Arctic Ocean, inferred from biomarker proxies. The Holocene 26, 1810–1821. https://doi.org/10.1177/0959683616645939

Polyakova, E.I., 1989. Diatoms in Arctic Shallow Seas Sediments, in: Herman, Y. (Ed.), The Arctic Seas. Springer US, Boston, MA, pp. 481–496. https://doi.org/10.1007/978-1-4613-0677-1_20

Ponel, P., 2013. BEETLE RECORDS | Postglacial Europe, in: Encyclopedia of Quaternary Science. Elsevier, pp. 274–281. https://doi.org/10.1016/B978-0-444-53643-3.00267-3

Poulin, M., 1990. Sea Ice Diatoms (bacillariophyceae) of the Canadian Arctic. I. the Genus Stenoneis1. Journal of Phycology 26, 156–167. https://doi.org/10.1111/j.0022-3646.1990.00156.x

Poulin, M., Cardinal, A., 1982. Sea ice diatoms from Manitounuk Sound, southeastern Hudson Bay (Quebec, Canada). : II. Naviculaceae, genus *Navicula*. Can. J. Bot. 60, 2825–2845. https://doi.org/10.1139/b82-343

Poulin, M., Daugbjerg, N., Gradinger, R., Ilyash, L., Ratkova, T., von Quillfeldt, C., 2011. The pan-Arctic biodiversity of marine pelagic and sea-ice unicellular eukaryotes: a first-attempt assessment. Mar Biodiv 41, 13–28. https://doi.org/10.1007/s12526-010-0058-8

Poulin, M., Underwood, G.J.C., Michel, C., 2014. Sub-ice colonial *Melosira arctica* in Arctic first-year ice. Diatom Research 29, 213–221. https://doi.org/10.1080/0269249X.2013.877085

Quillfeldt, C.H. von, 2001. Identification of Some Easily Confused Common Diatom Species in Arctic Spring Blooms 44, 375–389. https://doi.org/10.1515/BOT.2001.048

Quillfeldt, C.H. von, 2000. Common Diatom Species in Arctic Spring Blooms: Their Distribution and Abundance 43, 499–516. https://doi.org/10.1515/BOT.2000.050

Ragueneau, O., Leynaert, A., Tréguer, P., Demaster, D.J., Anderson, R.F., 1996. Opal studied as a marker of paleoproductivity. Eos, Transactions American Geophysical Union 77, 491–491. https://doi.org/10.1029/96EO00325

Ran, L., Chen, J., Jin, H., Li, H., Lu, Y., Wang, K., 2014. Diatom distribution of surface sediment in the Bering Sea and Chukchi Sea: Diatom distribution of surface sediment in the Bering Sea and Chukchi Sea. Advances in Polar Science 24, 106–112. https://doi.org/10.3724/SP.J.1085.2013.00106

Rothrock, D.A., Yu, Y., Maykut, G.A., 1999. Thinning of the Arctic sea-ice cover. Geophysical Research Letters 26, 3469–3472. https://doi.org/10.1029/1999GL010863

Ryves, D.B., Juggins, S., Fritz, S.C., Battarbee, R.W., 2001. Experimental diatom dissolution and the quantification of microfossil preservation in sediments. Palaeogreography, Palaeoclimatology, Palaeoecology 172, 99-113.

Sancetta, C., 1982. Distribution of Diatom Species in Surface Sediments of the Bering and Okhotsk Seas. Micropaleontology 28, 221. https://doi.org/10.2307/1485181

Sancetta, C., 1981. Oceanographic and ecologic significance of diatoms in surface sediments of the Bering and Okhotsk seas. Deep Sea Research Part A. Oceanographic Research Papers 28, 789–817. https://doi.org/10.1016/S0198-0149(81)80002-7

Schrader, H.-J., Gersonde, R., 1978. Diatoms and silicoflagellates. Utrecht Micropaleont. Bull. 17: 129–176. Bull. 17: 129-176.

Seidenkrantz, M.-S., Roncaglia, L., Fischel, A., Heilmann-Clausen, C., Kuijpers, A., Moros, M., 2008. Variable North Atlantic climate seesaw patterns documented by a late Holocene marine record from Disko Bugt, West Greenland. Marine Micropaleontology 68, 66–83. https://doi.org/10.1016/j.marmicro.2008.01.006

Selz, V., Laney, S., Arnsten, A.E., Lewis, K.M., Lowry, K.E., Joy-Warren, H.L., Mills, M.M., van Dijken, G.L., Arrigo, K.R., 2018. Ice algal communities in the Chukchi and Beaufort Seas in spring and early summer: Composition, distribution, and coupling with phytoplankton assemblages. Limnology and Oceanography 63, 1109–1133. https://doi.org/10.1002/lno.10757

Serreze, M.C., Barrett, A.P., Slater, A.G., Woodgate, R.A., Aagaard, K., Lammers, R.B., Steele, M., Moritz, R., Meredith, M., Lee, C.M., 2006. The large-scale freshwater cycle of the Arctic. Journal of Geophysical Research: Oceans 111. https://doi.org/10.1029/2005JC003424

Shannon, C.E., 1948. A mathematical theory of communication. The Bell System Technical Journal 27, 379–423. https://doi.org/10.1002/j.1538-7305.1948.tb01338.x

Shipilov, E.V., Senin, B.V., Yunov, A.Y., 1989. Sedimentary cover and basement of the Chukchi Sea from seismic data. Geotectonics 23, 456–463.

Simpson, E.H., 1949. Measurement of Diversity. Nature 163, 688–688. https://doi.org/10.1038/163688a0

Smol, J.P., Birks, H.J.B., Last, W.M., Bradley, R.S., Alverson, K. (Eds.), 2001. Tracking Environmental Change Using Lake Sediments: Terrestrial, Algal, and Siliceous Indicators, Developments in Paleoenvironmental Research. Springer Netherlands, Dordrecht. https://doi.org/10.1007/0-306-47668-1

Snoeijs, P., 1998. Intercalibration and distribution of diatom species in the Baltic Sea. Vol 5. Snoeijs, P., and Balashova, N. eds. Uppsala: Opulus press.

Snoeijs, P., 1996. Intercalibration and distribution of diatom species in the Baltic Sea. Vol 4. Snoeijs, P., and Kasperovičienė, J. eds. Uppsala: Opulus press.

Snoeijs, P., 1993a. Intercalibration and distribution of diatom species in the Baltic Sea. Vol 1. Snoeijs, P. ed. Uppsala: Opulus press.

Snoeijs, P., 1993b. Intercalibration and distribution of diatom species in the Baltic Sea. Vol. 1-5. Uppsala: Opulus press. Vol 1 (1993). Snoeijs, P. ed., Vol 2 (1994). Snoeijs, P., and Vilbaste, S. eds., Vol 3 (1995). Snoeijs, P., and Potapova, M. eds., Vol 4 (1996). Snoeijs, P., and Kasperovičienė, J. eds., Vol 5 (1998). Snoeijs, P., and Balashova, N. eds. Opulus Press.

Springer, A., McRoy, C.P., 1993. The paradox of pelagic food webs in the northern Bering Seao HI. Patterns of primary production 25.

Springer, A.M., McROY, C.P., Flint, M.V., 1996. The Bering Sea Green Belt: shelf-edge processes and ecosystem production. Fisheries Oceanography 5, 205–223. https://doi.org/10.1111/j.1365-2419.1996.tb00118.x

Stein, R., Fahl, K., Schade, I., Manerung, A., Wassmuth, S., Niessen, F., Nam, S.-I., 2017. Holocene variability in sea ice cover, primary production, and Pacific-Water inflow and climate change in the Chukchi and East Siberian Seas (Arctic Ocean). Journal of Quaternary Science 32, 362–379. https://doi.org/10.1002/jqs.2929

Stroeve, J., Holland, M.M., Meier, W., Scambos, T., Serreze, M., 2007. Arctic sea ice decline: Faster than forecast. Geophysical Research Letters 34. https://doi.org/10.1029/2007GL029703

Suzuki, K., Yoshino, Y., Nosaka, Y., Nishioka, J., Hooker, S.B., Hirawake, T., 2021. Diatoms contributing to new production in surface waters of the northern Bering and Chukchi Seas during summer with reference to water column stratification. Progress in Oceanography 199, 102692. https://doi.org/10.1016/j.pocean.2021.102692

Syvertsen, E.E., Hasle, G.R., 1984. Thalassiosira bulbosa Syvertsen, sp. nov., an arctic marine diatom. Polar Biol 3, 167–172. https://doi.org/10.1007/BF00442648

Tsoy, I., Obrezkova, M., 2017. Atlas of Diatom Algae and Silicoflagellates from Holocene Sediments of the Russian East Arctic Seas; V.I. Il'ichev Pacific Oceanological Institute branch. Russian Academy of Sciences: Vladivostok, Russia. 145p.

Tsoy, I.B., Obrezkova, M.S., Aksentov, K.I., Kolesnik, A.N., Panov, V.S., 2017. Late Holocene Environmental Changes in the Southwestern Chukchi Sea Inferred from Diatom Analysis 43, 10.

Tsoy, I.B., Obrezkova, M.S., Artemova, A.V., 2009. Diatoms in surface sediments of the Sea of Okhotsk and the northwest Pacific Ocean. Oceanology 49, 130–139. https://doi.org/10.1134/S0001437009010159

Vologina, E.G., Sturm, M., Kalugin, I.A., Darin, A.V., Astakhov, A.S., Chernyaeva, G.P., Kolesnik, A.N., Bosin, A.A., 2016. Reconstruction of the conditions of Late Holocene sedimentation by integrated analysis of a core of the bottom sediments from the Chukchi Sea. Dokl. Earth Sc. 469, 841–845. https://doi.org/10.1134/S1028334X16080183

von Quillfeldt, C.H., 2001. Identification of Some Easily Confused Common Diatom Species in Arctic Spring Blooms. Botanica Marina 44. https://doi.org/10.1515/BOT.2001.048

von Quillfeldt, C.H., Ambrose, W.G., Clough, L.M., 2003. High number of diatom species in first-year ice from the Chukchi Sea. Polar Biol 26, 806–818. https://doi.org/10.1007/s00300-003-0549-1

Warnock, J.P., Krueger, R.E., 2020. A record of diatom preservation from the AND-1B drillcore: The significance of taphofacies on diatom preservation. Marine Micropaleontology 158, 101887. https://doi.org/10.1016/j.marmicro.2020.101887

Warnock, J.P., Scherer, R.P., 2015. Diatom species abundance and morphologically-based dissolution proxies in coastal Southern Ocean assemblages. Continental Shelf Research 102, 1–8. https://doi.org/10.1016/j.csr.2015.04.012

Weingartner, T., Aagaard, K., Woodgate, R., Danielson, S., Sasaki, Y., Cavalieri, D., 2005a. Circulation on the north central Chukchi Sea shelf. Deep Sea Research Part II: Topical Studies in Oceanography, The Western Arctic Shelf-Basin Interactions (SBI) Project 52, 3150–3174. https://doi.org/10.1016/j.dsr2.2005.10.015

Weingartner, T., Aagaard, K., Woodgate, R., Danielson, S., Sasaki, Y., Cavalieri, D., 2005b. Circulation on the north central Chukchi Sea shelf. Deep Sea Research Part II: Topical Studies in Oceanography 52, 3150–3174. https://doi.org/10.1016/j.dsr2.2005.10.015

Weingartner, T.J., Danielson, S., Sasaki, Y., Pavlov, V., Kulakov, M., 1999. The Siberian Coastal Current: A wind- and buoyancy-forced Arctic coastal current. Journal of Geophysical Research: Oceans 104, 29697–29713. https://doi.org/10.1029/1999JC900161

West, G., Nilsson, A., Geels, A., Jakobsson, M., Moros, M., Muschitiello, F., Pearce, C., Snowball, I., O'Regan, M., 2022. Late Holocene Paleomagnetic Secular Variation in the Chukchi Sea, Arctic Ocean. Geochemistry, Geophysics, Geosystems 23, e2021GC010187. https://doi.org/10.1029/2021GC010187

Wolfe, A.P., 1997. On diatom concentrations in lake sediments: results from an inter-laboratory comparison and other tests performed on a uniform sample. Journal of Paleolimnology 18, 261–268. https://doi.org/10.1023/A:1007937300347

Woodgate, R. a. (1), Lindsay, R.(1), Weingartner, T.(2), 2010. The 2007 Bering Strait oceanic heat flux and anomalous Arctic sea-ice retreat. Geophysical Research Letters 37. https://doi.org/10.1029/2009GL041621

Woodgate, R., Cecilia Peralta-Ferriz, 2021. Warming and Freshening of the Pacific Inflow to the Arctic From 1990-2019 Implying Dramatic Shoaling in Pacific Winter Water Ventilation of the Arctic Water Column. Geophysical Research Letters 48, e2021GL092528. https://doi.org/10.1029/2021GL092528

Woodgate, R.A., Aagaard, K., Weingartner, T.J., 2006. Interannual changes in the Bering Strait fluxes of volume, heat and freshwater between 1991 and 2004. Geophysical Research Letters 33. https://doi.org/10.1029/2006GL026931

Woodgate, R.A., Aagaard, K., Weingartner, T.J., 2005a. A year in the physical oceanography of the Chukchi Sea: Moored measurements from autumn 1990–1991. Deep Sea Research Part II: Topical Studies in Oceanography 52, 3116–3149. https://doi.org/10.1016/j.dsr2.2005.10.016

Woodgate, R.A., Aagaard, K., Weingartner, T.J., 2005b. Monthly temperature, salinity, and transport variability of the Bering Strait through flow. Geophysical Research Letters 32. https://doi.org/10.1029/2004GL021880

Appendix A: Mg/Ca and Temperature from Core 2PC

Table S1. Core 2PC data, star (*): after Barrientos et al. in revision (2018a).

#	Sample id	Depth (cm)	Mg/Ca (mmol/mol)*	T (°C)*
1	1:1	1	0.75	-0.53
2	1:16	16	0.67	-1.168
3	1:36	36	0.58	-1.888
4	1:56	56	0.6	-1.728
5	1:76	76	0.51	-2.448
6	1:96	96	0.59	-1.808
7	2:11	109	0.59	-1.808
8	2:31	129	0.68	-1.088
9	2:56	154	0.65	-1.328
10	2:116	214	0.71	-0.848
11	3:11	259	0.72	-0.768
12	3:31	279	0.71	-0.848
13	3:51	299	0.64	-1.408
14	3:81	329	0.83	0.112
15	3:91	339	0.86	0.352
16	3:96	344	0.84	0.192
17	3:116	364	0.93	0.912
18	3:136	384	0.85	0.272
19	3:141	389	0.91	0.752
20	4:1	398	0.77	-0.368
21	4:16	413	0.7	-0.928
22	4:36	433	0.93	0.912
23	4:51	448	0.84	0.192
24	4:71	468	0.69	-1.008
25	4:76	473	0.66	-1.248
26	4:96	493	0.7	-0.928
27	4:116	513	0.71	-0.848
28	4:136	533	0.68	-1.088
29	5:1	547	0.65	-1.328
30	5:16	562	0.83	0.112
31	5:21	567	0.72	-0.768
32	5:61	607	0.86	0.352
33	5:81	627	0.88	0.512
34	5:116	662	0.84	0.192
35	6:11	685	0.85	0.272
36	6:21	695	0.81	-0.048
37	6:41	715	0.78	-0.288
38	6:56	730	0.67	-1.168
39	6:76	750	0.76	-0.448
40	6:101	775	0.79	-0.208
41	6:121	795	0.72	-0.768

Appendix B: Species list from Core 2PC

Table S2. A total of 126 diatom taxa were identified from 56 genera. Ecology acronyms as m: marine, b: benthic, n:neritc, o:oceanic, p: pelagic. Star sign (*): the taxonomic status of this species requires further investigation. Taxonomic species names according to www.algaebase.org [last visited: 2022-06-28].

#	Species	Synonym	Ecology
1	*Actinocyclus* cf. *octonarius* Ehrenberg 1837		m,bw,b,p
2	*Actinocyclus curvatulus* Janisch 1878		m,p,o
3	*Actinoptychus senarius* (Ehrenberg) Ehrenberg 1843	*Actinoptychus undulatus* Kützing 1844	m,b,p
4	*Attheya septentrionalis* (Østrup) Crawford 1994	*Chaetoceros septentrionalis* Østrup 1895	m,p,n
5	*Aulacoseira subarctica* (Müller) Haworth 1990		fw,p
6	*Bacillaria socialis* (Gregory) Ralfs 1861	*Nitzschia socialis* Gregory 1857	m,bw
7	*Bacterosira bathyomphala* Syvertsen & Hasle 1993		m,p,n
8	*Bacterosira constricta* (Gaarder) Park & Lee 2016	*Thalassiosira constricta* Gaarder 1938	m,p,n
9	*Chaetoceros cinctus* Gran 1897		m,p,n
10	*Chaetoceros debilis* Cleve 1894		m,p,n
11	*Chaetoceros diadema* (Ehrenberg) Gran 1897		m,p,n
12	*Chaetoceros didymus* Ehrenberg 1845		m,p,n
13	*Chaetoceros furcellatus* Yendo 1911	*Chaetoceros furcellatus* Bailey 1856	m,p,n
14	*Chaetoceros holsaticus* Schütt 1895		m,p,n
15	*Chaetoceros ingolfianus* Ostenfeld 1904		m,p,n
16	*Chaetoceros lorenzianus* Grunow 1863		m,p,n
17	*Chaetoceros mitra* (Bailey) Cleve 1896		m,p,n
18	*Chaetoceros C.* sp. *2* sensu Cremer 1998: pl. 5, fig. 5		m,p,n
19	*Chaetoceros C.* sp. *7*: Appendix E: suppl. fig. 1		
20	*Chaetoceros* spp.		m,p,n
21	*Chaetoceros vanheurckii* Gran 1897		m,p,n
22	*Cocconeis costata* W.Gregory 1855		m,b
23	*Coscinodiscus marginatus* Ehrenberg 1843		m,p,o
24	*Coscinodiscus oculus-iridis* (Ehrenberg) Ehrenberg 1840		m,p,o
25	*Coscinodiscus radiatus* Ehrenberg 1840		m,p,o,n
26	*Cyclotella striata* (Kützing) Grunow 1880		bw,m
27	*Cymbella gracilis* (Ehrenberg) Kützing 1844 *		
28	*Cymbella* spp.		fw
29	*Cymbella subcistula* Krammer 2002		fw
30	*Delphineis surirella* (Ehrenberg) Andrews 1981		bw,m, b
31	*Denticula subtilis* Grunow 1862		
32	*Detonula confervacea* (Cleve) Gran 1900		m,p,n
33	*Diploneis interrupta* (Kützing) Cleve 1894		bw,m,b
34	*Diploneis littoralis* var. clathrata (Østrup) Cleve 1896		m,b
35	*Diploneis smithii* (Brébisson) Cleve 1894		bw,m,b
36	*Encyonema silesiacum* (Bleisch) Mann 1990	*Cymbella silesiaca* Bleisch 1864	fw
37	*Entomoneis gigantea* var. *septentrionalis* (Grunow) Poulin & Cardinal 1983		m,b
38	*Entomoneis kjellmanii* (Cleve) Poulin & Cardinal 1983		m
39	*Entomoneis* spp.		m
40	*Eunotia praerupta* Ehrenberg 1843		fw
41	*Eunotia suecica* Cleve 1895		fw
42	*Fallacia forcipata* (Greville) Stickle & Mann 1990	*Navicula forcipata* Greville 1859	m,b
43	*Fallacia pygmaea* (Kützing) Stickle & Mann 1990		m,b
44	*Fossula arctica* Hasle, Syvertsen & Quillfeldt 1996		m,p
45	*Fragilaria capucina* Desmazières 1830		fw
46	*Fragilariopsis cylindrus* (Grunow ex Cleve) Helmcke & Krieger 1954	*Nitzschia cylindrus* (Grunow ex Cleve) Hasle 1972	m,p,n

47	*Fragilariopsis oceanica* (Cleve) Hasle 1965	*Nitzschia grunowii* Hasle 1972	m,p,n
48	*Fragilariopsis reginae-jahniae* Witkowski, Lange-Bertalot & Metzeltin 2000		m,p,n
49	*Grammatophora angulosa* Ehrenberg 1840		bw,m,b
50	*Grammatophora arcuata* Ehrenberg 1853		bw,m,b
51	*Gyrosigma diaphanum* Cleve 1894		m,b
52	*Haslea* cf. *spicula* (Hickie) Bukhtiyarova 1995		
53	*Melosira arctica* Dickie 1852		bw,m,p
54	*Melosira lineata* (Dillwyn) Agardh 1824		bw,m,p
55	*Navicula algida* Grunow 1884		fw
56	*Navicula asymmetrica* Cleve 1883		m
57	*Navicula directa* (Smith) Brébisson 1854		bw,m
58	*Navicula frigida* Grunow 1880	*Navicula kariana* var. *frigida* (Grunow) Cleve 1895	m
59	*Navicula geitleri* var. *asymmetrica* (Heiden) Desikachary & Sridharan 1989	*Navicula gelida* var. *assymetrica* Heiden 1905	m
60	*Navicula gelida* Grunow 1884		m
61	*Navicula imperfecta* Cleve 1883		m
62	*Navicula impexa* Hustedt 1961		fw
63	*Navicula kariana* var. *detersa* Grunow 1884		m
64	*Navicula novadecipiens* Hustedt 1966		m
65	*Navicula peregrina* (Ehrenberg) Kützing 1844		bw,m
66	*Navicula superba* var. *elliptica* Cleve 1883		m
67	*Navicula transitans* Cleve 1883		m
68	*Navicula transitans* var. *derasa* (Grunow) Cleve 1883		m
69	*Navicula valida* Cleve & Grunow 1880		m
70	*Navicula* spp.		
71	*Navigeia* cf. *paludosa* (Hustedt) Bukhtiyarova 2013	*Navicula paludosa* Hustedt 1957	
72	*Neodenticula seminae* (Simonsen & Kanaya) Akiba & Yanagisawa 1986		m,p,o
73	*Nitzschia angularis* Smith 1853		m
74	*Nitzschia hudsonii* Poulin & Cardinal 1983 *		m
75	*Nitzschia hybrida* Grunow 1880		m
76	*Nitzschia laevissima* Grunow 1883		m
77	*Nitzschia linearis* Smith 1853		fw
78	*Nitzschia polaris* Grunow 1883		m
79	*Nitzschia scabra* Cleve 1883		m
80	*Nitzschia* spp.		m
81	*Odontella aurita* (Lyngbye) Agardh 1832		m,b,p
82	*Odontidium mesodon* (Kützing) Kützing 1849	*Diatoma mesodon* (Ehrenberg) Kützing 1844	fw
83	*Opephora mutabilis* (Møller) Sabbe & Wyverman 1950 *	*Opephora olsenii* Møller 1950	m,bw
84	*Paralia sulcata* (Ehrenberg) Cleve 1873		m,b,p,n
85	*Paraplaconeis subplacentula* (Hustedt) Kulikovskiy & Lange-Bertalot 2012		fw
86	*Pauliella taeniata* (Grunow) Round & Basson 1997	*Achnanthes taeniata* Grunow 1880	m,bw
87	*Petroneis glacialis* (Cleve) Witkowski, Lange-Bertalot & Metzeltin 2000		m,b
88	*Pinnularia bihastata* (Mann) Mills 1934		fw,bw
89	*Pinnularia borealis* Ehrenberg 1843		fw
90	*Pinnularia quadratarea* var. *constricta* (Østrup) Gran 1900		m
91	*Pinnularia quadratarea* var. *cuneata* Østrup 1905 *		m
92	*Pinnularia quadratarea* var. *maxima* (Østrup) Boyer 1927 *		m
93	*Pinnularia quadratarea* var. *minor* (Østrup) Heiden 1905 *		m
94	*Pinnularia quadratarea* var. *subglabra* (Østrup) Poulin & Cardinal 1982 *		m
95	*Pinnularia subcapitata* Gregory 1856		

96	*Pinnularia* spp.		fw
97	*Pleurosigma rhomboides* Cleve Cleve 1880		m,bw
98	*Porosira glacialis* (Grunow) Jørgensen 1905		m,p,n
99	*Proboscia alata* (Brightwell) Sundström 1986		m,p,o
100	*Proboscia subarctica* Takahashi, Jordan & Priddle 1973		m,p,o
101	*Pseudogomphonema arcticum* (Grunow) Medlin 1986 *		m,b
102	*Pseudogomphonema kamtschaticum* (Grunow) Medlin 1986		m,b
103	*Pseudogomphonema septentrionale* (Grunow) Medlin 1986		m,b
104	*Pseudo-Nitzschia seriata* (Cleve) Peragallo 1899		m,p
105	*Rhizosolenia hebetata* Bailey 1856	*Rhizosolenia hebetata* f. *hiemalis* Gran 1904	m,p,o
106	*Rhizosolenia hebetata* f. *semispina* (Hensen) Gran 1908		m,p,o
107	*Rhizosolenia styliformis* Brightwell 1858		m,p,o
108	*Sellaphora bacillum* (Ehrenberg) Mann 2018	*Navicula bacillum* Ehrenberg 1839	fw
109	*Sellaphora laevissima* (Kützing) Mann 1989	*Navicula laevissima* Kützing 1844	fw
110	*Shionodiscus latimarginatus* (Makarova) Alverson, Kang et Theriot 1975 *	*Thalassiosira latimarginata* Makarova 1988	m,p,o
111	*Shionodiscus oestrupii* (Ostenfeld) Alverson, Kang & Theriot 2006	*Thalassiosira oestrupii* (Ostenfeld) Proshkina-Lavrenko ex Hasle 1960	m,p,o
112	*Sinerima marigela* Nesterovich & Caissie 2018		m
113	*Stauronella arctica* (Hustedt) Lange-Bertalot 1999		m
114	*Staurosirella martyi* (Héribaud) Morales & Manoylov 2006	*Opephora martyi* Héribaud 1902	fw
115	*Stenoneis inconspicua* var. baculus Cleve 1894	*Navicula baculus* Cleve 1883	m,bw
116	*Stenoneis obtuserostrata* (Hustedt) Poulin 1990		m,bw
117	*Stephanopyxis nipponica* Gran & Yendo 1914		m,p,n
118	*Stephanopyxis turris* (Greville) Ralfs 1861		m,p,n
119	*Tabularia fasciculata* (Agardh) Williams & Round 1986		fw
120	*Thalassionema nitzschioides* (Grunow) Mereschkowsky 1902		m,p,n
121	*Thalassiosira angustelineata* (Schmidt) Fryxell & Hasle 1977		m,p,o
122	*Thalassiosira antarctica* Comber 1896		m,p,n
123	*Thalassiosira bulbosa* Syvertsen 1984		m
124	*Thalassiosira* cf. *pacifica* Gran & Angst 1931		
125	*Thalassiosira eccentrica* (Ehrenberg) Cleve 1904		m,p,n,o
126	*Thalassiosira gravida* Cleve 1896		m,p,n
127	*Thalassiosira hyalina* (Grunow) Gran 1897		m,p,n
128	*Thalassiosira hyperborea* (Grunow) Hasle 1989		m,b
129	*Thalassiosira nordenskioeldii* Cleve 1873		m,p,n
130	*Thalassiosira simonsenii* Hasle & Fryxell 1977		m,p
131	*Thalassiosira* cf. spp. (<10 um diameter)		m,p,n
132	*Thalassiothrix longissima* Cleve & Grunow 1880		m,p,o
133	*Trachyneis aspera* (Ehrenberg) Cleve 1894	*Navicula aspera* Ehrenberg 1840	bw,b

Appendix C: LM micrographs

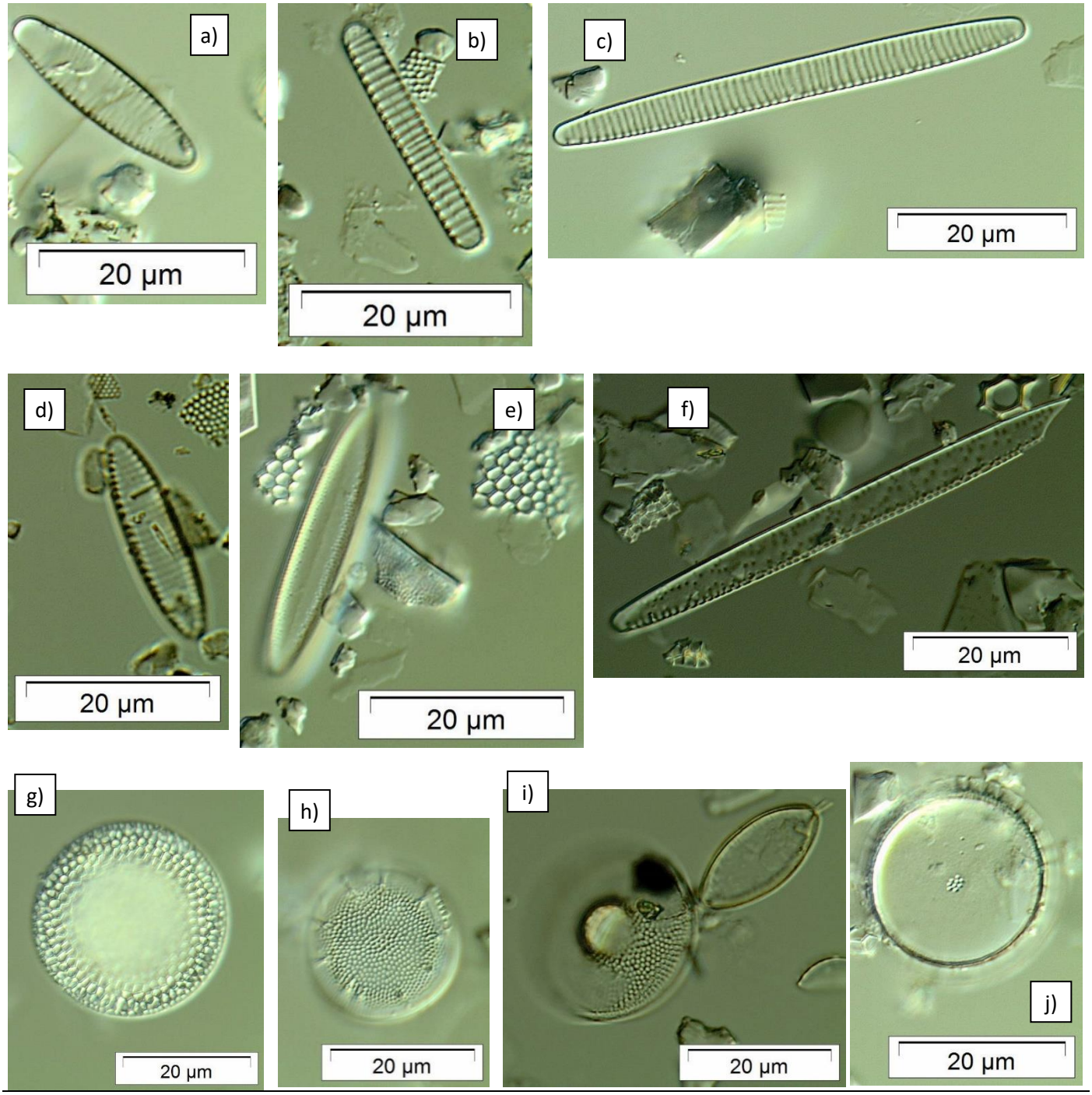

Plate 1: Sempagic ice algae and cold-water species. Diatoms in valve view and scalebar in each LM micrograph. Sympagic group: a-d **(a)** *Fossula arctica*, **(b)** *Fragilariopsis cylindrus*, **(c)** *Fragilariopsis reginae-jahniae*, **(d)** *Fragilariopsis oceanica*, **(e)** *Pauliella taenita* araphid valve, **(f)** *Fragilariopsis reginae-jahniae* heavy silicified variant, **(g)** *Thalassiosira antarctica*, **(h)** *Thalassiosira nordenskioldii*, **(i)** *Bacterosira bathyomphala* with a *Chaetoceros* valve to the right, and **(j)** *Bacterosira constricta*. Complete taxonomic names in appendix B.

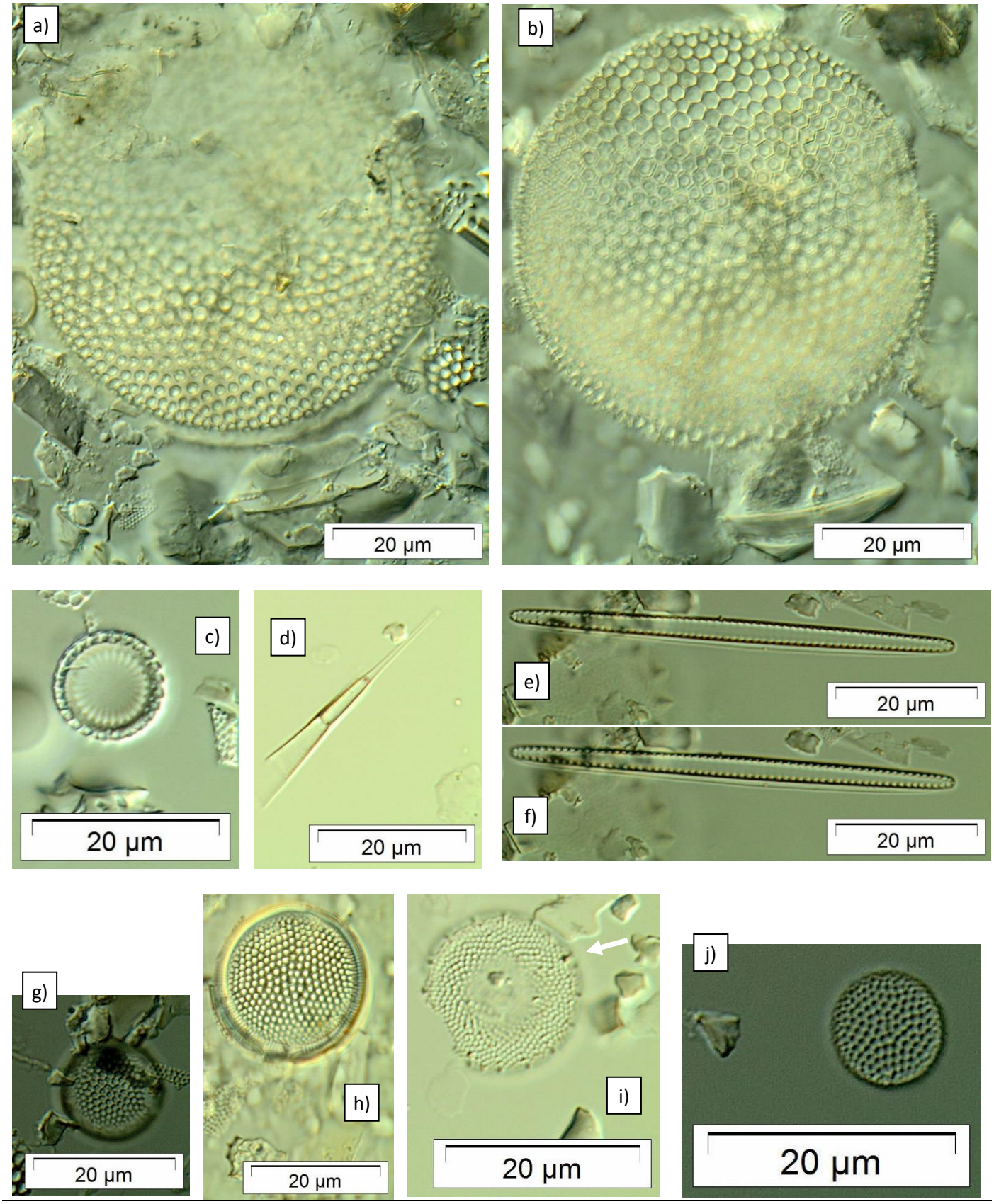

Plate 2: Warm water species and Paralia sulcata. LM-diatoms with scalebar in each micrograph. **(a,b)** Large specimen of *Coscinodiscus marginatus with* different foci, **(c)** *Paralia sulcata*, **(d)** *Rhizosolenia hebetata* f. *semispina*, **(e,f)** *Thalassionema nitzschioides* with different foci on apical ends, **(g)** *Shionodiscus oestrupii*, **(h)** *Thalassiosira simonsenii*, **(i)** *Thalassiosira* cf. *pacifica* slightly concave around valve center, process density 3/10 µm and a labiate process (arrow), and **(j)** *Thalassiosira* spp. ≤10 µm. Complete taxonomic names in appendix B.

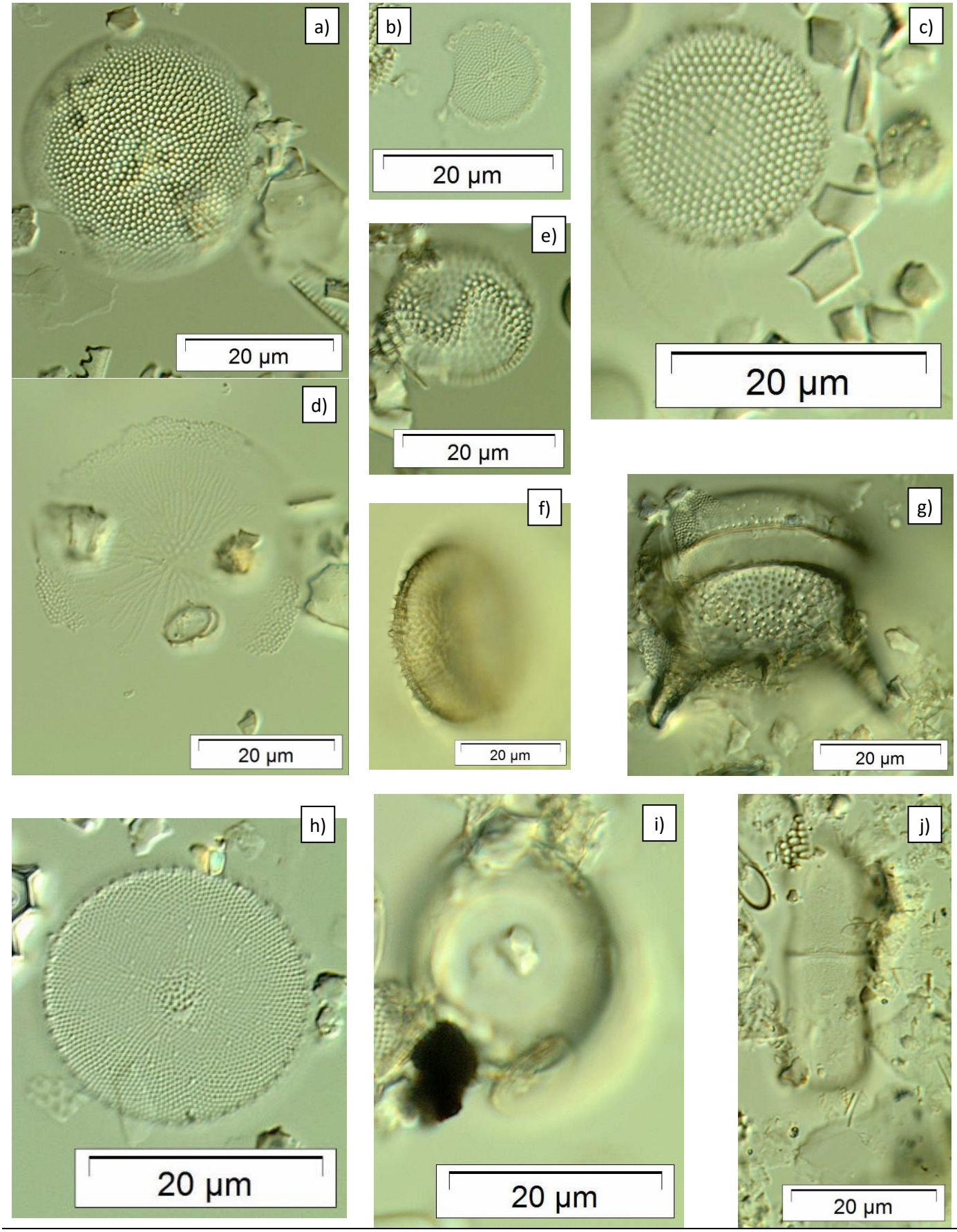

Plate 3: Various centrales diatoms. LM-diatoms with scalebar in each micrograph. **(a)** *Actinocyclus curvatulus*, **(b)** *Thalassiosira bulbosa*, **(c)** *Thalassiosira eccentrica*, **(d)** *Sinerima marigela*, **(e,f)** *Thalassiosira hyperborean, (f) in mantle view*, **(g)** *Odontella aurita* heavy silicified, **(h)** *Thalassiosira hyalina*, **(i)** *Melosira arctica*, and **(j)** *Melosira lineata* two valves in girdle view. Complete taxonomic names in appendix B.

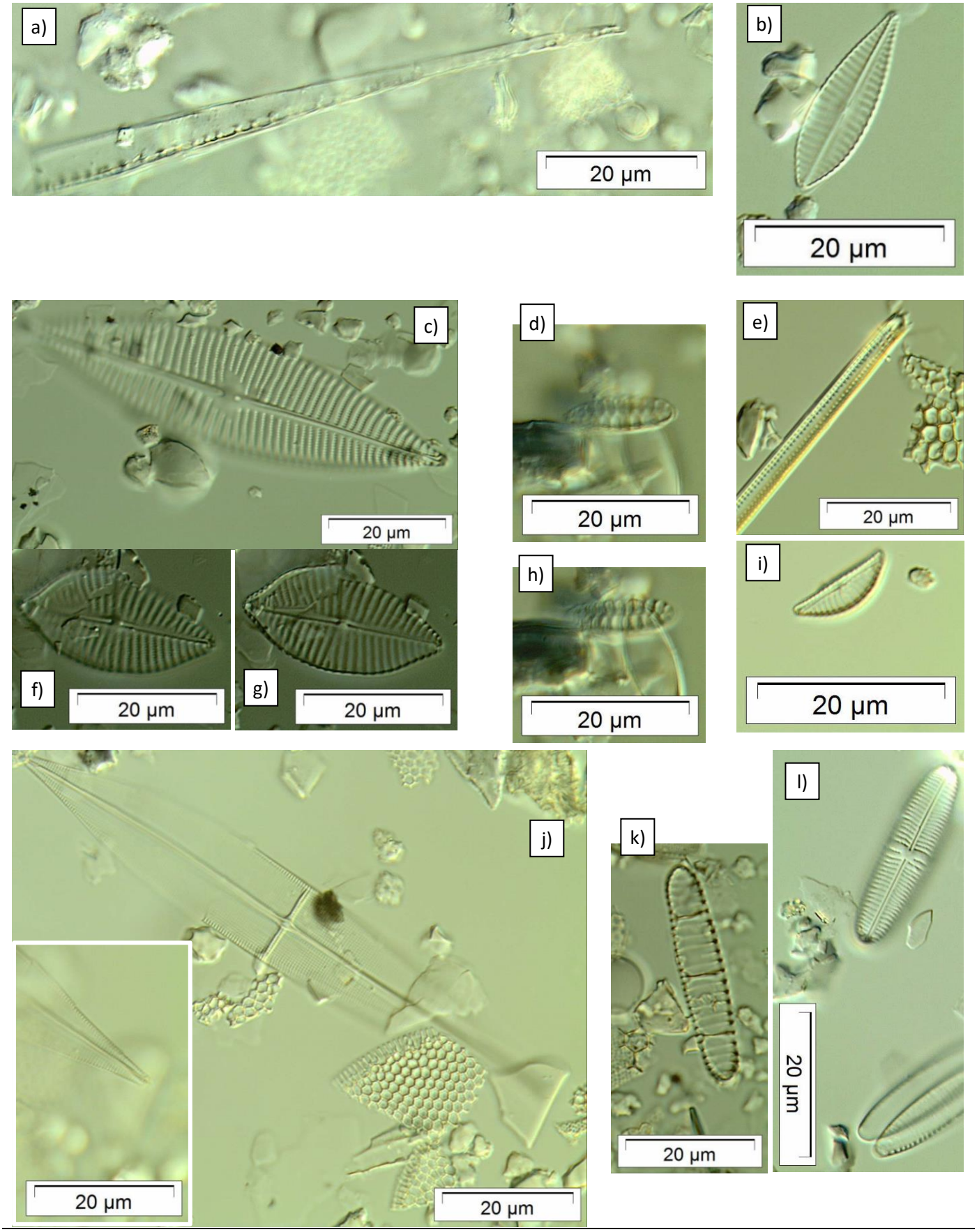

Plate 4: Various pennales diatoms. LM-diatoms in valve view, with scalebar = 20 µm in each micrograph. **(a)** *Nitzschia laevissima* broken valve, **(b)** *Pseudogomphonema arcticum*, **(c)** *Navicula transitans*, **(d,h)** *Opephora olsenii* with different foci **(e)** *Thalassiothrix longissima* (one terminal ending shown), **(f,g)** *Navicula valida* var. *minuta* different foci, **(i)** *Cymbella* cf. *silesiaca*, **(j)** *Haslea spicula* (overlapping valves) with extra inset figure of lower apical end, **(k)** *Neodenticula seminae*, **(l)** *Navicula ignota* var. *palustris* with two valves of *Fragilariopsis oceanica* on the bottom. Complete taxonomic names in appendix B.

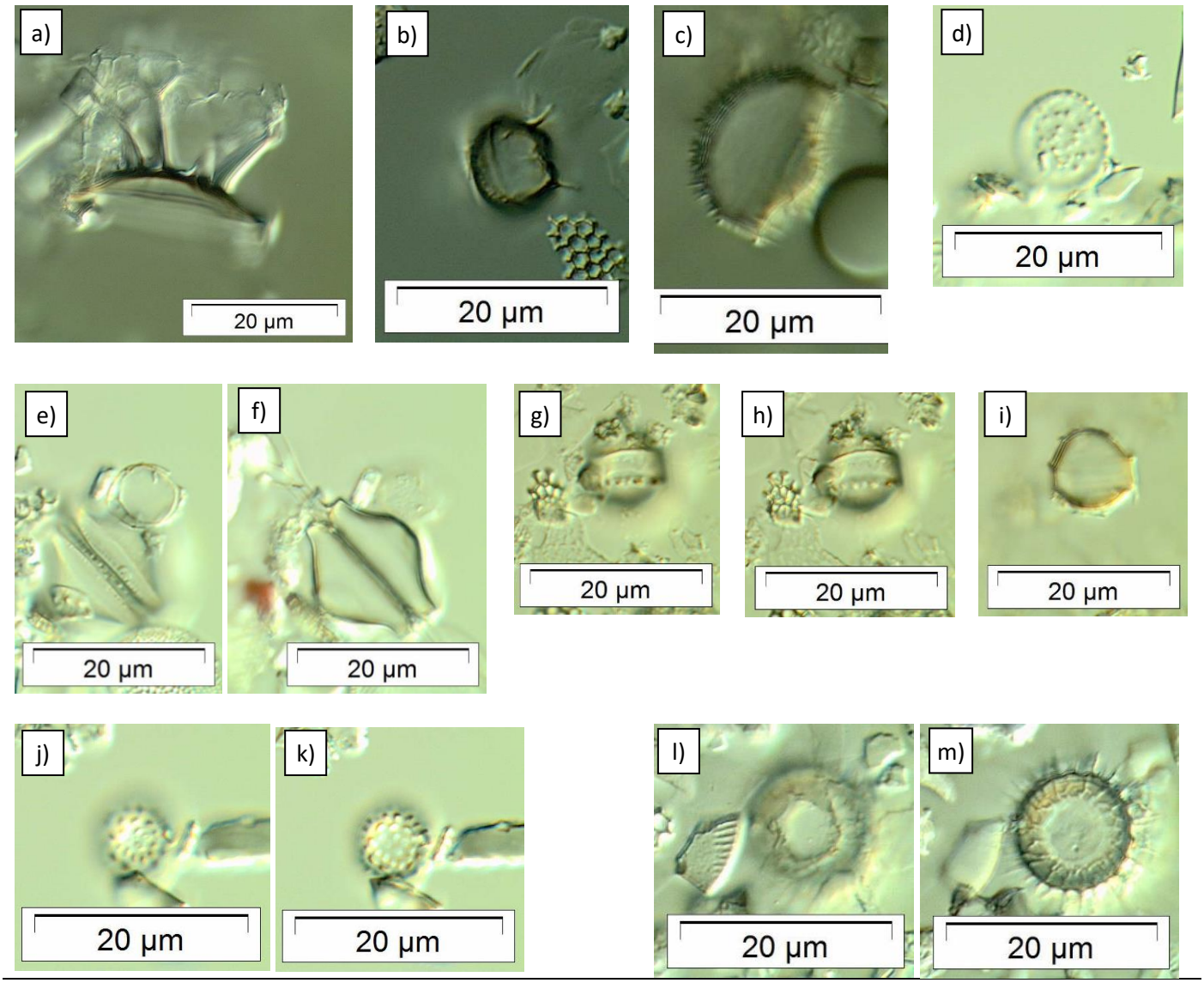

Plate 5: Chaetoceros, Chrysophyte and Dinoflagellate. LM-diatoms with scalebar in each micrograph. Figure e-m in different foci. **(a)** Epivalve of *Chaetoceros diadema*, **(b)** *Chaetoceros debilis* whole cell in mantle view, **(c)** *Chaetoceros holsaticus* with radial spines on epi- and hypovalve, **(d)** *Chaetoeros* sp. *3*, sensu *Ehrenbergiulvia granulosa* (Nesterovich, 2019: Figure C.3), **(e,f)** Chaetoceros furcellatus in pervalvar view and setae visible in fig. f, (**g-i**) *Chaetoceros C*. sp. *2* sensu Cremer 1998: pl. 5, fig. 5, **(j,k)** chrysophyte cyst, and **(l,m)** assumed dinoflagellate cyst. *Chaetoceros* taxonomic names in appendix B.

Appendix D: SEM micrographs

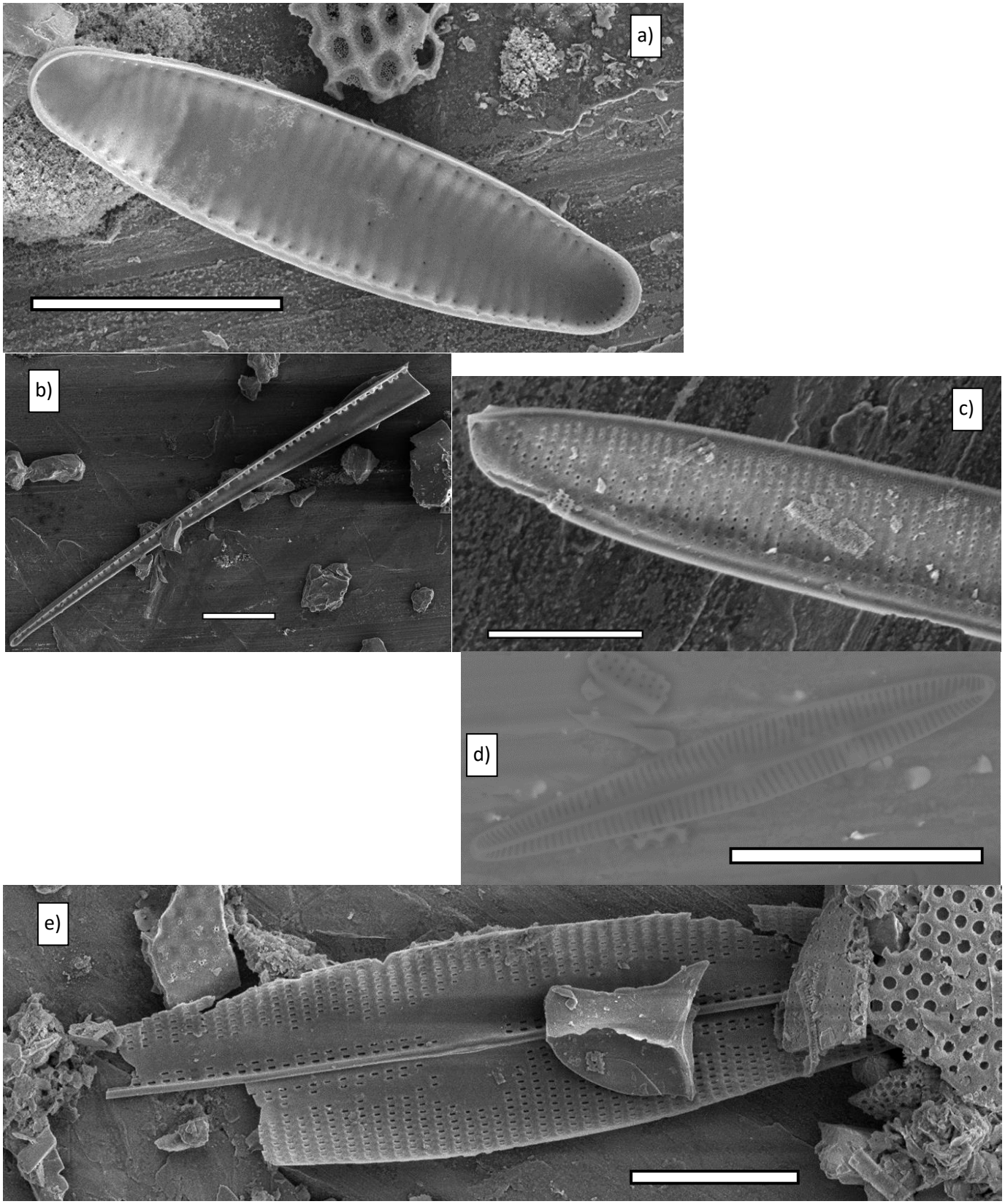

Pennales SEM images except image d: TM3000. White scale bar = 10 µm, except in image c: scale bar = 5 µm and image d: scale bar = 30 µm. Complete taxonomic names in appendix B. (a) *Fossula arctica*, (b) *Nitzschia laevissima* broken valve, (c) *Fragilariopsis reginae-jahniae* one terminal ending in valve view, (d) *Pseudogomphonema kamtschaticum* (TM3000) and (e) *Navicula transitans* broken valve.

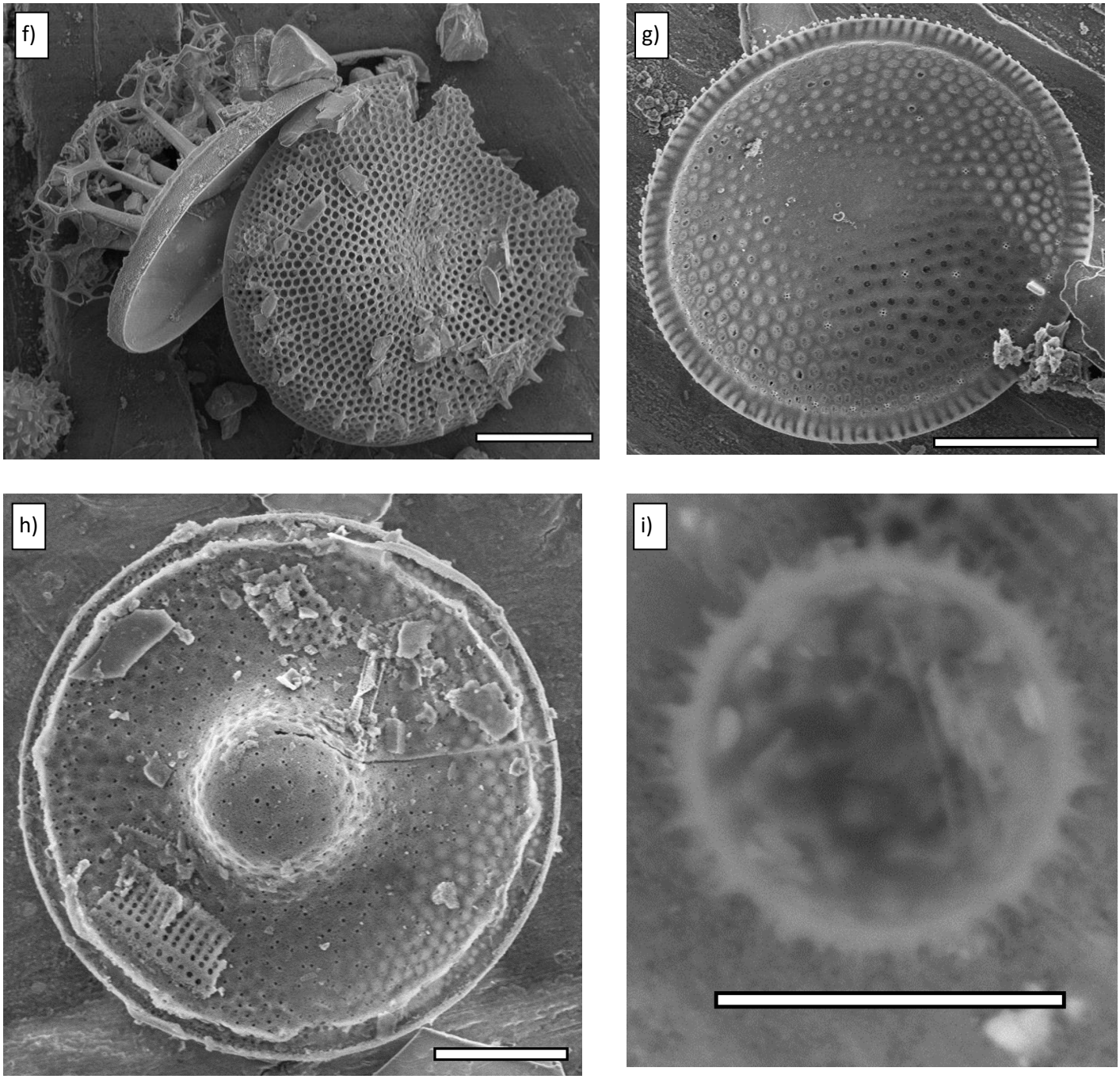

Centrales SEM images except image i: TM3000. White scale bar = 10 µm, except in image h: scale bar = 5 µm. Complete taxonomic names in appendix B. (f) *Thalassiosira nordenskioldii* with epivalve of *Chaetoceros diadema* to the right in pervalvar view, (g) *Thalassiosira antarctica,* (h) *Bacterosira bathyomphala and* (i) Crysophyte cyst.

Appendix E: Description of *Chaetoceros* sp. *7*

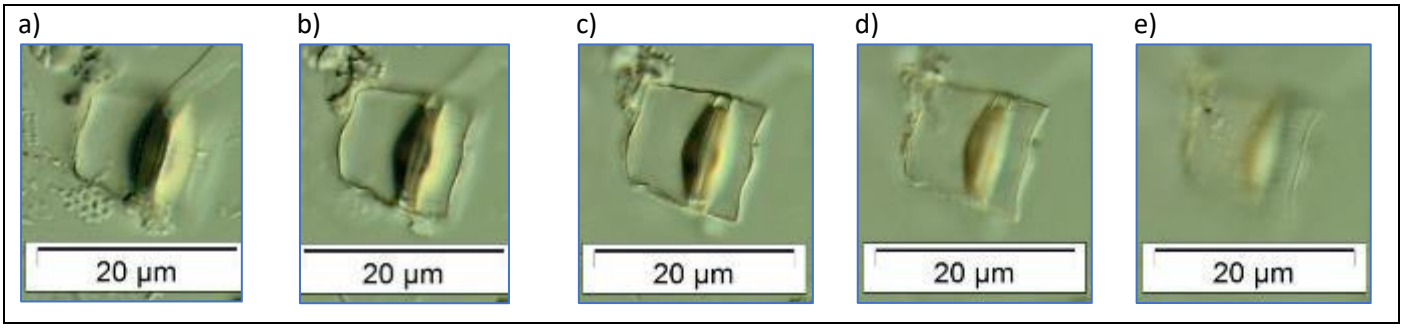

Supplementary figure 1. Micrographs a-e of *Chaetoceros* sp. *7* from the 2PC Core.

Chaetoceros sp. *7* (Phylum: Bacillariophyta, Class: Mediophyceae, Order: Chaetocerotales, Family: Chaetocerotaceae, Genus: Chaetoceros) was retrieved from Herald Canyon (57 m depth), Chukchi Sea from SWERUS-2014-L2-PC-1 (2PC) at a sample depth of 795 cm, aged set to 4129 cal. yr. BP (West et al., 2022). The taxon has neither been identified- nor seen earlier in the Laptev- East Siberian- and Chukchi Seas (Tsoy and Obrezkova, 2017; pers. comm. Ira Tsoy May 2022). The species *C.* sp. *7* from sample 6:121 is interpreted as a vegetative *Chaetoceros* cell and seen in girdle view (supplementary figure 1). Description with morphometric data, preservation, and distribution of *Chaetoceros* sp. *7* follows.

Description: *Chaetoceros* sp. *7* (apical length: <10 µm, pervalvar length: <4 µm) has dome-discoid shape in pervalvar view with a geoid-like-shaped fine delicate membrane surrounding the cell. The delicate fine structures, show small outgrowth in the pervalvar view, like a stem with small branching nodes on the top. In the images, the surrounding outgrowths are heading upwards enclosing the epivalve, like a hat. The second surrounding outgrowth is usually smaller, and it is observed this delicate cell structure is first missing if the specimen is not intact. The connecting outgrowth setae are enclosing the cell in bending curves 1 µm away from the cell in the perpendicular (90°) direction parallel to the pervalvar axis.

The Chaetoceros sp. *7* shows a complete frustule containing an assumed girdle ring in the middle and upper and lower single bands (supplementary figure a,b), assumed to include a single band of puncta in at least the lower band (not visible in the images). The upper valve has a dome-shaped structure, while the lower is less distinct, with a sudden inflated circular shape in the middle. The darker colour of the epi- and hypovalves (supplementary figure a-c) are not always dark and may be due to the image capture.

About the dark colour, Ira Tsoy, added: *"The dark part is probably an aperture. It is a space between valves of adjacent cells in colony of Chaetoceros or Attheya. But it cannot be ruled out that this is some stage of spore formation."*.

The valves show similarities in shape due to the apical- and pervalvar axis in the interpreted vegetative stage. When silicified, it may appear slightly larger to distinctive larger in those dimensions, but this is the rule of thumb based by LM-observations.

Preservation and distribution: This species have been interpreted as well preserved, possible due to a rapid sedimentation rate, the surrounding membrane around the lower valve (supplementary figure b-e) sometimes absent. Due to the delicate surrounding membrane structure, it was assumed that the *Chaetoceros* sp. *7* has not been transported, rather it is dwelled in the neritic sublittoral environment related to the 2PC Core, Herald Canyon, Chukchi Sea. *Chaetoceros C.* sp. *7* has been identified at various core depths.

The rectangular cell and the narrow possible aperture similar to *Chaetoceros affinis* Lauder 1864. However, the cell structure parallel to the hypo- and epivalves are more undulating, and doubtful if intercalary setae is present. Holotype sample 6:121 at Södertörn University.

The author suggests a dedication of *Chaetoceros C.* sp. *7*, to Ira Tsoy.